Synthesis and characterization of Ce^{3+} doped silica (SiO_2) nanophosphors co-doped with Al^{3+} or Mg^{2+} ions.

by

Lehlohonolo Fortune Koao

(B.Sc Hons)

A dissertation presented in fulfillment of the requirements for the degree

MAGISTER SCIENTIAE

in the

Faculty of Natural and Agricultural Sciences

Department of Physics

at the

University of the Free State, (Qwa Qwa Campus)

Republic of South Africa

Supervisor: Prof. B. F. Dejene

Co-supervisor: Prof. H. C. Swart

November 2009

This thesis is dedicated to my mother, father, brother, two sisters and my lovely daughter.

Acknowledgements

My sincere thanks and gratitude go to:

Abstract

In recent studies, amorphous silica (SiO_2) has been used as a host matrix for rare-earth ions to prepare luminescent materials that can be used in various light emitting devices. Sol-gel glasses have the potential to hold up to $\geq 10\%$ dopants without losing their amorphous structure. However, before rare earth (RE) - doped sol-gel glasses can be used as luminescent material, several fluorescence quenching mechanisms must be overcome. There are several quenching mechanisms which are present in all materials that are more serious in sol-gel glasses. The first is cross relaxation which involves energy transfer between RE elements; the others are energy transfer through lattice vibrations and to hydroxyl (OH) groups which are present due to the use of water as the solvent during the preparation process. A few studies have demonstrated that the luminescence intensity of rare-earth doped silica can be improved through incorporation of co-dopants such as Al, TiO_2, B and by annealing at high temperatures (e.g. $> 500^{\circ}C$).

Following their footsteps and in order to make comparisons, we used aluminum as the co-dopant in some samples to investigate the effects on luminescence yield for various RE concentrations. We also investigated the effects of magnesium co-dopant and high temperature annealing on the luminescence intensity of rare-earth doped silica. In this work, the highest emission intensity was observed for the sample with a composition of 0.5 mol% Ce^{3+}. Cerium doped silica glasses had broad blue emission corresponding to the $D_{3/2}$- F_J transition at 445 nm but exhibited apparent concentration quenching after higher concentrations of 0.5 mol% Ce^{3+}. Silica containing Mg^{2+} or Al^{3+} ions displayed an increase in luminescence intensity as the Mg^{2+} or Al^{3+} to Ce^{3+} ratio increases for the range investigated but significant luminescence enhancement was observed for Mg^{2+}:Ce ratio greater than 20, while that of Al^{3+} co-doping had the highest luminescent intensity when the ratio of Al:Ce is 10:1. This enhanced photoluminescence was assigned to an energy transfer from the Mg nanoparticles, to result in enhanced emission from Ce^{3+}. The Al^{3+} or Mg^{2+} ions disperses the Ce^{3+} clusters, enhancing $^2F_{5/2}$ and $^2F_{7/2}$ emissions due to increased ion-ion distances and decreased cross-relation.

TABLE OF CONTENTS

Chapter 1

Chapter 2: Background

Chapter 3: Experimental Procedure and an overview of Research techniques.

3.1 Experimental Procedure

3.2 Synthesis

3.3 Sample Characterization

Chapter 4: Characterization of pure silica nanoparticles (SiO$_2$) prepared by sol-gel method.

Chapter 5: Synthesis and characterization of Ce^{3+} doped silica (SiO$_2$) nanoparticles.

Chapter 6: The effect of Mg^{2+} ions on the Photoluminescence of Ce^{3+} doped silica.

Chapter 7: The effects of the Al^{3+} ions on the photoluminescence intensity and wavelength of Ce^{3+} with silica (SiO$_2$).

Chapter 8: Summary, Conclusion and future work.

LIST OF FIGURES

Chapter 1

1. Introduction

The term sol-gel process is a chemical synthesis technique for preparing gels, glasses and ceramic powders. The sol-gel process generally involves the use of metal alkoxides, which undergo hydrolysis and condensation polymerization reactions to give gels. Sol-gel glasses are of current interest because of their potential applications such as electronics and optics [1]. Glasses have been conventionally prepared by low temperature methods, but the use of the sol-gel process enables the preparation of porous or dense glasses with superior homogeneity, purity, and good optical qualities (high transmittance) at significantly lower temperature [2]. Sol-gel materials provide an excellent vehicle for the incorporation of secondary phase including metal ions, organic molecules or macromolecules. These species may be doped into the gel-matrix as it is being formed (pre-doping) [3] or incorporated after the glass has been prepared (post-doping). It is well recognized that impurity and defects [4-5] in silica glasses are important parameter that greatly influence properties of silica glasses.

Glasses doped with Ce^{3+} ions that emit optical transitions in the 300-500 nm wavelength range due to electric dipole allowed 5d-4f transitions, are useful in many applications including fiber optics, scintillators and tunable lasers [6]. Currently, much interest has emerged in the Ce^{3+} ion for its application in high energy physics, because of fast and efficient luminescence in the UV and blue spectral region. The emission of the Ce^{3+} ions produced by the electron transition of $4f^{n-1}$ 5d-4f^n, can be blue/red shifted depending on the type of co-doping solids [7, 8]. Also other factors such as modification of the ligand field around the Ce^{3+} ions in silica, presence of hydroxyl ions, energy transfer by cross-relaxation and the concentration of the co-dopants have significant effect on the luminescent wavelength and intensity. First, the hydroxyl groups (OH) which is a chemical impurity in silica glasses, causes luminescence quenching. OH is one of the most important impurities in glasses, having disproportionately large influences on various glass properties. A trace amount of water can reduce the viscosity [9-10], chemical stability [11] and density of the glass [12]. Even when water is not contained in a glass, it can enter into the glass surface through diffusion, thereby affecting the chemical, optical and mechanical properties of

the glass. Water in the surrounding atmosphere shortens the static fatigue life of silica glass [13-14]. Furthermore, water can interact with defects in glass. Still annealing the silica glasses at high temperature (e.g.>600 °C) does not necessarily remove all of the OH groups. The presence of OH groups near Ce^{3+} ions provides a non-radiative decay mechanism for the Ce, causing luminescence quenching.

Secondly, the clustering of the Ce^{3+} ions at higher concentrations causes luminescence quenching through cross relaxations [15, 8]. At higher Ce concentrations, most ions reside in clusters and the lattice defects become more important, the luminescence is observed from a minority of isolated ions. Low solubility of Ce^{3+} ions in silica, and the need to coordinate with limited numbers of non-bridging oxygen, make Ce^{3+} ions cluster on pore surface. The tendency of Ce^{3+} ions to cluster increases luminescence quenching by energy transfer among Ce^{3+} ions and the rate of energy transfer between Ce^{3+} ions is strongly dependent on the inter-ionic distance. These quenching mechanisms may be overcome or enhanced with the use of the co-dopants. Several research groups [8] have experimented with co-dopants and have found that aluminum produces the greatest enhancement on fluorescence of all rare-earth-doped materials. These researchers have found that the Al^{3+} co-doping improves fluorescence yield remarkably, but the mechanism is not yet understood [8]. One generally accepted explanation has been that Al^{3+} prevents Ce dopants from clustering in the glass, thus reducing ion-ion energy migration and cross-relaxation. The traditional interpretation of the enhancement of fluorescence is that Al^{3+} ions increases the number of non-bridging oxygen for Ce^{3+} ions to bond to, therefore dispersing clusters [16].

While Al-co-doping has been shown to reduce interactions among the Ce-O-Ce bonding, the exact nature of the way Al is incorporated into glass matrix is not well understood [17]. It is likely that the lower coordination number of aluminum increases the probability that Al-O-Ce bonds form. Aluminum may act as either network former or as a modifier. Its presence in the sol-gel glass is also known to increase the residual OH problem [18]. Recent work by Monteil et al [19] used numerical modeling to attempt a better understanding of the role Al^{3+} plays. Their numerical simulation predicted that RE ions in silica matrix containing Al^{3+} are found solely in aluminum-rich regions of the glass. However, the result also indicated that Al^{3+} co-doping does not prevent RE ions from forming clusters. At present, the researchers [8] have found that Al^{3+} co-doping has considerable impact on luminescence yields in these materials.

Following their footsteps and in order to make comparisons, we used aluminum as the co-dopant in some samples to investigate the effects on luminescence yield for various RE concentrations. We also investigated the effects of magnesium co-dopant and high temperature annealing on the luminescence intensity of rare-earth doped silica. It was observed the magnesium or aluminum co-dopants and annealing temperature significantly affect the luminescence intensity. This enhancement may be due to the Mg/Al reducing the charge defects or OH induced reduction by substitution of trivalent rare-earth ion site into the silica or dispersing the Ce^{3+} ions.

2. The problems.

The specific objectives of this study are:

- To synthesis and characterize silica nanoparticles in order to study defects centers and luminescence properties of pure silica grown by the so-gel technique since this is an important parameter that influence the properties of silica glass and its applications.

- To synthesize and characterize Ce^{3+} doped silica (SiO_2) nanophosphors in order to investigate the concentration quenching effects of Ce ions on the PL luminescence.

- To study the effect of Mg or Al ions co-doping on the Ce^{3+} doped silica (SiO_2) nanophosphors. Specifically, it was intended to experimentally determine the variation in the luminescence intensity and wavelength with Al or Mg concentrations.

- To investigate the influence of the annealing temperature on the material properties of pure or doped silica nanophosphors (SiO_2, SiO_2:0.5%Ce^{3+}, SiO_2:0.5%Ce^{3+}:1%Al^{3+} and SiO_2:0.5%Ce^{3+}:1%Mg^{2+}).

3. Aim of this study.

Our rural communities are disadvantaged in terms of service delivery such as electricity; this is due to the unavailability of main grids reaching these areas. This research will give rural people an opportunity to have lighting materials at home and safety on the roads by use of the phosphor nanoparticles. However, sol-gel optical materials have diverse potential applications in phosphor, laser, and amplifier technologies, but RE-doped sol-gel glasses are known to suffer from three luminescence − quenching mechanisms. **Firstly** there is natural tendency for RE ions to form clusters in the sol-gel preparation, **secondly** the cause of low luminescence efficiency is quenching due to residual hydroxyl (OH^-) group in the glass (SiO_2). The hydroxyl group can associate with an RE ion, providing a non-radiative de-excitation channel for the excited ion that lowers luminescence yield and **thirdly** is due to energy transfer to the matrix.

The clustering of the Ce^{3+} ions can be reduced by adding Al or Mg as a co-dopant, so the co-dopant (e.g. Al^{3+}) disperses the RE clusters and the lower coordination number of Al^{3+} increases the probability that Al-O-RE bonds form. The reduction of OH^- groups is accomplished by annealing the gels at high temperature.

4. Thesis Layout.

This thesis is organized into eight chapters. In Chapter 1 introduction, aim of this study and the statement of the problem of this project are expressed. In Chapter 2, literature survey and background information is presented on the relevant theoretical aspects of present research on synthesis and characterization of Ce^{3+} doped silica (SiO_2) nanophosphors. The typical sol-gel process is discussed as well as highlighting its important advantages of easy, cheap, and scalable process of synthesis of nanoparticles. Attention is also focused on the luminescence properties, quenching mechanisms and the critical relationship between the material properties and the growth conditions of these nanoparticles. The experimental procedures followed during the preparation of Ce^{3+} doped silica (SiO_2) nanophosphors as well as the deposition techniques used are discussed in detail in chapter 3. An important aspect of this study was the accurate characterization of the Ce^{3+} doped silica (SiO_2) nanophosphors. A large number of structural,

morphological and optical characterization techniques were used in this study, and these are thus discussed in this chapter. The experimental results that followed from the detailed study of the influence of growth parameters and the doping or co-doping effects on the ultimate nanophosphor material quality are presented and discussed in Chapter 4, 5, 6 and 7. These results take the form of SEM micrographs, PL, EDS and XRD measurements of composition as well as x-ray diffraction patterns to determine the presence of crystalline phases. Finally, in Chapter 8, the most significant results are summarized and conclusions are drawn, with suggestions for future research.

Reference

[1]. L. Hench, J. West, *Chemistry Review* **90** (1990) 33.

[2]. L.L. Hench, *Ceram. Int*. **17** (1990) 206.

[3]. O. Svelto, *Principles of Lasers*, Plum Press, New York, 1989.

[4]. D.L. Griscom, *J. Ceram. Soc. Jpn*. **99** (1991) 923.

[5]. L. Skuja, M. Hirano, H. Hosono, K. Kajihara, *Phys. Stat. Sol.* (c) **2** (2005) 15.

[6]. P Moulton, M. Bass and M. Stitch, 1985 *Laser Handbook* (Amsterdam: North-Holland), **5 (**1985) 282.

[7]. V. R. Kharabe1, S. J. Dhoble and S. V. Moharil, *J. Phys. D: Appl. Phys.* **41** (2008) 205413.

[8]. A.J. Silversmith, N.T.T. Nguyen, B.W. Sullivan, D.M. Boye, C. Ortiz, K.R. Hoffman, *J. Lumin*. **128** (2008) 931

[9]. H. Scholze, *Glass Ind*. **47** (1966) 546, 622, 670.

[10]. E.N. Boulos, N.J. Kreidl, *J. Can. Ceram. Soc*. **41** (1972) 83.

[11]. M. Tomozawa, C.Y. Erwin, M. Takata, E.B. Watson, *J. Am. Ceram. Soc*. **65** (1982) 182.

[12]. G. Hetherington, K.H. Jack, *Phys. Chem. Glasses* **3** (1962) 129.

[13]. T.A. Michalske, S.T. Freiman, *J. Am. Ceram. Soc*. **66** (1983) 284.

[14]. K. Hirao, M. Tomozawa, *J. Am. Ceram. Soc*. **70** (1987) 377.

[15]. D.M. Boye, A.J. Silversmith, A.J. Silversmith, Thao Nguyen Nguyen, K.R. Hoffman*, J. Non-Cryst. Solids* **353** (2007) 2350.

[16]. M. J. Lochhead, Ph.D. Dissertation, *Luminescence Spectroscopy of Europium (III) – Doped Silica Gels and Silicate Glasses*. Florida State University, (1992).

[17]. R.M. Almeida, H.C. Vasconcelos, M.C. Goncalves, L.F. Santos, *J. Non-Cryst. Solids* **65** (1998) 232.

[18]. M.J. Lochhead, K.L. Bray*, Chem. Mater*. **7** (1995) 572.

[19]. A. Monteil, S. Chaussedent, G. Alombert-Goget, N.Gaumer, J. Obriot, S.J.L. Ribeiro, Y. Messaddeq, A.Chiasera, M. Ferrari, *J. Non-Cryst. Solids* **348** (2004) 44.

Chapter 2: Background

2.1 General Sol-gel process

The sol-gel process is the name given to any processes that involve a solution or sol that undergoes a sol-gel transition. At the transition, the solution becomes rigid, porous mass through destabilization, precipitation, or supersaturation [1-4]. The sol-gel is one of the most suitable ways for producing glasses and glass nanoparticles. As an alternative to melted glass, a sol-gel derived glass is a good medium for studying crystallization and phase separation [6]. The relatively mild reaction conditions, purity, homogeneity and simplicity of the sol-gel method make it an excellent tool for producing substances with precisely tailored properties [5].

The sol-gel process (see Fig. 2.1) involves the simultaneous hydrolysis and condensation reaction of metal alkoxide [7]. In general, the synthesis of sol-gels begins with an organosilicate precursor such as tetramethylorthosilicate (TMOS) or tetraethylorthosilicate (TEOS), since it is easier to undergo the chemical reaction with water. The first stage is a hydrolysis reaction where a proton from the water molecule reacts with the oxygen of the OCH_2CH_3 group in the precursor molecule as shown in Fig. 2.1. The intermediates produced by this stage are ethanol and TEOS derivative with a very unstable Si-OH bond in place of an OCH_2CH_3 group. The hydrolysis reaction is reversible, therefore excess water is needed in order to drive the equilibrium to the right and an acid is added as a catalyst to speed up the reaction. The unstable Si-OH bond immediately undergoes either a water or alcohol condensation reaction as shown in Fig. 2.1. In the water condensation reaction a proton from one of the OH groups reacts with the oxygen of another OH group to produce water and a Si-O-Si bond between two former TEOS molecules. In the alcohol condensation reaction the proton of the OH group reacts with the oxygen of nearby OCH_2CH_3 group to produce ethanol and a Si-O-Si bond [9]. The byproducts are the only difference between these two reactions.

The reaction continues until nearly all the OCH_2CH_3 groups react and a network of silicon-oxygen bonds form throughout the former solution or sol. The reaction is a polycondensation reaction and occurs during the gelation stage of sol-gel formation.
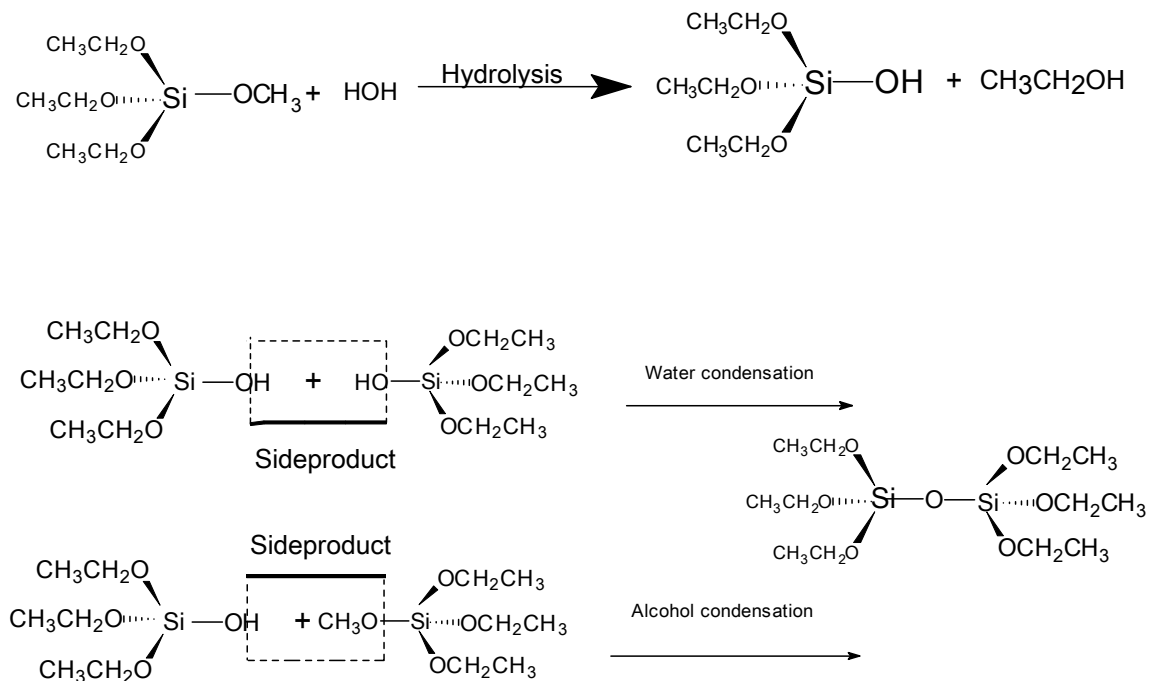
Figure 2.1: Synthesis reaction for the formation of each Si-O-Si.

For polycondensation the water and alcohol by products from the reaction remains in the pores of the network, see Fig. 2.1. This phase establishes a 3D network which invades the whole volume of the container. As the reaction progresses, each side of the tetrahedral formed around silica becomes connected through oxygen to another silicon atom and forms a three dimensional network. This network is best described as possessing an order as described for an amorphous glass [6]. Thus a gel is obtained and for these two syntheses the liquid used as a solvent to perform the different chemical reaction remains within the pores of the solid network. Once the sol reactions are complete, temperature dependent gelation, aging and drying processes take over. To increase the density of the material and remove the byproducts, we must follow the sol-gel synthesis process by a high annealing schedule.

2.1.1 Gelation

The gelation point of any system, including sol-gel silica, is easy to observe qualitatively (by turning the capped or closed Erlenmeyer flask upside-down), but extremely difficult to measure analytically. As the solution particles grow and collide, condensation occurs and macroparticles form, this is where the sol becomes a gel. Gelation is determined by checking whether the solution no longer runs free which means when it has a high viscosity [10]. Gelation of the solution occurs within approximately one week (or can take 24hrs with the help of a catalyst). An acid or base catalyst such as nitric acid or ammonium hydroxide increases the rate of polycondensation and gelation. Extra protons provided by the acid interact with the unreacted OCH_2CH_3 groups, vastly increasing the number of molecules undergoing reaction at any particular time. West and Hench [11] noted that base catalyzed solutions gel faster than acid catalyzed solutions. The gelled samples occupy the same volume as the ungeeled samples and the transition is irreversible, at this point samples crumbles easily when removed from the Erlenmeyer flask.

2.1.2 Aging

After the gel has formed and is completely aged at room temperature to let all available bonds connect, it sits in a solution of alcohol solvent and water for a period of time (hours to days). It occurs slowly allows time for the sol-gel to undergo further condensation forming more Si-O-Si linkages and its density increases causing the siloxanes (Si-O-Si) network to become more rigid. Samples shrink and its density increases as the solvent leave the pores of the sol-gel decreasing the number of the pores [2, 12 and 13]. The shrinkage rate increases with concentration of silica in the sol and temperature.

2.1.3 Drying

The gels (Xerogel) were then dried at temperature close to room temperature and under atmospheric pressure [14], retaining their original shape, but often crack. No further weight loss occurs over time during the drying process. Samples do not show effects from ambient conditions. The xerogel are hard and also porous. The transparent nature of these glasses makes them suitable for optical applications and allows the xerogels to be studied by standard spectroscopic techniques, like absorption, Raman and PL spectroscopy. No matter how drying is accomplished, the gel is not truly dry until it is subjected to some stabilizing heat treatment.

2.1.4 Densification

Annealing the porous xerogel at high temperature causes densification to occur. In the gelation process, dry gels formed through hydrolysis always entrap some water, alcohol, and other organic groups reducing the density. Annealing sol-gel glasses reduce or eliminate residual hydroxyl groups therefore increases the density of the samples. It also activates the lattice relaxation of the glass network, and encourages ion migration in the glass host. During the annealing process, the rare earth ions are thermally activated into migration forming clusters.
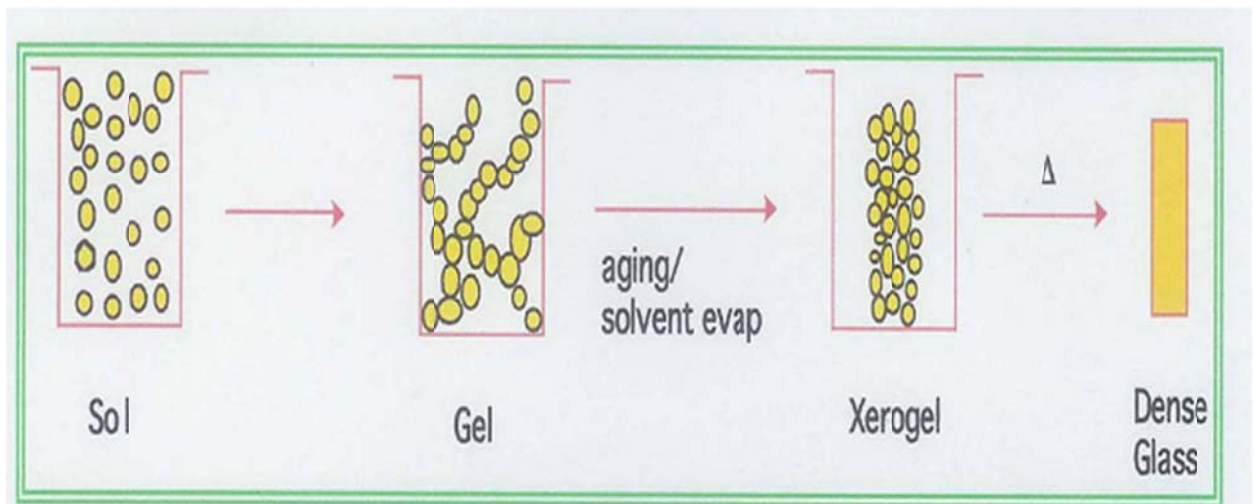
FIGURE 2.2: Depiction of the Sol-Gel Process [20].

The driving force behind annealing effect is reduction in surface area of the materials attributed to the removal of water and organics [15-17]. However, certain samples material properties do not exhibit a linear relationship with surface area [18,19].

2.2 The properties of silica (SiO_2) glasses.

The chemical compound silica or silicon dioxide is an oxide of silicon with a chemical formula of SiO_2. It has three dimensional network structures in which each silicon atom is bonded to four oxygen atoms, which are tetrahedrally arranged. Each oxygen atom is being shared by two silicon atoms. Since Si-O bonds are very strong, therefore, silica is relatively inert and has a very high melting point. Pure silica is colorless but sand is brownish or yellowish due to the presence of impurities of ferric oxide. Silica, as sand, is a principal ingredient of glass, one of the most inexpensive of materials with excellent mechanical, optical, thermal, and electrical insulator properties. Silica is a group IV metal oxide, with molar mass of 60.0843 g/mol, its electron configuration is $1s^2\, 2s^2\, p^6\, 3s^2\, p^2$, oxidation states of 4, valence electrons of 4 and energy gap of around 9 eV at 300K. It is one of the most abundant oxide materials in the earth's crust; silica is insoluble in water and resists the action of all acids except hydrofluoric acid which readily acts on it.

The glass has very high viscosity, and this property allows the glass to be formed, cooled and annealed without crystallizing. Silica, its physical structure may exist in either crystalline or amorphous forms (non-crystalline). Fig. 2.3 shows the two-dimensional representation of the difference between crystalline and non-crystalline silicon structure [21]. Crystalline silica has its oxygen and silicon atoms arranged in a three dimensional repeating pattern. Non- Crystalline forms of silica have a random pattern. Consequently, while in a crystalline form every dopant ion will be surrounded by essentially the same electronic environment, in an amorphous form every dopant will be surrounded by a slightly different electronic environment.

The electronic environment of an ion affects the stability of excited species, thus affecting the position of energy levels slightly and the transition rate from one energy level to another slightly.
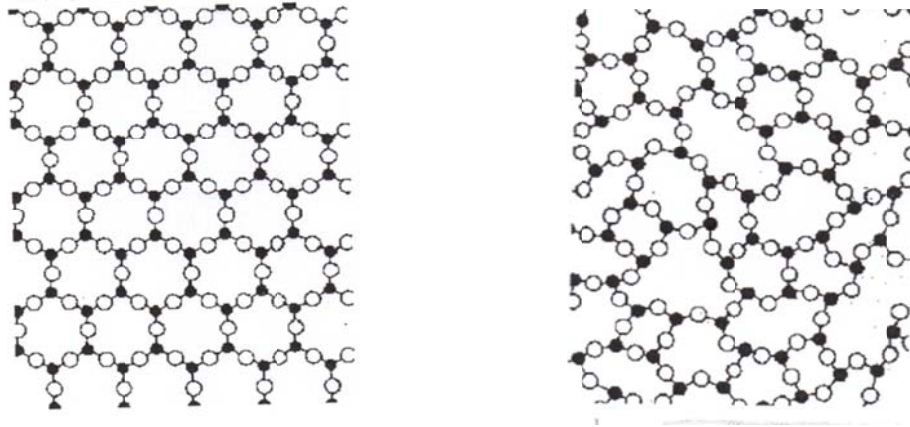
Figure 2.3: Representations of molecular arrangements in a crystalline and non-crystalline silicon glass. In crystalline, there is high degree of long range and short range in silicon glass, non-crystalline, the order is only in the range of a few molecules [21].

2.3 Doping Silica

The common method of improving the conductivity of a semiconductor is to add impurity atoms to silica which in turn creates more free charge carriers. This process of adding impurity atoms to a semiconductor is called Doping. The concentration of either free electrons or the free holes can be raised by the electrically active impurities in a semiconductor by donating electrons to the conduction band or by accepting them from the valence band [22]. Doping causes the semiconductor material to become impure or extrinsic. There are two different types of doping atoms, namely donors (p-type) and acceptors (n-type)

Consider, for instance, a specimen of Si (silicon) which has been doped by As (arsenic). By introducing a donor atom impurity substance with five valence electrons into the lattice structure of the intrinsic (pure) silicon, four of its valence electrons will immediately form bonds with the four silicon atoms immediately closest to it leaving one electron un-bonded. Since these fifth electron cannot enter the bond, which is now saturated and so it exists at a higher energy level than its surrounding bonded electrons (in their valence band), and hence this electron detaches from the impurity and is free to migrate through the crystal as a conduction band electron (e.g. the electron enters the C.B). Once it loses its fifth electron the donor atom becomes a positively charged ion (As^+). Therefore only the free un-bonded electron contributes to conduction and not

13

the remaining positive ion. As is a donor, having a valence greater than the host. These new high energy donor electrons contribute to a general raising of the average energy level of all of the electrons in the body, which in turn causes the donor level of an n-doped silicon to be slightly raised below the conduction band as shown in Fig. 2.4(a). Because the level is so close to the C.B, almost all the donors are ionized at room temperature, their electrons having been excited into the C.B [23]. Note that the electrons have been created without the generation of holes as compared to an intrinsic semiconductor. The concentration of electrons for doped samples [23] is determined using equation 2.1:

$$n = 2(\frac{k_B T}{2\pi\hbar^2})^{\frac{3}{2}} \ (m_e m_h)^{\frac{3}{4}} \ e^{\frac{-E_g}{2k_B T}} \qquad\qquad 2.1$$

where k_B is Boltzmann constant, T is the temperature, m_e is mass of electron and m_h is mass of hole. When a dopant (impurity) atom is introduced in a crystal, the perfect periodicity of the crystal is destroyed; at a particular atomic site background potential of the host lattice is replaced by the potential of the impurity.
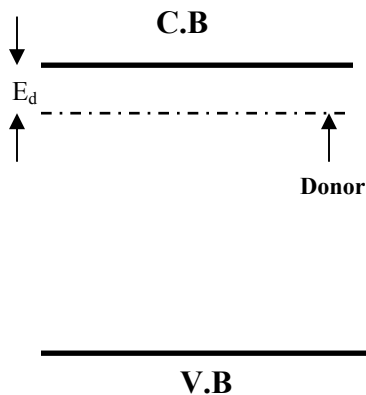
Figure 2.4 (a): Shows the donor level in a semiconductor

Similarly an impurity substance with three valence electrons such as boron (B), aluminium (Al) and gallium (Ga) could be added to the intrinsic semiconductor material. An appropriate choice

14

of impurity may produce holes instead of electrons. Suppose that the Si crystal is doped with B impurity atom. As each of these three electrons form bonds with their neighboring semiconductor atoms, there is a fourth bond which is not able to be formed. This leaves one bond unable to be formed. These impurity atoms are known as acceptor atoms as they each create a hole in the structure. This hole possesses an effective "positive" charge in the valence band of the acceptor atom and it can participate in the hole drift during conduction. The acceptor is negatively charged, by virtue of the additional electron it has entrapped. Since the acceptor holes, introduced into the sample by doping, have slightly higher energy levels than the silicon's valence band, any electron which falls into one of these holes must loose energy. The holes removing any potential "free" electrons which may have been gathering enough energy to break across the forbidden energy gap to become free. This has the overall effect of lowering the acceptor level of a p-type doped substance very slightly, as shown in Fig. 2.4(b).

C.B

Acceptor

E_a

V.B
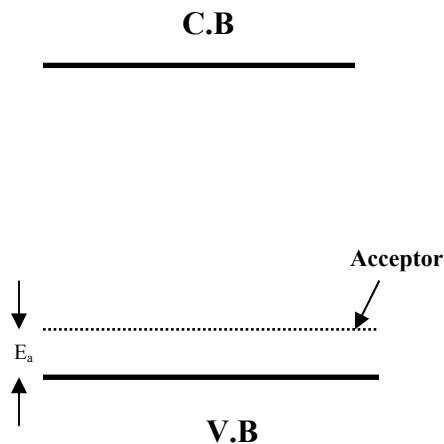
Figure 2.4 (b): Shows the acceptor level in a semiconductor

Because the acceptor level lies in the energy gap, slightly above the edge of the V.B, almost all the acceptors are ionized at room temperature, the electrons excited from the top of the V.B to fill this hole, then the holes falls to the top of the V.B becoming a free carrier [23]. Therefore Boron (B) is an acceptor, having a valence less than the host (Si). The concentration of holes can be calculated by using equation 2.2 which is valid for pure and doped sample [22].

$$p = 2\left(\frac{m_h k_B T}{2\pi\hbar^2}\right)^{\frac{3}{2}} e^{\frac{-EF}{k_B T}} \qquad\qquad 2.2$$

An acceptor is neutral at very low temperature; it becomes ionized when an electron obtains sufficient energy to be lifted from the valence band to the so-called acceptor level [22]. A semiconductor may of course contain many impurities and defects that cannot be ionized as easily and thus do not affect the electrical conductivity.

In this project silica (SiO_2) is doped with Cerium (iii) nitrate hexahydrate (Si^{4+} doped with Ce^{3+} ions). Since the host has 4 valence electron while dopant has 3 valence electron, the Ce^{3+} is an acceptor. Therefore three of its valence electrons will immediately form bonds with the three silica atoms immediately closest to it leaving one electron un-bond, creating a hole (or vacancy).

2.4 Luminescence
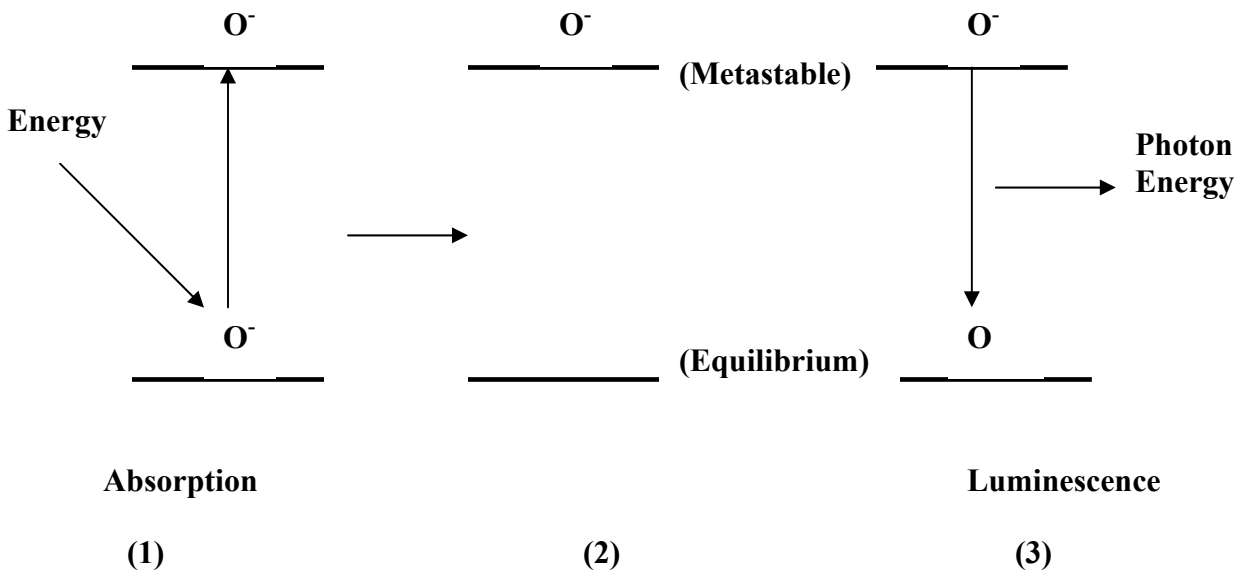
Figure 2.5: Shows the process luminescence.

Luminescence may be defined as the process in which electron that have been excited to higher energy states decay back into lower states at equilibrium thereby emitting radiation in the form

16

of a photon. Clearly, luminescence is the opposite of absorption. In the absorption process the energy of the photon must be at least equal to E_g (the band gap energy):

$$hv \geq E_g \qquad\qquad 2.3$$

$$v \geq E_g \qquad\qquad 2.4$$

where h is Planck's constant. Again in the absorption, the total energy and total momentum are conserved, where

$$E_F = E_i + hv \qquad\qquad 2.5$$

$$k_F = k_i + q \qquad\qquad 2.6$$

where E_i is the initial electron energy in the valence band, E_F is the final electron energy in conduction band and q is the wave vector of the photon. In the conduction band E_i is zero and in the visible spectrum $q \rightarrow 0$, therefore

$$k_F = k_i \qquad\qquad 2.7$$

This result ($k_F = k_i$) is known as the selection rule and means that only vertical transitions in K-space are allowed between valence band and conduction band [22]. It is important to realize that at step (1) in Fig. 2.5 above, the incident energy need not be only from a photon. It may well be temperature effect, a photon and electrical stimulus. For example, in a p-n junction an electric current result in luminescence that is subsequently classified as electroluminescence. In the same token, luminescence due to a photonic absorption is referred to as photoluminescence.

The processes involved in luminescence are the exact opposite of the electron excitation. The fundamental decay transition occurs between the C.B and V.B. However, other transitions will occur also between these bands and the various impurity levels (both acceptors and donors).

2.5 Rare Earth metal ions

The lanthanide metals or Rare Earth metals are all relatively electropositive metals that strongly, although not exclusively, favor the tripositive oxidation state. During the last few decades, the application of RE doped sol-gel glasses have grown significantly in scope coming to include sensors, waveguides and solid state laser materials. They all can enter a +3 oxidation state in which both s electrons are lost and either d or f electron as well, but some of the lanthanide rare earths also show +2 or +4 oxidation state. The lanthanides metals (La-Gd) are the lighter metals. In their magnetic and spectroscopic properties the lanthanides show important differences from the d-block elements, this happens because the 4f electrons are pretty well (although not totally) shielded from the external fields by overlying $5s^2$ and $5p^6$ shells. The states arising from the various $4f^n$ configurations therefore tend to remain nearly invariant for a given ion [24]. The lanthanides ions have ground states with a single well-defined value of total angular momentum J, with the next lowest J state at energies many times kT above, hence virtually unpopulated.

Even though the 4f orbital are well shielded, however, they become more attractive as Z increases [25]. Ce (Z=58) the 4f orbitals become more stable than the 5d orbitals, since the 5d state is easily affected by the ligands. All the lanthanides neutral atoms have the configuration $6S^2 4F^n$ except where the minimization of electron-electron repulsion associated with a set of orbital completely filled by parallel spins makes the F^n configuration preferable (e.g. Gadolinium). The ions, lose the 6s electrons first, but in general lanthanides do not have a stable +2 oxidation state in compound, instead, they all show a stable +3 oxidation state, which is the net charge that strikes the best balance between the ionization energy or solvation energy stabilization of the ion. For the lanthanides, whose 4f electrons are entirely buried in the inner core, the increasing nuclear charge leads to a smooth contraction from Z= 57 to 71. This trend is known as the lanthanides contraction. It has some chemical effects of interests. The lanthanides contraction lead to essentially identical radii (e.g. Europium (Eu) is 1.09Å, Terbium (Tb) is 1.08Å, Cerium (Ce) is 1.15Å and Praseodymium (Pr) is 1.15Å [25].

2.5.1 Energy levels of Ce^{3+}.

The electron configuration of cerium atom is [Xe] $4f^1 5d^1 6s^2$. In liquids and solids Ce can occur in a trivalent or tetravalent state, by losing its two 6s electron and one or both of its 4f electrons. Trivalent Cerium ion is the most important activator in various fluoride and oxide materials for its allowed optical transitions of $4F^n$-$4F^{n-1}5d$ [5, 6]. The triply charged cerium ions with one 4f electron are optically active; the resulting electronic energy level in a solid structure is shown in Fig. 2.6. The 4f electrons, though they are not the outermost electrons, can be excited to 5d electron shells when excited by the photons, electrons and other energetic particles which can yield the emission when the excited $4f^{n-1}5d$ electrons transfer back to $4f^n$ electron shells.

When cerium enters a liquid or a solid, the expansion of the electron shells that decreases the electrostatic interaction between the electrons results in a reduction of the energy of the excited states from that of the free ion values. This nephelauxetic shift increases with the degree of covalency of the cerium-anion band. The spin orbit interaction splits the ^2F ground state into two J states separated by ~ 2000 cm^{-1}. Because the $4f^n$ electron is shielded from the ligand field by the closed 5s and 5p electron shells, the overall splitting of the ^2F_j states is small. When the 4f electron is excited to the outer 5d state, however, it experiences the full effect of the ligands. In general, the electronic d-state splits into several energy levels whose degeneracy in the crystalline field depends on the site symmetry. The overall splitting of the 5d manifold is typically of the order of 5000-10000 cm^{-1}.

In the case of Ce^{3+}, the transitions from the 4f ground state to the lowest 5d energy level may occur anywhere from the UV to the visible for silica host, depending on the symmetry and the strength of the ligand field [26]. Electric-dipole transitions between the 4f ground state and the 5d excited state of Ce^{3+} ion are parity allowed and have a large oscillator strength. Trivalent cerium ions may be excited to a 5d state by ionizing radiation either directly by intraionic processes within Ce^{3+} or indirectly. In the first case the excited Ce^{3+} will emit a 5d~5f photon (*hv*) via [26]:

$$Ce^{3+} \rightarrow Ce^{3+} + hv \qquad\qquad 2.8$$

Ce^{3+} may also lose its 4f electron to form Ce^{4+} either by direct ionization or by capturing a hole created in the valence states of the anions, for example by atomic-like 2p~3s transitions of oxygen or fluorine. The process

$$Ce^{3+} + h\nu \rightarrow Ce^{4+} \qquad\qquad 2.9$$

may be prompt if the hole is nearby or delayed if the hole must diffuse to the vicinity of cerium site. The resulting Ce^{4+} may then capture an electron,

$$Ce^{4+} + e \rightarrow Ce^{3+} \qquad\qquad 2.10$$

and subsequently decay by the process in Equation 2.10 [26]. Usually the emission and absorption spectra of the Ce^{3+} ion consists of broad bands due to transitions between the ground state of the $4f^1$ configuration (a doublet $^2F_{5/2}$ and $^2F_{7/2}$) and the lower excited states (the crystal field components of the 5d configuration). Three electronic transitions are possible (see Fig. 2.7). The lowest energy transition, $^2F_{5/2} \rightarrow {}^2F_{7/2}$ (2000 cm^{-1}), is a Laporte forbidden $\mu \rightarrow \mu$ transition and corresponds to an $f^n \rightarrow f^n$ transition [27]. The other two transitions, $^2F_{5/2} \rightarrow {}^2D_{3/2.5/2}$, are laporte allowed nf$\rightarrow$n-1fd transitions [28].
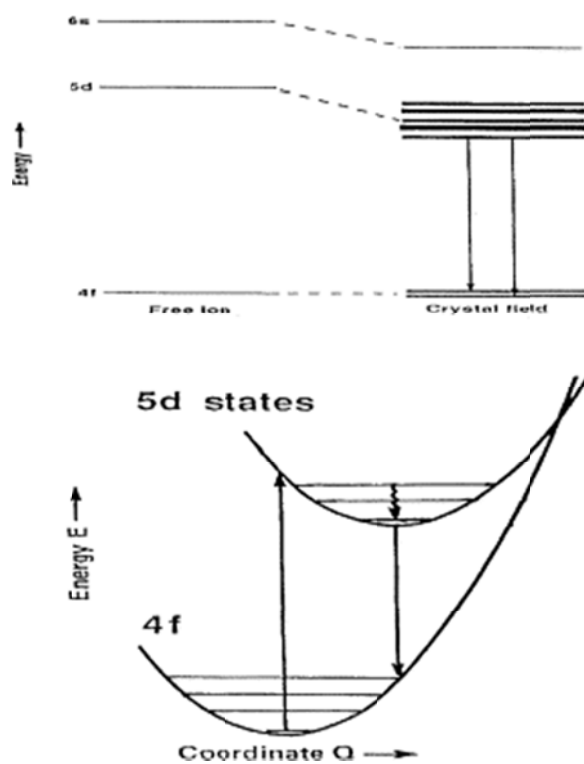
Figure 2.6: Electronic energy levels of Ce^{3+} (upper) and configuration diagram of Ce^{3+} (lower). This partial energy level diagram shows the transitions that produce emission in the visible and UV range of spectrum.

The f→f transition is of low energy and is expected to appear in the visible region (λ_{max}~440 nm), whereas the f→d transitions are observed in the ultra violet region (λ~190-300).

Jorgensen [29] suggested that Ce^{3+} ions might exist with a lower coordination number, producing the weak band. The intensity of the weak band is strongly dependent on the temperature, the presence of the other ion, and even the substitution of heavy water as a solvent [27]. The 4F-5d transition is an allowed electric dipole transition and therefore high emissions can be achieved. The wavelengths of absorption and emissions are more strongly affected by the host lattice because of a strong interaction of the 5d-electron with the neighboring anion ligands in the compounds, most of the Ce^{3+}-activated phosphors show a blue or nearly ultraviolet emission [30-35] and others show the blue and UV emission [32-35]. These two emission bands, at 385 nm and 436 nm are the characteristic of Ce^{3+} transitions from the 5d to $^2F_{7/2}$ and $^2F_{5/2}$ states, respectively.
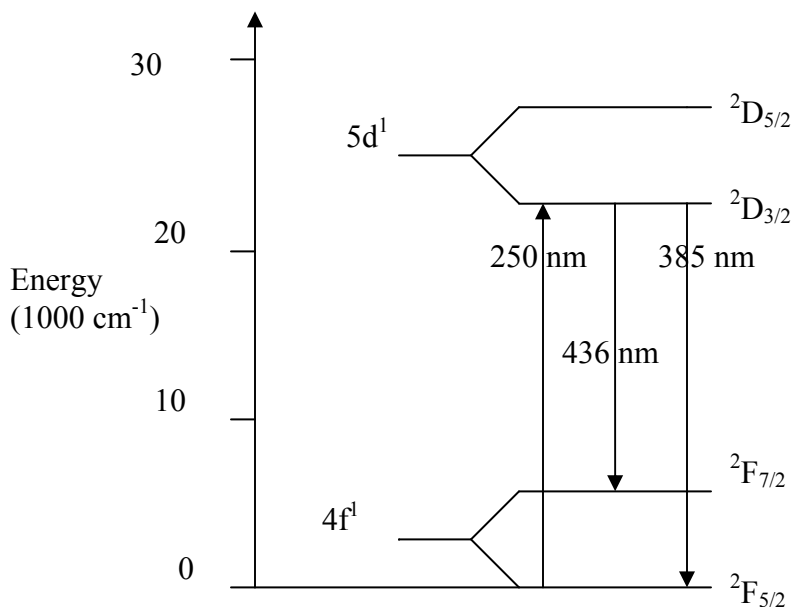
Figure 2.7 (a): Shows Ce^{3+} expected emission spectrum [36].

2.6 Defects in silica

Defects simply mean an imperfection of material. Silica glass has been widely used in many fields due to its unique properties. It has been well recognized that impurity in silica glasses, and thermal history, affect the properties of silica glasses. Chemical impurities in silica glasses have been greatly reduced by doping, co-doping and annealing. However, even in the absence of such impurities, structural point defects such as E' centers and non-bridging oxygen hole centers (NBOHCs) can exist. The variety of structural defects [37] can be introduced in silica glass during its fabrication process [38] or post-treatment [39] and play important role by affecting various properties of silica glass, such as optical absorption, luminescence bands [40], refractive index [41] and density of silica glasses [42]. Compared with the traditional silica material, nano-sized silica has a huge surface area. Low coordinated elements (SiO_2) are easy to form many kinds of the surface, which may make nano-sized silica having much different optical property from traditional silica materials. The effect of defects formation on the phosphor samples can influence the PL intensity and thus lead to the quenching effect. Many Researchers have reported several kinds of optical active centers in nature, such as:

1) **Neutral Oxygen Vacancy**

The simplest defects is a vacancy which is a missing atom (Oxygen), and often known as the Schottky defects. The oxygen deficiency is obtained by adding any missing bond of a silicon atom and any additional bond of an oxygen atom as one-half oxygen vacancy each. Oxygen vacancies are also introduced during the fabrication process. The removal of an oxygen atom is accompanied by a ≡Si-Si≡ [43] bond formation, where "≡" denotes bonding with three separate atoms. Neutral oxygen vacancy defects, which are the most characteristic lattice imperfections of crystalline and glassy quartz, cause a large number of radiatively stimulated phenomena.

22

(2) Non-bridge oxygen hole center (NBOHC)

One of the most studied luminescent defects in silica is the NBOHC or oxygen dangling bond ($\equiv$Si-O$^.$). The non-bridging oxygen hole center is obtained from the precursor after hole capture [44]. It occurs predominantly in synthetic silica with excess oxygen. The formation of a non-bridging oxygen hole center (NBOHC) defect [45,46] is;

$$\equiv\text{Si-O-Si}\equiv \rightarrow \equiv\text{Si-O}^. + {}^.\text{Si}\equiv \qquad\qquad 2.11$$

Where "$\equiv$" and "$^.$" Denotes or symbolize the bond with three oxygen and unpaired electron respectively, lastly we have $\equiv$Si-O$^.$, which is a NBOHC (oxygen dangling bond). The majority of the dangling bond centers are unpuckered. From Skuja et al most NBOHC's disappear within few seconds after the photolysis pulse [47]. The remaining small fraction of room temperature-stable NBOHC's is usually assigned to an intrinsic process [48].

(3) Peroxy radicals

The peroxy radical is fundamental oxygen associated paramagnetic defects in SiO_2 glass. Peroxy-center is associated with oxygen, formed by the action of an O_2^- (Super oxide ion) ion on a silicon atom to lead to Si–O–O$^.$.This structural identification of peroxy radical has stimulated studies on reactions involving peroxy radicals. The most studied channel is the formation of peroxy radical from the E' center (a silicon dangling bond,$\equiv$Si$^.$) in SiO_2 glass stuffed with the interstitial O_2 [49],

$$\equiv\text{Si}^. + O_2 \rightarrow \equiv\text{Si-O-O}^. \qquad\qquad 2.12$$

4) E' center (a silicon dangling bond)

E' center is the most studied defect in silica (SiO_2) and is an unpaired electron in a tetrahedral sp^3 hybrid orbital of silicon atom bonded with three separate oxygen atoms [50]. In the E'-center, an electron is trapped in an oxygen vacancy to give $\equiv$Si$^.$ [51]. E' center in amorphous silica can be

formed at favorable precursor sites and can only be formed in the amorphous structure. The E'-center is assigned to a silicon dangling bond ($\equiv$Si$^{.}$), with the Si atom bonded by two bridging oxygen and an OH group (E'(OH)').

2.7. Clustering of Ce^{3+} ions.

Cerium, like other rare-earths, has a low solubility in the glass matrix; therefore, Ce^{3+} ions tend to migrate to the sol-gel pores. In particular, because clusters are formed around non-bridging oxygen, the clusters are formed at the pore surface. Because Ce^{3+} has a high coordination number (meaning it can have a large number of ligands), Ce^{3+} can form partial bonds with several of the lone pair of electrons on the network oxygen, forming a layer of Ce^{3+} at the pore glass interface. However, by increasing the cerium concentration increases the probability of clustering.
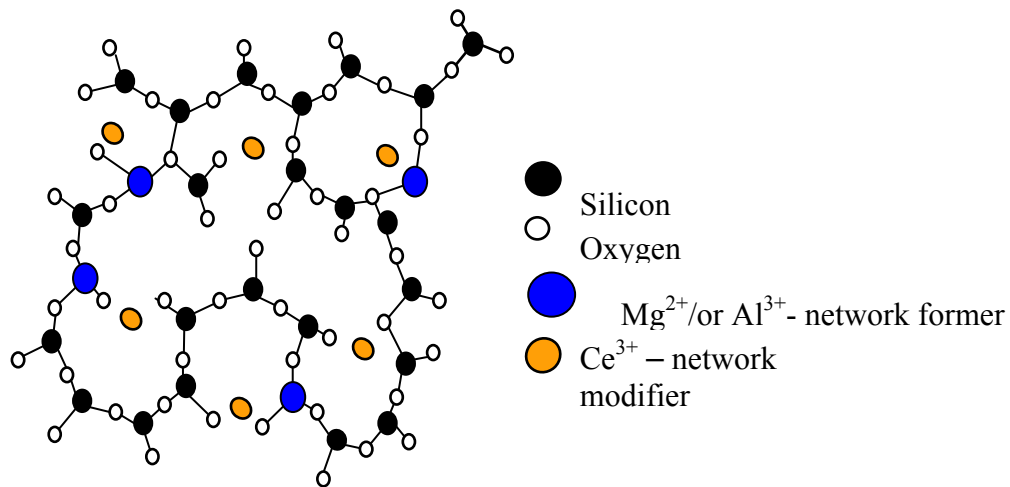
Figure 2.9: Sol gel glass structure shows that dopant (Ce^{3+}) acts as network Modifier and the Co-dopants (Mg^{2+} and Al^{3+}) acts as a network former. [52]

By looking at Fig. 2.9, the Ce^{3+} ions dope crystals substitutionally, in so-gel glass, Ce^{3+} ions prefer not to join the network. Instead, they become network modifiers, by coordinating with

multiple oxygen atoms. The cerium ions choose non-bridging oxygen atoms preferentially, as their electron density is considerably higher than that of other nodes in the network.

2.8 Introduction for types of the luminescence quenching mechanisms:

In this part, we will discuss interactions that reduce luminescence in materials. There are many mechanisms that cause losses in luminescence, firstly is Energy transfer to matrix vibrations, second Concentration Quenching and thirdly is The Residual Hydroxyl ($^-$OH) groups. Luminescence occurs when the excited ions release energy in the form of photon. The excited ion may be coupled with its environment, which may result in fast, non-radiative energy transfers. Energy dissipation reduces the efficiency of the luminescence processes. In order for Ce-doped sol-gel glasses to fulfill their application potential, we must maximize the luminescence yield. To this end, we must reduce these energy transfer effects.

2.8.1 Energy transfer to matrix

The first quenching mechanism is the energy loss due to matrix vibrations of the host material, in our case is silica (SiO_2) glass, by exciting silica matrix with energy there is going to be energy transfer between Si^{2+} ions and the emission will be Non-Radiative Recombination. Matrix vibrations are present in any host material, and are difficult if not impossible to control. All of our samples are made with a silica host material, so this quenching effect is expected to be uniform across our samples. The maximum energy corresponding to lattice vibrations depends on the host material [53]. In oxide glass, this is about 800 cm^{-1} [54].

2.8.2 Concentration Quenching

Concentration quenching is the process in which the excitation energy reaches a site causing nonradiatively transitions (a killer or quenching site), lowering the luminescence efficiency of that composition. This type of quenching usually occurs at higher concentrations of the dopant, because then the average distance of the Ce ions is so small that there is energy migration among REs elements. At low concentrations of Ce^{3+}, the distribution of Ce^{3+} in SiO_2 is not uniformly

distributed and the distance between Ce^{3+} ions are very large. Maximum luminescence intensity is observed when the Ce^{3+} ions are distributed uniformly in the host (SiO_2) and bound to non-network oxygen atoms in Si-O-Ce, however, luminescence decreased with increasing in the Ce^{3+} content, because the distance between the Ce^{3+}-O-Ce^{3+} ion becomes short or clustered.

The source or cause of this quenching (decrease in luminescence intensity) process is due to clustering of Rare-earth ions (RE-O-RE) ions in sol-gel glass pore at high doping levels. The clustering of Rare-earth in so-gel decreases the luminescence intensity of certain susceptible transitions, in Ce^{3+} ions, it quenches the intensity of the 5d-4f transitions. At higher RE concentrations, most ions reside in cluster, the luminescence is observed from minority of isolated ions and the distribution of Ce^{3+} ions is not uniformly, there are regions of high and low distributions in the host. Tightly clustered RE ions do not contribute to the luminescence intensity peak because of strong cross-relaxation. This clusters of the Rare-earth ions on pore surface firstly, may be due to the low solubility [55,56] of RE_s in SiO_2. The low solubility may be due to the Rare-earth ions which are bigger in atomic or ionic radius than the host matrix (e.g. atomic radius of Ce^{3+} is 2.7Å and for silica (Si^{2+}) is 1.46Å) and secondly, the need to coordinate with limited numbers of non-bridging oxygen [57].
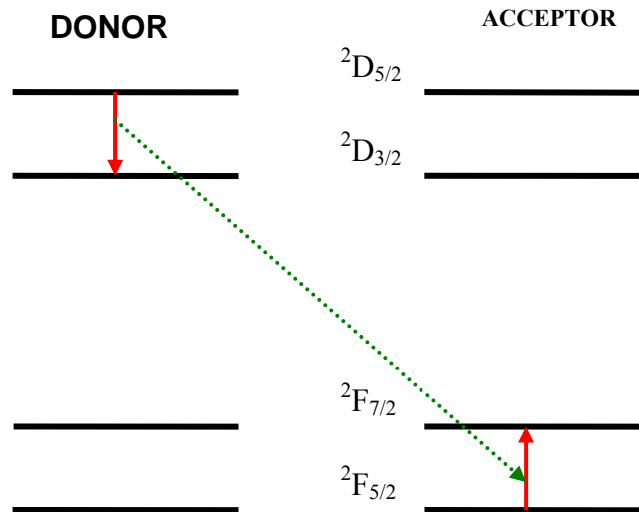
Figure 2.10: The cross-relaxation between two Rare-earth ions

Cross-relaxation (CR) is an energy transfer process between two ions. The CR rate depends strongly on the average distance between RE ions. The quenching of the Rare-earth causes the non-radiative decay. Fig. 2.10 shows the process of cross-relaxation (CR). In our work, we only focus on CR between Ce ions. The specific interaction between clustered Ce^{3+} ions that depopulate the ^2D_J excited state is suggested to be CR. The process involves an electron excited to the $^2D_{5/2}$ energy level drops to the lower $^2D_{3/2}$ energy level. The energy from this transition is transferred non-radiatively to the second ion. The close match in energy between the $^2D_{5/2} \rightarrow {}^2D_{3/2}$ and $^2F_{7/2} \rightarrow {}^2F_{5/2}$ makes this process highly effective at quenching radiative emissions in samples with doping levels above optimum Ce^{3+} ions. Because no photon is emitted in this energy process, we call it a non-radiative relaxation. The energy transfer mechanism involves multipolar interactions, the cross-relaxation rates depend strongly on separation distance between Ce^{3+} ions. In rare-earth, it is well known that dipole-dipole interactions dominate the process [58].

2.8.3 Non-radiative Vibrational Excitation of Residual hydroxyl ($^-$OH) group.

The third important quenching mechanism is as a result of residual hydroxyl group ($^-$OH) remaining in the sol-gel material, even after annealing at high temperature (e.g. 600 °C). When located near RE_s in the matrix (RE-OH), $^-$OH ions provide non-radiative decay, as shown in Fig. 2.11. The presence of water in the starting solution (sol), and water generated during condensation reactions in the sol-gel process, causes an abundance of OH in the material.

Secondly, water molecules in the atmosphere diffuse into the samples after annealed process such as during crushing the samples. This process is called Rehydration. Rehydration happens because glasses made using the so-gel method are typically less dense and more porous than melt glasses. Water and many other solvents have vibration energies from 2000 cm^{-1} to 3000 cm^{-1} [59]. A glass with $^-$OH group (HO-Si-OH), the $^-$OH group absorbs excitation energy causing bond vibrations; hence it will not release or emit photons leading to the luminescence quenching.
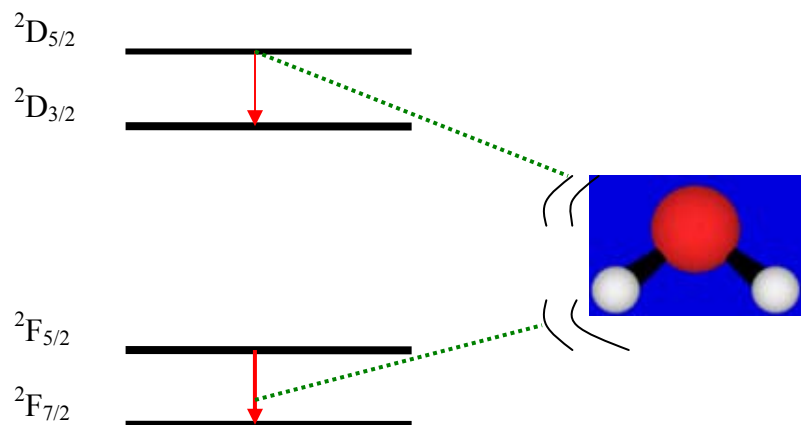
Figure 2.11: Vibrational excitation of water.

2.9 Magnesium and aluminium co-doping

Magnesium appears in Group 2 in Periodic Table and is known as the alkaline earth metal. It is a silver-white metal of low density mainly used in making light alloys e.g. magnalium and electron [60]. The alkaline earth metals have a fixed oxidation state of +2 (e.g. Mg^{2+}), and their compounds are mainly stable ionic solids, which are colorless unless a colored anion is present. The metals are electropositive, readily forming Mg^{2+} ions. Magnesium nitrate hexahydrate is very soluble in both water and ethanol and its melting point is 89 °C (362K). Magnesium nitrate hexahydrate is a white crystal and decomposes at 330 °C. Because of its smaller size Mg^{2+} is the hardest of the ions. The electron configuration of Mg is $1s^2 2s^2 2p^6 3s^2$ and Mg^{2+} has $1s^2 2s^2 2p^6$. Aluminium nitrate is a salt of aluminium and nitric acid, existing generally as a crystalline hydrate. Its melting point is 73 °C, decompose at 135 °C and exhibit an oxidation state of +3. Aluminium is used in making electric cables, pots and pans. It has electron configuration of $1s^2 2s^2 2p^6 3s^2 3p^1$ and Al^{3+} has $1s^2 2s^2 2p^6$. Aluminium is a metal which does form trivalent ions, but many of its compounds are predominately covalent and form no compounds with metal, only one simple hydride, its oxide and hydroxide are amphoteric, it dissolves in acids to give aluminium

salts (Al^{3+}) [60]. Anhydrous Al^{3+} ions occur in anhydrous AlF_3 and the hydrated ion, (Al $(H_2O)_6)^{3+}$, is found in many hydrates e.g. $Al(NO_3)_3 \cdot 9H_2O$, and in aqueous solution [60]. $Al(NO_3)_3 \cdot 9H_2O$ is a white refractory material that is almost insoluble in water but soluble in acids and alkalis because it is amphoteric.

Many Researchers shows that the Al is the most effective rare-earth fluorescence enhancing co-dopant [58] than other co-dopants such as Ti [61] and P [62], but the exact mechanism for fluorescence enhancement is not yet understood. Many Researchers [58] suggests that rare-earth ions form RE-O-RE bond with one another, especially at higher concentration doping. Since both Aluminium and rare-earth ions are trivalent rare-earth would likely to form RE-O-Al bonds as well. Aluminium substitutes itself into the SiO_2 matrix during synthesis and could thereby prevent clusters of rare-earth (e.g. Ce^{3+}) ions from forming [63]. Aluminium may act as a network former, as shown in Fig. 2.9. Laegsgaard et al. showed that Al ions substitute for Si ions, forming triangles in which a RE ion is situated [52]. Although the study showed that only three Al ions are required to dissolve one RE ion, the Al/RE ratio had to be 10:1 to ensure complete cluster dissolution, which means Al creates Al rich regions where RE ions are located [63]. Even our experimental data indicate that Al disperses Ce^{3+} ions when the Al:Ce ratio is at least 10:1 and at higher percentages luminescence quenching effect (above 5% Al) is observed. The best sample is SiO_2:0.5%Ce^{3+}:5%Al^{3+}, which reduces the rate of non-radiative decay and improves or increases the quantum yield. Aluminium increases the luminescence in UV region of 350 nm ($^2D_{3/2} \rightarrow ^2F_{5/2}$) while $^2D_{3/2} \rightarrow ^2F_{7/2}$ luminescence decays for Al^{3+} samples containing.

In contrast to Al co-doped samples, the luminescence intensity is greatly improved when Mg co-dopant is introduced into the Ce systems. Luminescence in samples containing more than 0.5% of dopants is strongly quenched. Thus, the enhancement of luminescence intensity when Mg is added to the samples has been ascribed to Mg^{2+} ions dispersing Ce^{3+} ions clusters, reducing the inter-ion distance between Ce^{3+} ions and luminescence quenching. Also the Mg^{2+} ions network former, see Fig. 2.9. Even Our experimental data indicate that Mg dispersing Ce^{3+} ions when the Mg:Ce ratio is at least 20:1. The luminescent was observed with the SiO_2:0.5%Ce^{3+}:10%Mg^{2+}, so above the 10%Mg^{2+} ions we don't know whether luminescence intensity keep on increasing or quenching, however in future we have to determine or check. The Mg^{2+} improves the

luminescence in blue region of 436 nm ($^2D_{3/2} \rightarrow {}^2F_{7/2}$), while the luminescence of $^2D_{3/2} \rightarrow {}^2F_{5/2}$ disappears.

In agreements with finding of other researchers, Al co-doping relatively improves the luminescence intensity as compared to Mg. The reason being that the electronic configuration, of Al^{2+} is $1s^2\, 2s^2\, 2p^6\, 3s^2\, 3p^1$, thus behaving more like a metal since its valence band is only partially filled but in its Al^{3+} oxidation state, it's completely full ($1s^2\, 2s^2\, 2p^6$) exhibiting very low conductivity. Mg has the electron configuration of $1s^2\, 2s^2\, 2p^6\, 3s^2$, so its band is completely filled up, resulting in an insulator like property, however, in reality Mg is a metal, although a poor one with low conductivity. A very similar property is displayed by Mg^{2+} in its oxidation state of 2+. Since the solids are divided into two major classes: metal and insulator, the difference between the two can be easily understandable by the basis of the energy band theory.

Reference

[1]. D.P.Partlow, B.E Yoldas, 1981. *J. Non-Cryst.Solids* **46** (1981)153.

[2]. R.K. Iler, *The Chemistry of Silica*; Wiley: New York, 1979.

[3]. K.S.Mazdiyasni, R.T.Dolloff, J.S.II Smith, 1969.*J. Am. Ceram. Soc.* **52 (**1969) 523.

[4]. J. M.Pope, K.C.Radford, 1974. *Am. Ceram. Soc. Bull*. **53** (1974) 574.

[5]. mhtml:file://C:\Documents and Settings\uvp\My Document\Wiley *InterScience Jour…*

[6]. G.F.Neilson, M.C. Weinberg*, J.Non-Cryst.Solids* **63** (1984)365.

[7]. L. L. Hench, J. K .West, *Chemistry Reviews* **90 (**1991) 133.

[8]. R. H. Doremus*, Glass Science*, 2nd Edition. John Wiley & Sons. New York, (1994).

[9]. C.J.Brinker , G.W. Scherer, *Sol-Gel Science*. New York: Academic Press, 1990.

[10]. S.Sakka, K. Kamiya, K. Makita, Y. Yamamoto, 1984. *J. Non-Cryst. Solids* **63 (**1984) 223.

[11]. L. L. Hench, J. K. West, *Chemistry Reviews* **90 (**1990) 37.

 [12]. G.W. Scherer, *In Better Ceramics Through Chemistry III*; C.J.Brinker, D.E.   Clark, D.R. Ulrich, Eds.; *Materials Research Society*: Pittsburgh, PA, **121** (1988) 179.

[13]. B.E. Yoldas, *J. Mater. Sci*. **21** (1986) 1087.

[14]. L. M. Sorensen*, Msc. Dissertion*, University of Florida,Florida, (2006)

[15]. M.J.S, Dewar, W. Theil, *J. Am. Chem. Soc*. **99** (1977) 4899.

[16]. R.K. Harris; C.T. G. Knight, W.E. Hull. In soluble silicates; J.S.Falcone, Ed.;ACS Symposium Series No. **194**; *American Chemical Society*: Washington, D.C., 1982; p. 79.

[17]. S. P. Mukherjee.; *Thin Solid Films Lett*. **81** (1981) L89.

[18]. L.C. Klein.; T.A. Gallo.; G.J. Garvey. *J. Non-Cryst. Solids* **63** (1984) 23.

[19]. C.J. Brinker.; E.P. Roth.; D.R. Tallant.,; G.W. Scherer. *In Science of Ceramic Chemical Processing*; L.L. Hench, D.R.Ulrich., Eds.; Wiley: New York, 1986; p. 37.

[20]. C. E. Brown, Ph.D. dissertation, The Florida State University College of Arts and Sciences, 2006.

[21]. http://math.ucr.edu/home/baez/physics/General/Glass/glass.html [Online], [Accessed 24 July 2009].

[22]. H. Ibach, H. Lüth, *Solid-State Physics, An Introduction to Principles of materials Science (2nd Ed)*, Springer, Berlin, Heidelberg (1993, 1995 and 1996), p. 336.

[23]. M.A. Omar, *Elementary Solid State Physics (Revised Printing)*, Longman, 1993, p. 265.

[24]. F.A. Cotton, G. Wilkinson, C.A. Murillo, M. Bochmann, *Advanced Inorganic Chemistry (6th ed)*, Wiley-Interscience, UK (1999), p. 1113.

[25]. W.W. Portefield, *Inorganic Chemistry, A Unified Approach (2nd Ed),* Academic Press, 1993, p. 498.

[26]. R. Reisfeld, A. Patra, G. Panczer, M. Gaft, *Optical Materials* **13** (1999) 81.

[27]. R.H. Abu-Eittah, S.A. Marie, M.B. Salem, **49** (2004) 4.

[28]. C.K. Jorgensen, "*Absorption Spectra and Chemical Bonding in Complexes.*" Pergamon Press, New York (1964).

[29]. C.K. Jorgensen, Mat. Fys. Medd. Dan. Vid. Selsk, **30** (1965) No. 22 Taken from ref. 18.

[30]. V. R. Kharabe1, S. J. Dhoble and S. V. Moharil*, J. Phys. D: Appl. Phys*. **41** (2008) 205413.

[31]. G.Q. Xu, Z.X. Zheng_, W.M. Tang, Y.C. Wu, *J. Lumin* **126** (2007) 475.

[32]. G.E. Malashkevich, I.M. Melichenko, E.N. Poddenezhny, A.A. Boiko, *J. Non-Cryst. Solids* **260** (1999) 141.

[33]. H. Bi, W. Cai, L. Zhang, *Mater. Res. Bul*. **35** (2000) 1495.

[34]. R. Reisfeld, H. Minti, A. Patra, D. Ganguli, M. Gaft, *Spectrochimica Acta A* **54** (1998) 2143.

[35]. V.P. Dotsenko, I.V. Berezozskaya, N.P. Efryushina, A.S. Voloshinovskii, P.Dorenbos, C.W.E. van Eijk., *J. Lumin.* **93** (2001) 137.

[36]. O.D. Ntwaeaborwa, *PhD. Dissertation*, University of the Free State, Free State, (2006).

[37]. L. Skuja, M. Hirano, H. Hosono, K. Kajihara*, Phys. Stat. Sol*. (c) **2**(2005) 15.

[38]. J.W. Lee, G.H. Sigel Jr., J. Li, *J. Non-Cryst. Solids* **239** (1998) 57.

[39]. S. Agnello, N. Chiodini, A. Paleari, A. Parlato, *J. Non-Cryst. Solids* **353** (2007) 573.

[40]. D.L. Griscom, *J. Ceram. Soc. Jpn*. **99** (1991) 923.

[41]. M. Rothschild, D.J. Ehrlich, D.C. Shaver, *Appl. Phys. Lett*. **55** (1989) 1276.

[42]. J.A. Ruller, E.J. Friebele, *J. Non-Cryst. Solids* **136** (1991) 163.

[43]. L. Skuja, *J. Non-Cryst. Solids* **239** (1998) 16.

[44]. M. Stapelbroek, D.L. Griscom, E.J. Friebele, G.H. Sigel Jr., *J. Non-Cryst. Solids* **32** (1979) 313.

[45]. C. Itoh, T. Suzuki, and N. Itoh, *Phys. Rev*. B **41** (1990) 3794.

[46]. P. N. Saeta and B. I. Greene, *Phys. Rev. Lett*. **70** (1993) 3588.

[47]. L. Skuja, K. Kajihara, M. Hirano, A. Saitoh, H. Hosono , J. of Non-Cryst. Solids **352** (2006) 2297.

[48]. K. Kajihara, L. Skuja, M. Hirano, H. Hosono, *Appl. Phys. Lett.* **79** (2001) 1757.

[49]. A.H. Edwards, W.B. Fowler, *Phys. Rev. B* **26** (1982) 6649.

[50]. D.L. Griscom, *J. Ceram. Soc. Jpn*. **99** (1991) 923.

[51]. J. R. Chavez, S. P. Karna, K. Vanheusden, C. P. Brothers, R. D. Pugh, B. K. Singaraju, W. L. Warren, and R. A. B. Devine, *IEEE Trans. Nucl. Sci*. **44** (1997) 1799.

[52]. J. Laegsgaard, *Physical Review B* **65** (2002) 174114.

[53]. S. Shinoya, W. M. Yen, *Phosphor Handbook, CRC Press, Boca Raton* (1999).

[54]. C. Armellini, M. Ferrari, M. Montagna, G. Pucker, C. Bernard, and A. Monteil., *J. Non-*

Cryst. Solids **245** (1999) 115.

[55]. W. Jia, Y. Wang, M. Santiago, L. Castro, H. Liu, *Res., Mater. Res.Soc. Symp. Proc*. 519Ž1998.**271**.

[56]. W. Jia, H. Liu, S.P. Felofilov, R. Meltzer, J. Jiao, *J. Alloys Compd*.311Ž2000.**11**.

[57]. R.M. Almeida, H.C. Vasconcelos, M.C. Gonçalves, L.F. Santos., *J. Non-Cryst. Solids* **65** (1998) 232.

[58]. A.J. Silversmith, N.T.T. Nguyen, B.W. Sullivan, D.M. Boye, C. Ortiz, K.R. Hoffman, *J. Lumin* **128** (2008) 931.

[59]. C. J. Brinker, G. W. Scherer, *Sol-Gel Science: The Physics and Chemistry of Sol-Gel Processing. Academic Press, Boston* (1990).

[60]. G.I. Brown*, Introduction to Inorganic Chemistry (2nd Ed*.), Longman,Harlow, UK(1985), p. **179.**

[61]. A. J. Silversmith, D.M. Boye, R.E. Anderman, K.S. Brewer, *J. Lumin* **(94-95)** (2001) 275.

[62]. K. Arai, H. Namikawa, K. Kumata, T. Honda, Y. Ishii, T. Handa, *J. Appl. Phys*. **59** (1986) 3430.

[63]. A. Monteil, S. Chaussedent, G. Alombert-Goget, N. Gaumer, J. Obriot, S.J.L. Ribeiro, Y. Messaddeq, A. Chiasera, M. Ferrari, *J. Non-Cryst. Solids* **348** (2004) 50.

Chapter 3

Experimental Procedure and Overview of Research techniques

3.1 Experimental Procedure

3.1.1 Introduction

The study of the sol-gel process started back in the late 19th century and this section focus on the synthesis of silica, Ce-doped silica and co-doped with Al^{3+} and Mg^{2+} respectively. Sol-gel process commonly starts with homogenous solutions of metal salts or metal organic precursors in mixture of H_2O and alcohols. Due to starting with homogenous solutions, the sol-gel technique is considered as an alternative way for the preparation of silica with a more homogenous distribution of rare-earth ions. Sol-gel process is well known and widely used for creation of glasses and ceramic materials. The wet-gel is obtained by adding silica alkoxide precursors together with ethanol as solvent and again adding water simultaneously with acid. Sol-gel chemistry begins as soon as the precursors are added together. For more information on the preparation of sol-gel you can go to [1].

3.2 Synthesis

3.2.1 Synthesis of silica, Ce^{3+} doped silica, Ce^{3+} doped silica nanoparticles co-doped with different mol% of Mg^{2+} and Al^{3+}, respectively.

Silica glasses were synthesized by the sol-gel technique [2] using tetraethylorthosilicate (Si $(OC2H5)_4$, TEOS), ethanol (ETOH), distilled water and Nitric Acid (HNO_3, as a catalyst) as material sources. The purities of these reagents are similar to those of analytically pure reagent. During preparation of pure silica 10 mL of tetra-ethylorthosilicate (TEOS, Si $(OC_2H_5)_4$) dissolved in 10 mL ethanol. The resulting clear solution was stirred for about 10 minutes. To catalyze the hydrolysis and polymerization reactions, 5 mL of concentrated nitric acid was added simultaneously with 14 mL of de-ionised water and the mixture stirred for 24 hours at ambient

temperature until gel point. The volume ratio of TEOS, ETOH, WATER, and HNO_3 was 1:1:1.4:0.5.

Silica doped with different mol% of Ce^{3+} were synthesized using the same material sources of the preparation of silica and cerium nitrate (Ce $(NO_3)_3$) was used as dopants. When synthesizing series of cerium doped silica, the similar procedure of synthesizing pure silica was followed, but this time the solution of silica was stirred for 30 minutes. After that the various mass of cerium (III) nitrate was dissolved in 5 ml of ethanol and was added to the foregoing mixture of silica solution and the solution further stirred till gel point.

Similar experimental procedure was followed during synthesis of Al or Mg co-doped samples. In this case the concentration of Cerium (III) nitrate was hold constant while mol% of magnesium nitrate (Mg $(NO_3)_3$) or aluminium nitrate (Al $(NO_3)_3$) were varied from 0-20%. The salt mixture were dissolved in 5 or/and 2.5 mL of ethanol and added to the stirred silica solution. The combined solutions were further stirred till gel point.

The gels were then dried at room temperature for approximately 5 to 14 days. Dried gels were crushed and sintered in a furnace at 600 $^{\circ}C$ for two hours to remove solvent and organic ligands and to obtain full densification. The powders were re-crushed and were ready for characterization. The preparation was done at ambient conditions.
.

3.3 Sample Characterization

3.3.1 Introduction

In this study, a wide variety of characterization techniques were used to evaluate the material quality of the semiconductor nanoparticles. The techniques broadly deal with the issues such as sample surface topography, morphology including grain size, shape, evidence of voids, the presence of crystalline or amorphous phases and detection of shallow-level impurities. The thermal analyses of the samples were determined by differential scanning calorimetry (DSC) and thermo gravimetric analyses (TGA). The structural properties of the polycrystalline nanoparticles

were studied by scanning electron microscopy (SEM) and the presence of crystalline phases by x-ray diffraction (XRD). The stoichiometric ratios of pure, Ce^{3+} doped and Mg or Al ions co-doped silica nanoparticles were determined by energy dispersive x-ray spectroscopy (EDS). The optical properties of the nanoparticles were evaluated by photoluminescence spectroscopy (PL) and UV-vis spectroscopy. The most important features of these characterization techniques are outlined in the following sections.

3.3.2 Thermal Analysis

3.3.2.1 Differential Scanning Calorimetry (DSC)

DSC is a thermal analysis technique used to measure changes in heat flows associated with material transitions. DSC measurements provide both qualitative and quantitative data on endothermic (heat absorbing) and exothermic (heat evolving) processes. DSC is commonly used to determine the glass transition temperature and crystalline melting point of materials (e.g. polymers) [3]. In the DSC, a material specimen is weighed and placed into DSC sample pan. The sample pan and empty reference pan are placed within the DSC apparatus. The DSC cell is heated or cooled at some controlled rate while continuously monitoring the differential heat flow between the sample and reference pans. The heat flow profile obtained during the DSC heating or cooling run is subsequently analyzed for any of several endothermic and / or exothermic transitions. The undoped,doped and co-doped xerogels were used as precursor for DSC. Thermal analysis was performed using Perkin Elmer DSC 7 differential scanning calorimeter, under flowing nitrogen atmosphere, as shown in Fig. 3.1. The samples approximately weighed in the range of 5-10 mg, were heated from 25 to 200 °C at the heating rate of 10 °C min^{-1}. Peak temperatures of melting and enthalpies were determined from the scan. The instrument was computer controlled and calculations were performed using Pyris Software. Fig. 3.1 shows the DSC model used in this study.

Figure 3.1: The Perkin-Elmer DSC7 thermal analyzer.

3.3.2.2 Thermogravimetric Analysis (TGA)

Thermogravimetric Analysis (TGA) is a thermal analysis technique used to measure changes in the weight (mass) of a sample as function of temperature and or time. Its principal uses include measurement of a material's thermal stability, absorbed moisture content and composition. It is useful to determine the amount of material lost as the sample is heated [4]. In TGA, a sample is placed into a tared TGA sample pan which is attached to a sensitive microbalance assembly, as shown in Fig. 3.2. The sample holder portion of the TGA balance assembly is subsequently placed into a high temperature furnace. The balance assembly measures the initial sample weight at room temperature and then continuously as the temperature increases the material loses weight as species decompose or evaporate from the sample. These changes are detected by the analytical balance from which the sample is suspended. A plot of TGA data is typically weight percent on the y-axis and temperature on the x-axis. The data would be plotted with weight percent as the y-axis and time as the x-axis. The undoped, doped and co-doped xerogels were used as a precursor for TGA. In order to determine the thermal stability of the various xerogels, thermogravimetric analyses were performed in a Perkin-Elmer TGA7 thermal analyzer in the flowing nitrogen atmosphere under the constant flow rate 20 ml min^{-1}, as shown in Fig. 3.2. The xerogels were

also annealed at 600 °C and the resulting powders were used as precursor for other techniques. The samples approximately weighting 5-10 mg each were then heated from 25 to 600 °C at a heating rate of 10 °C min^{-1}. The instrument was computer controlled and calculations were done using Pyris Software.

Figure 3.2: Photo of TGA apparatus.

3.3.3 Structural Analysis

3.3.3.1 Scanning Electron Microscope (SEM)

SEM is a type of electron microscope that images the sample surface by scanning it with a high energy beam of electrons in a raster scan pattern. SEM is used to determine the topography, morphology, composition and crystallographic information of a sample. It has a greater depth of field, higher resolution and higher magnification than ordinary optical microscope. The SEM only produces high-resolution images of the sample surface. Hence, the internal structure of the sample cannot be determined unless cross-section is performed. Scanning electron microscopy was conducted using a SHIMADZU SSX-550 Superscan SEM Model operating in standard high vacuum mode and is equipped with energy dispersive spectroscope, see Fig. 3.3. The filament used was standard tungsten cathode and the images were taken at 5 keV depending on the

sensitivity of the material to the electron beam. Samples were placed on a specimen stub lined with double sided adhesive, conducting tape and then coated with a thin layer of gold to reduce sample charging. Sputter coating is done because samples are semiconductors. The sputter coating is done to prevent the accumulation of static electric charge on the specimen during electron irradiation, and secondly the sputter coating is done to improve contrast and resolution. The SEM generates a beam of electrons in a vacuum.

Figure 3.3: SHIMADZU SSX-550 Superscan SEM Model with EDS.

3.3.3.2 Energy Dispersive Spectroscopy (EDS)

EDS is a spectrographic technique that identifies elemental composition within single particles in a sample matrix, providing qualitative and semi-quantitative information [5]. As a type of spectroscopy, it relies on the investigation of a sample through interactions between electromagnetic radiation and matter, analyzing X-rays emitted by the matter in response to being hit with charged particles. Its characterization capabilities are due in large part to the fundamental principle that each element has a unique atomic structure allowing x-rays that are characteristic of an element's atomic structure to be identified uniquely from each other. To

stimulate the emission of characteristic X-rays from a specimen, a high energy beam of charged particles such as electrons or a beam of X-rays, is focused into the sample being studied.

At rest, an atom within the sample contains ground state (or unexcited) electrons in discrete energy levels or electron shells bound to the nuclear. The incident beam may excite an electron in an inner shell, ejecting it from the shell while creating an electron hole where the electron was. An electron from an outer, higher-energy shell then fills the hole, and the difference in energy between the higher-energy shell and the lower energy shell may be released in the form of an X-ray. The number and energy of the X-rays emitted from a specimen can be measured by an energy dispersive spectrometer. As the energy of the X-rays is characteristic of the difference in energy between the two shells, and of the atomic structure of the element from which they were emitted, this allows the elemental composition of the specimen to be measured.

However, EDS systems are most commonly found on Scanning Electron Microscopes (SEM-EDS) and EDS used in this study is shown in Fig. 3.3.

3.3.3.3 X-ray Diffraction (XRD)

XRD is the science of determining the arrangement of atoms within a crystal from the manner in which a beam of X-rays is scattered from the electrons within the crystal. A crystal is a solid in which a particular arrangement of atoms (its unit cell) is repeated indefinitely along three principal directions known as the basis (or lattice) vectors. It is a technique used to characterize the crystallography structure, crystallite size (grain size), and preferred orientation in polycrystalline or powdered solid samples. It is also a common method for determining strains in crystalline materials. An effect of the finite crystallite sizes is seen as a broadening of the peaks in an X-ray diffraction as is explained by the Scherer equation. In XRD spectroscopy the wave nature of the X-rays are diffracted by the lattice of the crystal to give a unique pattern of peaks of reflectors at different angles and of different intensity, just as light can be diffracted by a grating of suitably spaced lines. The diffracted beams from atoms in successive planes cancel unless they are in phase, and the condition for this is given by the Bragg's law [6]:

$$2dsin\theta = n\lambda \qquad\qquad 3.1$$

Here d is the spacing between diffracting planes, θ is the incident angle, n is any integer and λ is wavelength of the beam. The X-ray detector moves around the sample and measures the intensity of these peaks and the position of these peaks at diffraction angle of 2θ. The X-ray Diffractometer used in this study is Bruker AXS Discover diffractometer, as shown in Fig 3.4.

Figure 3.4: The X-ray Diffractometer used in this study is Bruker AXS Discover diffractometer.

3.3.4 Optical Properties

3.3.4.1 UV-VIS-NIR Spectroscopy

Ultraviolet and visible (UV-Vis) absorption spectroscopy is the measurement of the attenuation of a beam of light after it passes through a sample or after reflection from a sample surface. Ultraviolet and visible light are energetic enough to promote outer electrons to higher energy levels. UV-Vis spectroscopy is usually applied to molecules or inorganic complexes in solution. Since the ultraviolet (UV) region scanned is normally from 200 to 400 nm, and the visible portion is from 400 to 800 nm, UV-Vis spectroscopy is useful to characterize the absorption, transmission, and reflectivity of a variety of technologically important materials, such as pigments, coatings, windows, and filters. It measures the intensity of light passing through a

sample (I), and compares it to the intensity of light before it passes through the sample (I_o). The ratio I / I_o are called the transmittance, and are usually expressed as a percentage (%T). The absorbance, A, is based on the transmittance [7]:

$$A = -\log(\frac{\%T}{100\%})$$
<div align="right">3.2</div>

The basic parts of a spectrophotometer are a light source, a holder for the sample, a diffraction grating or monochromator to separate the different wavelengths of light, and a detector, check Fig. 3.6. A spectrophotometer can be either single beam or double beam. In a single beam instrument all of the light passes through the sample cell. I_o must be measured by removing the sample. In a double-beam instrument, the light is split into two beams before it reaches the sample. One beam is used as the reference; the other beam passes through the sample. Some double-beam instruments have two detectors (photodiodes), and the sample and reference beam are measured at the same time, check Fig 3.5.
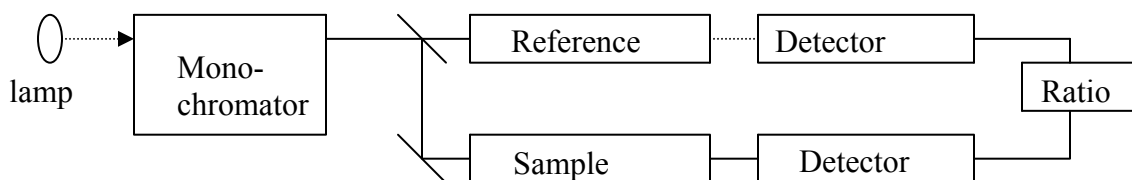
Figure 3.5: The schematic of a double-beam UV-vis spectrophotometer [8].

Samples for UV/Vis spectrophotometer are most often liquids, although the absorbance of gases and even of solids can also be measured. Samples are typically placed in a transparent cell, known as a cuvette. Cuvettes are typically rectangular in shape, commonly with an internal width of 1 cm. The type of sample container used must allow radiation to pass over the spectral region of interest. The most widely applicable cuvettes are made of high quality fused silica or quartz glass because these are transparent throughout the UV, visible and near infrared regions. Glass and plastic cuvettes are also common, although glass and most plastics absorb in the UV, which limits their usefulness to visible wavelengths [9]. The UV-vis Spectroscopy used in this study was from Shmadzu Corporation, Model-UV-vis 1700 Pharmospec, and show in Fig 3.6.

Figure 3.6: UV-vis Spectrophotometer from Shmadzu Corporation, Model-UV-vis 1700 Pharmospec.

3.3.4.2 Photoluminescence Spectroscopy (PL).

PL Spectroscopy is a process in which a substance absorbs photons (electromagnetic radiation) and then re-radiates photons. Quantum mechanically, this can be described as an excitation to a higher energy state and then a return to a lower energy state accompanied by the emission of a photons. This is one of many forms of luminescence (emission of light) and is distinguished by photoexcitation (excitation by photons). PL Spectroscopy concerns monitoring the light emitted from atoms or molecules after they have absorbed photons [10]. PL spectroscopy is suitable for the characterization of both organic and inorganic materials of virtually any size, and the samples can be in solid, liquid, or gaseous forms.

Electromagnetic radiation in the UV and visible ranges is utilized in PL spectroscopy. The sample's PL emission properties are characterized by four parameters: intensity, emission wavelength, bandwidth of the emission peak, and the emission stability [11]. PL emission properties can change, in particular a size dependent shift in the emission wavelength can be observed. Additionally, because the released photon corresponds to the energy difference between the states, PL spectroscopy can be utilized to study material properties such as band

gap, recombination mechanisms, and impurity levels. Solid sample can also be analyzed, with the incident beam impinging on material (powder). Generally an emission spectrum is recorded, where the sample is irradiated with a single wavelength and the intensity of the luminescence emission is recorded as a function of wavelength. In this study Photoluminescence measurements were done on a Carry Eclipse Fluorescence Spectrophotometer system, equipped with a 150 W xenon lamp as the excitation source as shown in Fig 3.7 and secondly using a SPEX 1870, 0.5M Spectrometer, equipped with a He-Cd laser lamp as the excitation source.

Figure 3.7: PL spectroscopy from Carry Eclipse Fluorescence Spectrophotometer System, equipped with a 150 W xenon lamp as the excitation source.

References

[1]. L. Hench, J. West, *Chemistry Review*, **90** (1990) 33.

[2]. O.M. Ntwaeaborwa, P.H. Holloway*, Nanotechnology*, **16** (2005) 865.

[3]. P. J. Haines, *Thermal Methods of Analysis, Principles, Applications and Problems, Blackie Academic and Professional, London*, 1995, p. 64.

[4]. T. Hatakeyama, F.X. Quinn, *Thermal Analysis, Fundamentals and Applications to Polymer Science, Wileys, New York*, 1995, p. 39.

[5]. Scanning Electron Microscopy and Energy Dispersive Spectroscopy [online]. Available From http://www.sixsigmaservices.com/sem-eds.asp [Accessed 14 May 2009].

[6]. E. J. A. Pope, M. Asami, J.D. Mackenzie, *J. Mater. Res.* **1989**. *4*. 1018.

[7]. UV-Visible Spectroscopy [online]. Available From http://www.cem.msu.edu/~reusch/VirtualText/Spectrpy/UV-Vis/uvspec.htm≠uv 1 [Accessed 21 May 2009].

[8]. UV-Vis Absorption Spectroscopy [online]. Available From http://www.files.chem.vt.edu/chem-ed/spec/uv-vis/uv-vis.html [Accessed 21 May 2009].

[9]. Skoog, Holler & Crouch, *Principles of Instrumental Analysis, 6th ed.*; Thomson Brooks/Cole: Belmont, CA, 2007, **351**.

[10]. M. Brust, C.J. Kiely, *Colloids and Surface A-Physicochemical and Engineering Aspects* 202, **175-186** (2002).

[11]. J. Turkevich, P.C. Stevenson, J. Hillier, *Discussions of the Fara-day Society* 11, **55-75** (1951).

Chapter 4

Characterization of pure SiO$_2$ nanoparticles prepared by sol-gel method.

4.1 Introduction

Sol-gel silicate glasses are SiO$_2$ glass monoliths made by the sol-gel process using silicate precursors. The sol-gel process has been extensively studied and used for preparation of high optical quality transparent monoliths by incorporating transition metals in a SiO$_2$ matrix [1-2]. The versatility of sol-gel technology provides control over the surface, shape, morphology of materials from the earliest stages of production until the final stages of the process.

The different molar ratios of reagents and the concentrations of reactants decide the density, morphology (whether they are clustered or dispersed) and transparency of sol-gel [3]. The sol-gel process can be dried by the two products through xerogel which takes long time and aerogel often achieved by supercritical. SiO$_2$ glass is one of the most important optical materials for technologies and applications. It is used for optical fibers, UV and Vis-UV lasers because of its wideband gap. In sol-gel processing, the SiO$_2$ gel backbone is O-Si-O network, which is susceptible to various defects [4, 5]. Many researchers have reported several kinds of optical active centers in nature SiO$_2$ such as oxygen vacancy (-Si-S-), non-bridge oxygen hole center (-Si-O), which give birth to the luminescence bands at 2.7, 3.1, 4.2 and 1.9 eV respectively [6-8].

Many researchers have observed optic-active defect centers in UV region [9-13] of SiO$_2$. Defects in SiO$_2$ have been widely studied in the last decades. The prepared SiO$_2$ nanoparticles show the photoluminescence in the blue region or blue emission at maximum luminescence band of 448 nm (2.7 eV), with the shoulders around 422 nm (2.9 eV), 471 nm (2.6 eV) and 540 nm (2.3 eV). Some researchers have reported the luminescence property of SiO$_2$ in the UV region [14] and others in the visible region [15, 11, and 12]. In this sector we present the thermal, morphological, structural and luminescent characteristic of SiO$_2$ prepared by the sol-gel method.

4.2 Result and Discussion

4.2.1 Thermal analysis

Fig.4.1 (a) shows the Differential thermal analysis of SiO_2 xerogel nanoparticles. The SiO_2 xerogel has an endothermic or melting peak at 105.4 °C and the enthalpy of 880.2 J/g. This endothermic peak is due to free adsorbed water. The SiO_2 xerogel has high enthalpy due to the large crystallites in SiO_2 xerogel chains which melt at high temperature compared to the small crystallites. At the melting temperature, the SiO_2 xerogel chains come out of their ordered arrangements by absorbing heat and begin to move around freely; hence the melting is an endothermic transition. The presence of OH groups in SiO_2 also contributes to absorption at high temperature and high enthalpy.

Fig. 4.1 (b) shows the TGA thermodiagram for SiO_2 xerogel nanoparticles. It is observed that the SiO_2 weight sharply decreases from room temperature up to 150 °C while no significant weight loss was recorded from 150 °C to 600 °C. The TGA shows that from 25-95 °C a 40 wt% losses were also observed, attributed to removal of water in a gel. From 95 °C-150 °C again there is the loss of 30 wt% removal of water and ethanol and again the weight loss of almost 5 wt. % from 150 °C – 600 °C which is due to the vaporization of organic solvent, the decomposition of nitrates in precursor gel and relaxation of the SiO_2 skeleton. SiO_2 xerogel is more thermally stable, by thermally stable it means it can melt at high temperature and it can withstand heat. Since at temperature around 600 °C the graph is considerably stable which means we have used that temperature to anneal the samples.
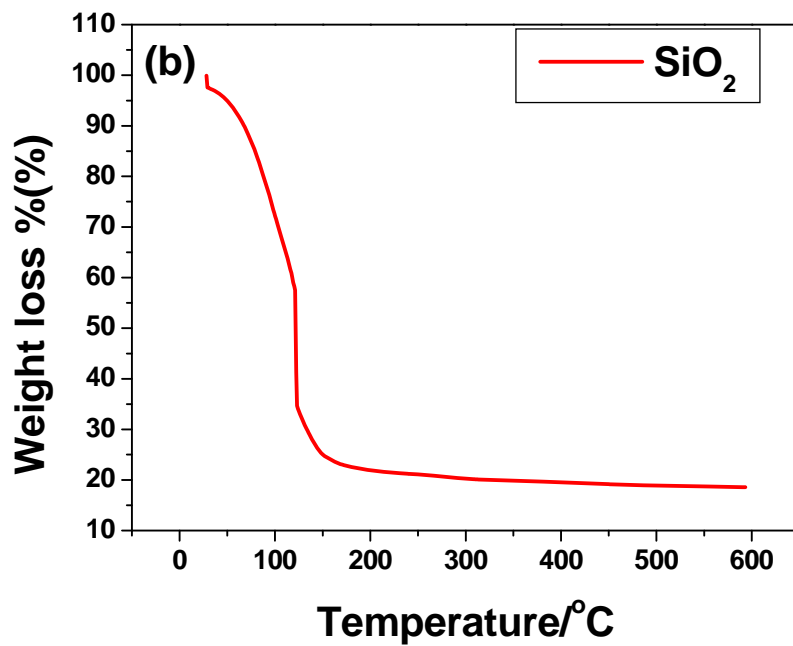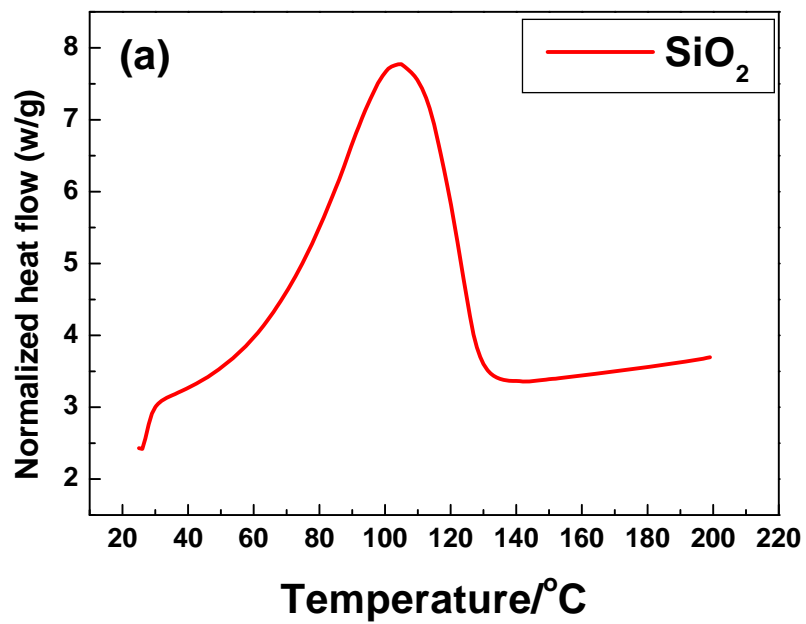
Figure 4.1: (a) DSC and (b) TGA measurements of unannealed SiO₂ xerogel.

4.2.2 Morphological and Structural properties.

Fig. 4.2 Shows the SEM micrograph of SiO$_2$ xerogel nanoparticles annealed at 600 °C for 2 hours. The surface aspects of the SiO$_2$ nanoparticles at high magnification are spherical, smooth and homogenous but with isolated aggregates. At low magnification the micrograph show that that the particles are micro, irregular shape and aggregated.
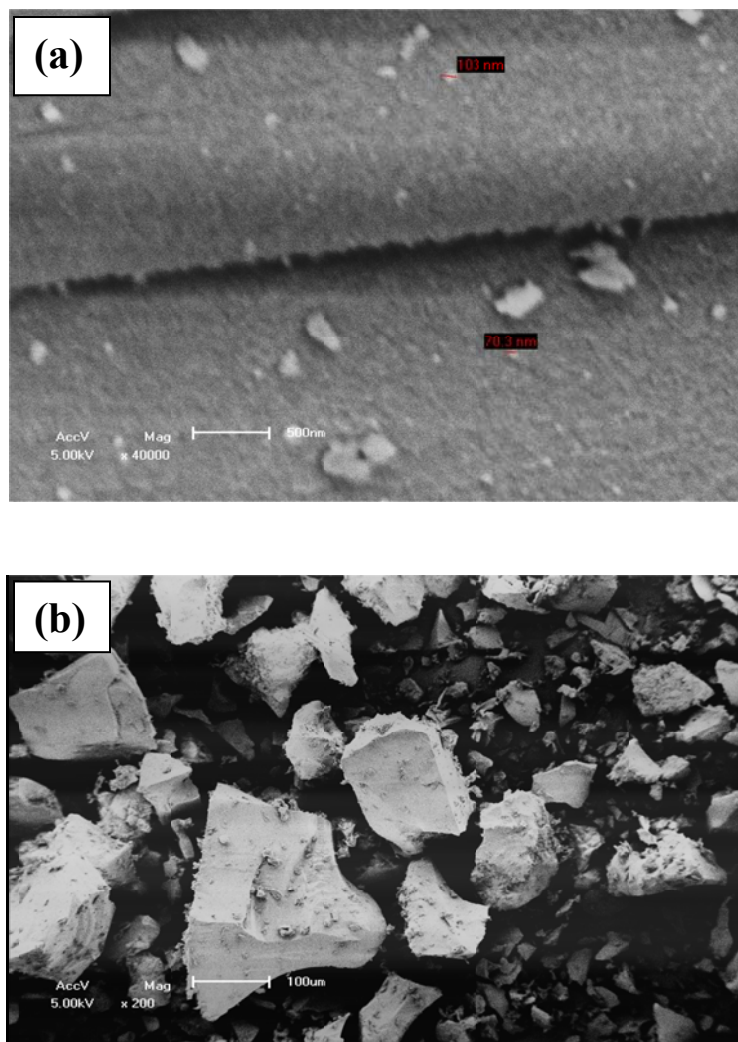
Figure 4.2: SEM image of a xerogel SiO$_2$ at (a) high and (b) low magnifications.

Due to low solubility of SiO_2 in the acidic aqueous/ alcohol media, siloxane bonds hardly break and hence no rearrangement of chains occur [16]. Fig. 4.3 shows the energy dispersive X-ray spectrum of xerogel SiO_2. The composition analysis of the nanoparticles suggests the existence of Si, O, (from the cores and the outside shell), C (from the copper (Cu) gridding for measurement) and Au (from thin gold overlayer).
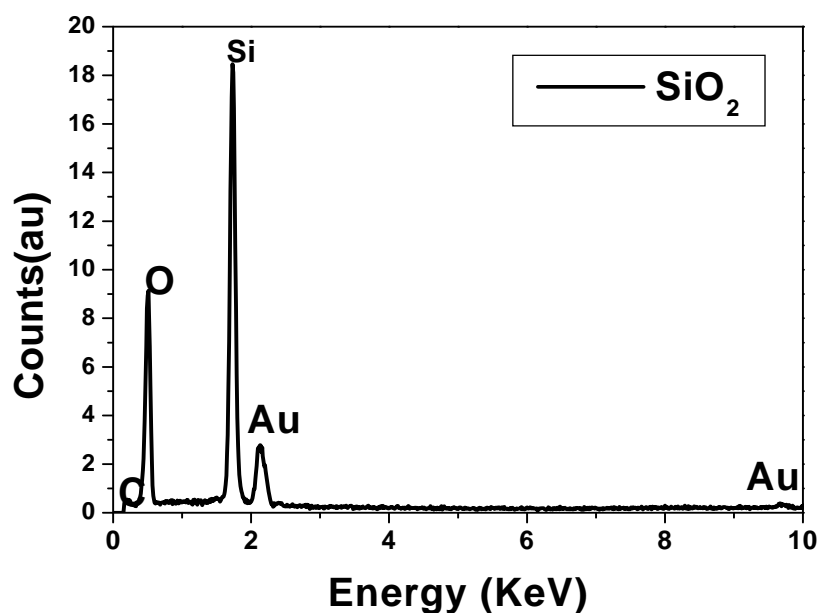
Figure 4.3: EDS shows elemental component of the synthesized samples for a xerogel SiO_2 annealed at 600 °C for 2 hours.

An X-ray diffraction pattern of xerogel SiO_2 is shown in Fig. 4.4 (a). The spectra have only one dispersive broad peak, which indicate that all the samples are non-crystalline solids [17, 3]. The broad diffraction peak signifies small sized particles (in nano range). The heat-treatment in air using furnace at 600 °C for 2 hours have minimal effect on the structure of pure SiO_2.
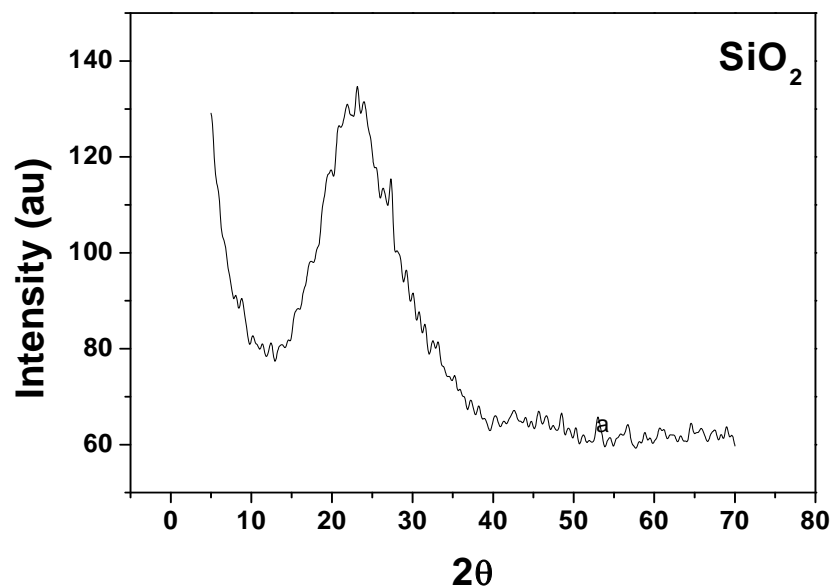
Figure 4.4: XRD spectra of xerogel SiO$_2$ nanoparticles annealed at 600 °C for 2 hours.

4.2.3 Absorbance and Transmittance of pure Silica nanoparticles.

Fig. 4.5 shows the UV-VIS spectrum and optical absorption spectrum of xerogel SiO$_2$ nanoparticles dispersed in ethanol. It is seen from the spectra that the SiO$_2$ has an absorption peak at around 275 nm, which correspond to the 4f and 5d transition [18-19] and is similar to the corresponding reference sample in this study (see transmission and absorption curve of SiO$_2$ in Fig. 4.5). The annealed xerogel SiO$_2$ nanoparticles in ethanol displayed a fair transparency in the visible region.
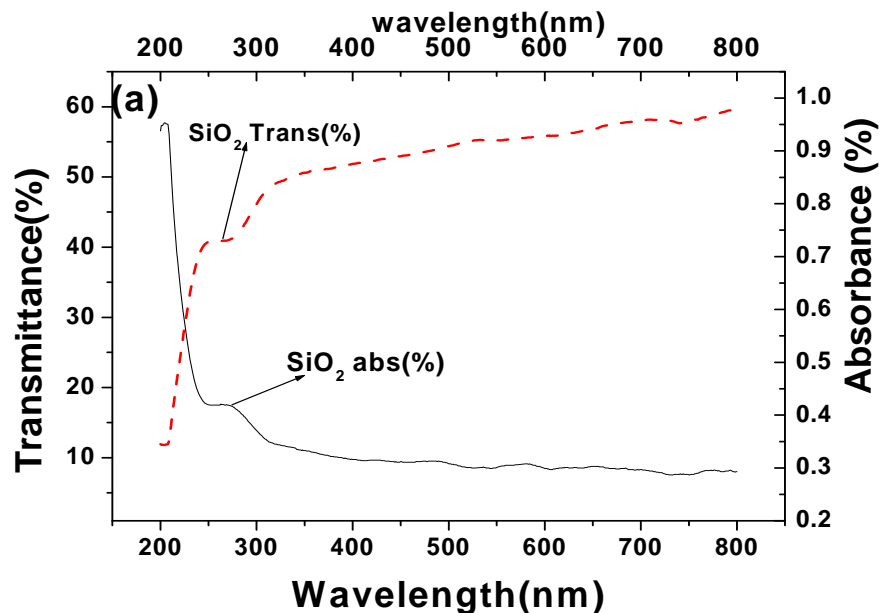
Figure 4.5: UV-VIS spectrum and Optical absorption spectrum of xerogel SiO$_2$ nanoparticles annealed at 600 °C for 2 hours.

4.2.4 Photoluminescence properties

Fig. 4.6(a) presents the luminescence spectra of xerogel SiO$_2$ heat-treated at 600 °C in air for 2 hours excited at 325 nm using He-Cd laser lamp. A broad emission with maximum peak at 448 nm was detected in the blue region of the visible spectrum. The analysis on this broad band with the Gaussian function is shown in this pattern. Four luminescence bands contribute to this broad band with the maximum at 422, 448, 471 and 540 nm as shown in Fig. 4.6(a). These luminescence bands are attributed to the defects in SiO$_2$. Since xerogel SiO$_2$ has low coordination number (which forms bond with few metals or elements and also have a low number of ligands), it easily forms many kinds of defects [4-5] on the surface, which may make nano-sized SiO$_2$ having much different optic property.

The SiO$_2$ gel backbone of the O-Si-O network is susceptible to various defects. Some of the common defects in SiO$_2$ are neutral oxygen vacancies [20], and the O$^-$ states (or positive holes), known as non-bridge oxygen hole center [21]. In the present work, the intense blue emission

around 448 nm was reported, but other researcher reported the luminescence band of xerogel SiO$_2$ nanoparticles in the UV region [14] and other in the visible region [22].

In this work, a major emission peak is observed in the blue region of the visible region at 448 nm (2.7 eV) with shoulders at 422, 470 and 540 nm. The emission peak at 2.7 eV has been attributed by researchers [23-24] to neutral oxygen vacancy (-Si-Si-) in SiO$_2$. The luminescence band at around 422 nm (2.9 eV) and 470 nm (2.6 eV) may be attributed to the some kind of oxygen deficiency center (-Si-O-) [21], while the luminescence band at around 540 nm (2.3 eV) to the impurities in SiO$_2$. The PL emission spectra of xerogel SiO$_2$ annealed at 600 °C for 2 hours, excited by the xenon lamp operating at 250 nm, is shown in Fig. 4.6(b). The spectrum shows several emission bands at 418, 436 and 368 nm. The major two unresolved peaks were detected in the blue region of the visible spectrum at 418 nm and 436 nm with minor peak detected in UV region at 368 nm. These emissions are due to the structural defects in SiO$_2$ [11-13].
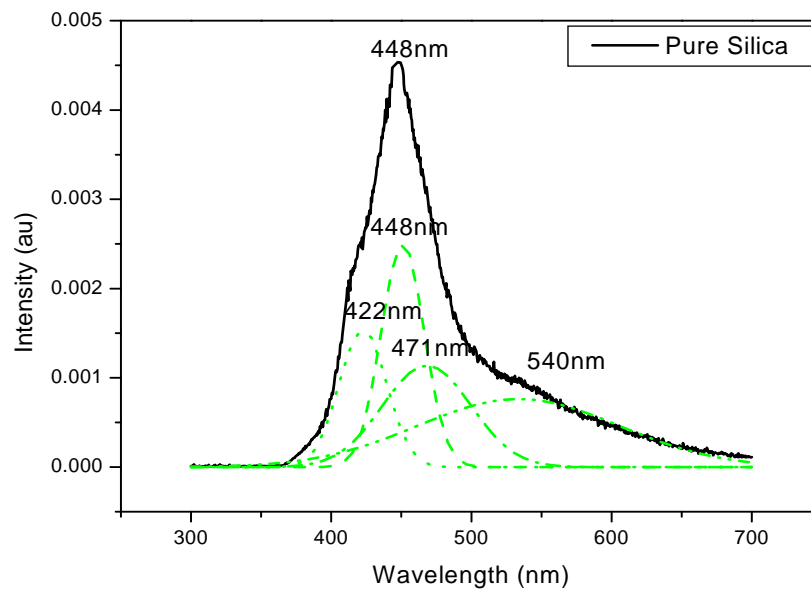
Figure 4.6: (a) Photoluminescence emission spectrum for xerogel SiO$_2$ using He-Cd laser lamp.
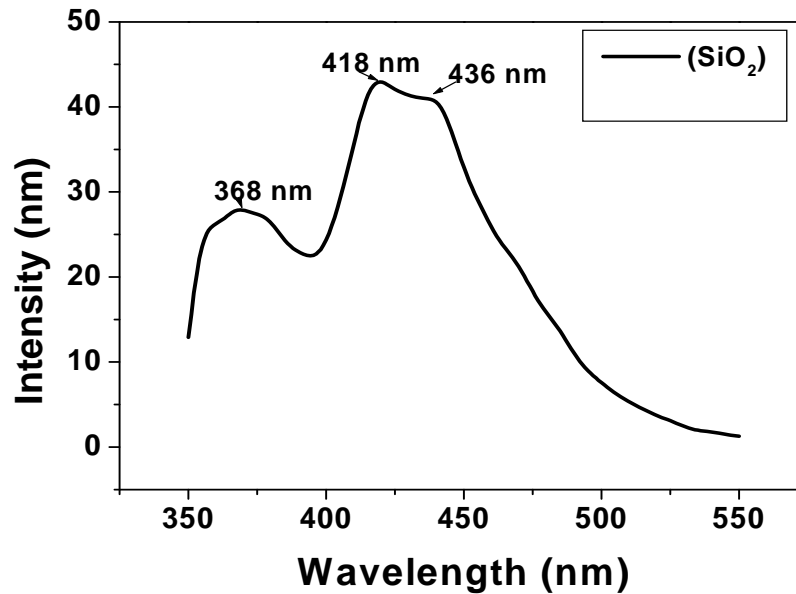
Figure 4.6: (b) Photoluminescence emission spectrum for xerogel SiO$_2$ using xenon lamp.

4.3 Conclusion

Spherical SiO$_2$ particles with nanometer particle size distribution have been synthesized by the hydrolysis reaction of TEOS in ethanol containing deionized water and nitric acid. The particles showed sharp UV absorption bands at around 270 nm. The bright PL emission band was observed with the maximum at 448 nm with the shoulder around 422, 478, and 540 nm. The luminescence characteristic of SiO$_2$ is found to be excitation energy dependent. The XRD analysis shows that the SiO$_2$ nanoparticles are amorphous and TGA shows that the amount lost as a sample is heated.

References

[1]. S. McCulloch, R. M. Stewart, R. M. Guppy, J. O. W. Norris, *Int. J. Optoelec*. **9** (1994) 235.

[2]. M. D. Curran, D. D. Poore, A. E. Stiegman, *Chem. Mater*. **10** (1998) 3156.

[3]. S. Tabatabaei, A. Shukohfar, R . Aghababazadeh1, A. Mirhabibi**,** *Journal of Physics: Conference Series* **26** (2006) 371.

[4]. J. Zink, B. Dunn, *J. Ceram. Soc., Jpn.* **99** (1991) 878.

[5]. A. Patra, D. Ganguli, *J. Non-Cryst. Solids* **144** (1992) 111.

[6]. Y. Sakurai, K. Nagasawa, *J. Non-Cryst. Solids* **290** (2001) 189.

[7]. M. Leone, R. Boscaino, M. Cannas, *et al., J. Non-Cryst. Solids* **245** (1999) 196.

[8]. Y. Sakurai, *J. Non-Cryst. Solids* **271** (2000) 218.

[9]. L. Skuja, *J. Non-Crystal. Solids* **239** (1998) 16.

[10]. M. Leone, R. Boscaino, M. Cannas, *J. Non-Cryst. Solids* **245** (1999) 196.

[11]. Y. Han; J. Lin; H. Zhang, *Mater. Lett.* **54** (2002) 389.

[12]. T. Inokuma, Y. Kuruta, S. Hasegawa, *J. Lumin.* **80** (1990) 247.

[13] W.H. Green, K.P. Le, J. Grey, T.T Au; M. Sailor, *J. Science*. **276** (1997) 1826.

[14]. G.Q. Xu, Z.X. Zheng, W.M. Tang, Y.C. Wu, *J. of Lumin.* **126** (2007) 43.

[15]. J. Lin, K. Baerner, *Mater. Lett*. **46** (2000) 86.

[16]. R.D. Shoup, *J. Sol–Gel Sci. Technol*. **2** (1994) 861.

[17]. F. Yuan-Xiang, S. Yan-Hui, *J. of Alloys and Compounds*. **471** (2009) 190.

[18]. J. Zink, B. Dunn, *J. Ceram. Soc., Jpn*. **99** (1991) 878.

[19]. A. Patra, D. Ganguli, *J. Non-Cryst. Solids* **144** (1992) 111.

[20]. R. Reisfeld, A. Patra, G. Panczer, M. Gaft, *Optical Material*, in press.

[21]. A. Mohammed, T. Zaitoun, T. Kim, C.T. Lin, *J. Phys. Chem*. B. **102** (1998) 1123.

[22]. O.M. Ntwaeabora, Ph.D. *thesis*, University of the Free State, South Africa 2006.

[23]. H. Nishikawa, T. Shiroyama, R. Nakamura, Y. Ohki, K. Nagasawa, Y. Hama, *Phys. Rev*. B **45** (1992) 586.

[24]. Y. Sakurai, K. Nagasawa, *J. Non-Cryst. Solids* **290** (2001) 189.

[25]. A.N. Trukhin, H.J. Fitting, *J. Non-Cryst. Solids.* **248** (1999) 49.

Chapter 5

Synthesis and characterization of Ce³⁺ doped SiO₂ nanoparticles

5.1 Introduction

The so-gel technique that involves the simultaneous hydrolysis and condensation reaction of the metal alkoxide [1] is one of the most common methods of synthesizing SiO_2 nanoparticles. It has simple chemical manipulations and a greater homogeneity of samples. It is well known that almost every element in the periodic table can be stuffed into glasses, to control its quality and opto-electronic properties. Glass hosts with their superior properties such as optical, flexible geometry, higher doping levels and fiberization capability are a viable alternative to crystal. Glass matrices also provide a wider tunability range because of varied site geometries available to the active species. Cerium doped sol-gel SiO_2 glasses seems to be a promising material for diverse applications such as phosphors, lasers, amplifiers and radiation detection technologies [2, 3]. Ce^{3+} ions were widely used as activators in various oxides materials for its allowed optical transitions of 4f–5d. A strong overlap of the activator 5d orbitals with ligand orbital causes high sensitivity of their spectral characteristics to the local structural environment. Many researchers have mentioned two main luminescent bands of Ce^{3+} ions at 357 and 450 nm in the samples of Ce^{3+}-doped glasses and crystals [4-6]. Both of the two bands were attributed to the 4f–5d transitions of triply charged cerium. There is still no doubtless conclusion about the relationship between the luminescence bands and the environment structure. In some Ce^{3+}-doped materials, there was only one luminescence band with the maximum at 357 nm [5,6], but in other samples luminescence bands at 450 nm appeared [5]. The luminescence of Ce doped silica is influenced by factors such as the modification of the ligand field around the Ce^{3+} ions in SiO_2, presence of hydroxyl ions, energy transfer by cross relaxation and the concentration of dopants [7]. It was therefore of great interest to distinguish between the luminescence arising from Ce^{3+} ions and of that arising from defect centers in the silica matrix. Thus, the purpose of this paper is to study the absorption and luminescent properties by using UV (Ultra Violet) and PL (photoluminescence)

spectroscopy of Ce-doped SiO_2 glasses made by the sol-gel process. Secondly the dependence of the PL wavelengths and intensity on the Ce^{3+} concentrations was investigated.

5.2 Result and Discussion

5.2.1 Thermal analysis
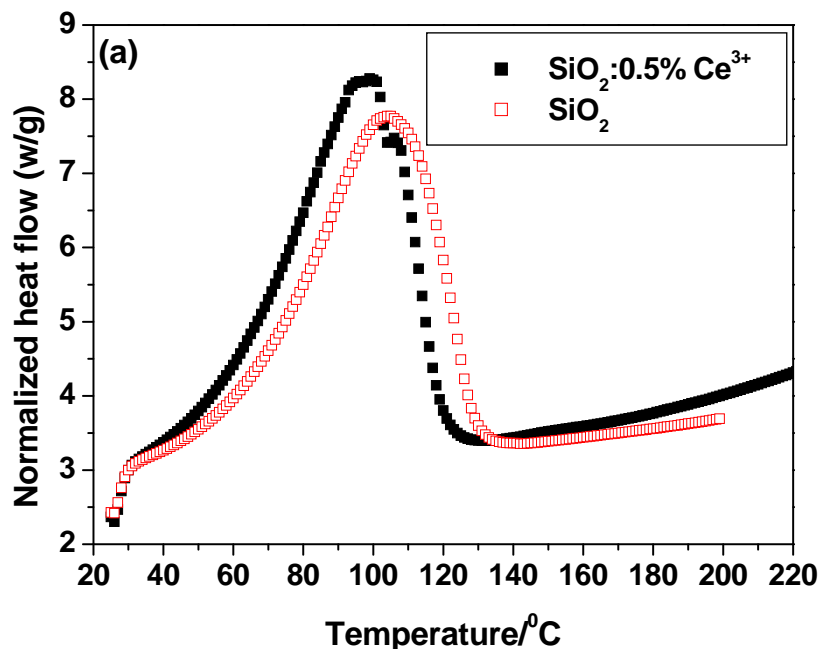
Figure 5.1: (a) DSC measurements of unannealed SiO_2 and SiO_2:0.5% Ce^{3+} xerogels.

The differential thermal analyses (DTA) of samples are shown in Fig. 5.1(a). SiO_2 xerogel has a melting peak at 105.4 °C and the enthalpy of 880.2 J/g observed in the heating and cooling process [8]. The peak correspond well to the desorption of physically adsorbed water, the removal of chemically adsorbed water, and the decomposition of organic matter and hydroxide groups. The results of DSC indicate the presence of organic matter in the monodispersed sample and the higher melting peak of SiO_2 xerogel compared to the Ce-doped implies the stronger bond between the Si-O networks. This means the high melting peak shows that the bonding between the metals is strong. The presence of Ce in the SiO_2 matrix decreases the melting peak temperature to 100.8 °C and reduces the enthalpy to 868.2 J/g.
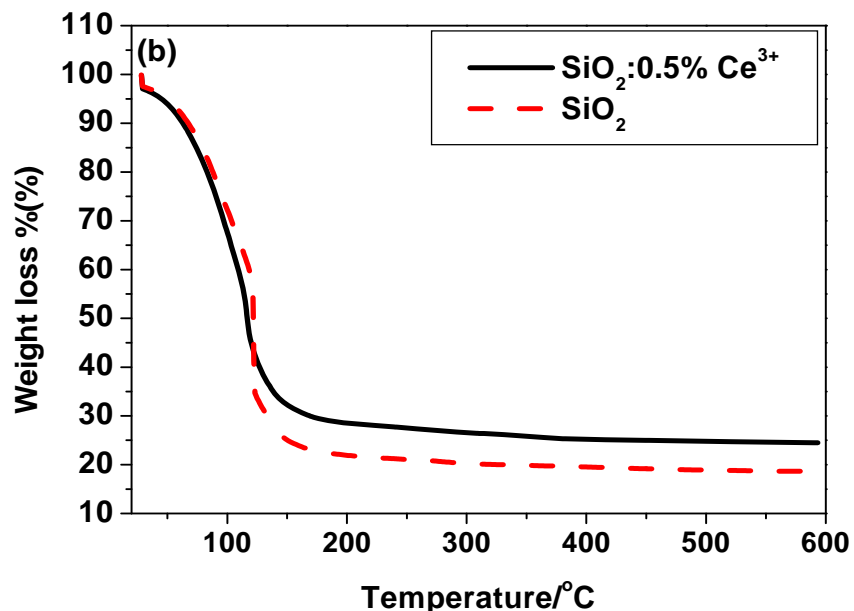
Figure 5.1: (b) TGA measurements of unannealed SiO₂ and SiO₂:0.5% Ce³⁺ xerogels.

SiO$_2$-Ce melts at lower temperature as compared to SiO$_2$ because of the weak intermolecular forces between the Si-O-Ce or Si-Ce. The temperatures of DSC start at 25 °C and stop at 200 °C because from 200 °C to 600 °C there was just a constant line or straight line.

Thermogravimetric analyses (TGA) were carried out to determine the content of organic matter in the SiO$_2$ nanoparticles. As shown by Fig. 5.1 (b) weight loss of about 40 wt. % from room temperature to 125 °C was due to the desorption of physically adsorbed water and chemically adsorbed alcohol. The weight loss of 20 wt. % from 125 to 135 °C was due to the removal of chemically adsorbed water. Weight loss of almost 5 wt. % from 135 to 600 °C was mostly due to the decomposition of organic matter and the hydroxide groups. There was a total weight loss of 75 wt. % when SiO$_2$ xerogel sample was heated from room temperature to 600 °C. The presence of Ce as a do-pant significantly reduces the residual mater due to existence of weak bonds relative to that of SiO$_2$ xerogel. The do-pants partly participate in the removal of ⁻OH group thus reducing the number of pores.

5.2.2 Morphological and structural properties.

Fig. 5.2 show SEM micrographs of SiO_2:0.5% Ce^{3+} samples' annealed at 600 °C. Since SiO_2 is a semiconductor, therefore injection of large number of high energy electrons on to its surface causes surface charging. To circumvent this, samples were sputter coated with Gold (Au) in order to be able to monitor the surface morphology of the samples. The surface aspects of the nanoparticles are found to be spherical, smooth and homogenous in all cases but with isolated aggregates of SiO_2/ SiO_2:Ce. However, small nano-sized particles on some of the large agglomerated particles are clearly evident. It was observed that the concentration of the Ce ions have less effect on the morphology of the samples. Figure 5.3 (a) and (b) show the EDS spectra performed on the particles (a) SiO_2: 0.5% Ce^{3+} (b) SiO_2 xerogels. The components analysis of the particles suggests the existence of Si (from the cores and the outside shell), oxygen (O) (from the cores and the shells) and carbon (C) (from the Cu(copper) gridding for measurement) and SiO_2: 0.5% Ce^{3+} shows Si, O, C, and Ce^{3+} but cerium peak are small due to the low concentration of it.

Figure 5.2: SEM images of SiO_2:0.5%Ce^{3+} nanoparticles showing aggregation and spherical nanoparticles.
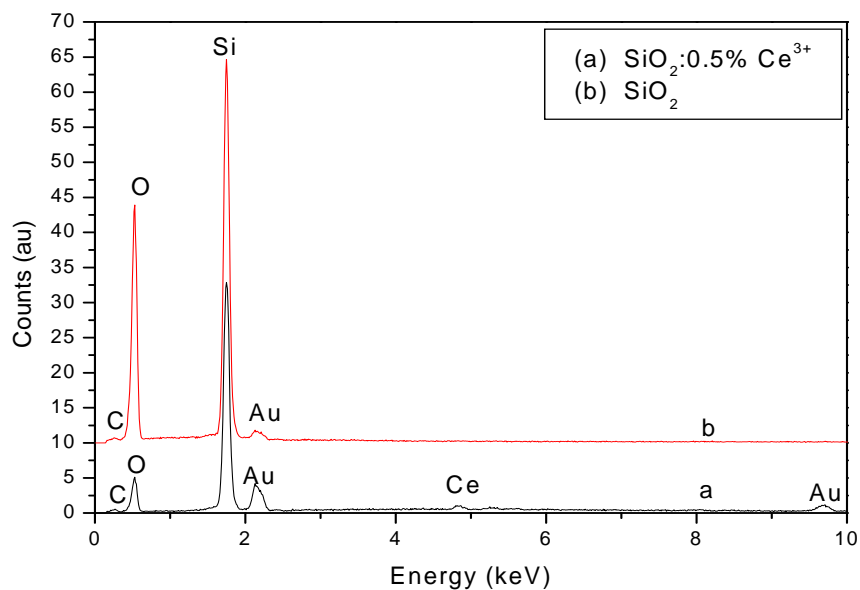
Figure 5.3: EDS shows elemental component of the synthesized samples (a) SiO$_2$: 0.5% Ce^{3+} and (b) SiO$_2$ xerogels.
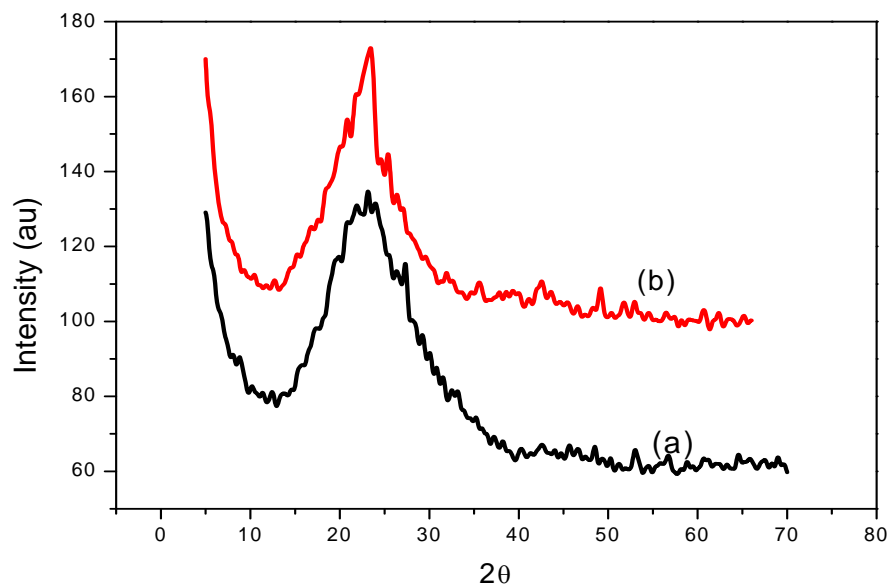
Figure 5.4: XRD spectra of (a) SiO$_2$ and (b) SiO$_2$:0.5% Ce^{3+} xerogels.

Since we have coated our samples with Gold (Au) to prevent charging, small amount of Gold is also observed on the spectrum. X-ray diffraction patterns of SiO_2 and $SiO_2:Ce^{3+}$ is shown in Fig. 5.4. All of the spectra are similar and only have one dispersive broad peak, which indicate that all the samples are non-crystalline solids. The heat-treatment of samples in air using furnace at 600 °C for 2 hours have minimal effect on the structure of SiO_2 and Ce-doped SiO_2.

5.2.3 Absorbance and Transmittance of SiO_2 and SiO_2: 0.5% Ce^{3+}.
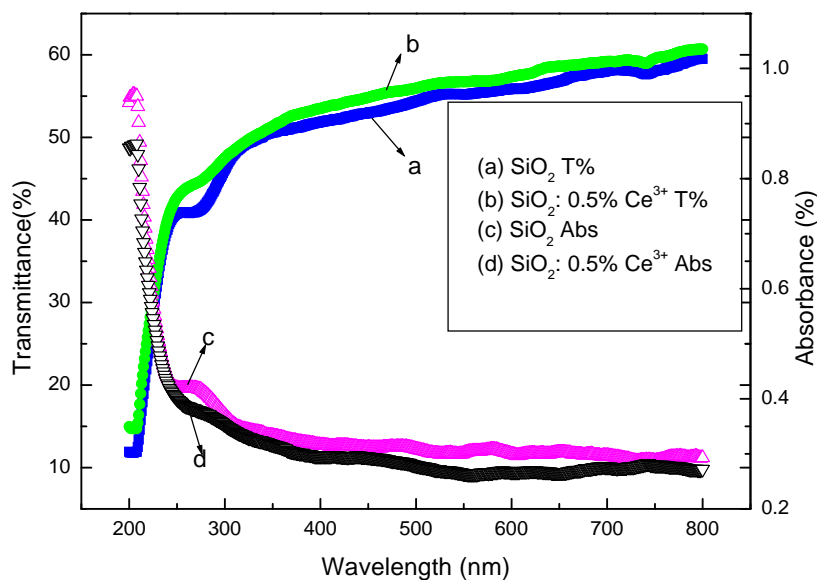
Figure 5.5: Transmittance and absorbance measurement of SiO_2 and SiO_2: 0.5% Ce^{3+} xerogel.

The SiO_2 nanoparticles in ethanol solution displayed a fair transparency in the visible region. The presence of Ce^{3+} in the matrix slightly increases the transmission intensity and lower absorption peak of SiO_2. For SiO_2, there is an absorption peak at around 275 nm, which correspond to the 4f and 5d transition [9,10] and is similar to the corresponding reference sample in this study (see transmission and absorption curve of $SiO_2:Ce^{3+}$) in Fig. 5.5. In contrast for samples containing Ce^{3+} ions, no clear absorption peak but an absorption edge was observed.

5.2.4 Photoluminescence properties

Fig. 5.6 (a) presents the photoluminescence spectra of SiO_2 xerogel excited at 325 nm after heat-treated at 600 °C in air for 2 hours. A broad emission with maximum peak at 448 nm (2.7 eV) was detected in the blue region of the visible spectrum. The analysis on this broad band with the Gaussian function is shown in this pattern. Four luminescence bands contribute to this broad band with the maximum at 422, 448, 471 and 540 nm. Three luminescence bands (422 (2.9 eV), 471 (2.6 eV) and 540 nm (2.3 eV)) can be due to the defects in SiO_2. These values which are slightly blue shifted may be due to the size of the nanoparticles but comparable to luminescence peaks at 450, 560 and 650 nm for SiO_2 xerogel as reported by some researchers [11]. This assumption of an indication of quantum confinement is in agreement to the SEM results where nano-sized particles are observed as reported above. Since SiO_2 has a low coordinated elements (this means it can have a low number of ligands) and therefore easily form many kinds of defects on the surface, which may make nano-sized SiO_2 to have much different optic property (e.g. figure of SiO_2).
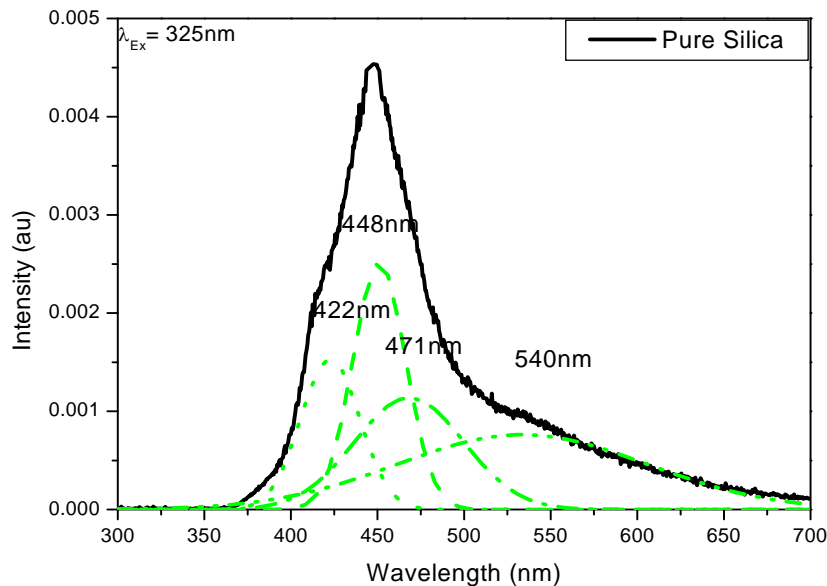
Figure 5.6(a): Photoluminescence emission spectrum for SiO_2 xerogel.

Three luminescence bands are attributed to the defects in SiO_2 gel backbone of the O-Si-O network, which is susceptible to various defects [12,13]. Some of common defects in SiO_2 are neutral oxygen vacancy [14], and the O^- states (or positive holes), also called non-bridge oxygen hole center [15]. Fig. 5.6 (b) shows the photoluminescence emission spectra of SiO_2:0.5% Ce^{3+} excited by 325 nm photon after heat treated in air at 600 °C for 2 hours. A broad emission with maximum peak at 445 nm (2.8 eV) was observed in the violet and blue region of the visible spectrum. The broad emission can also be decomposed to two luminescence bands with the maximum wavelength at 442 nm (22624.43 cm^{-1}) and 467 nm (21413.28 cm^{-1}). Two main luminescence bands of Ce^{3+} ions at 357 and 450 nm in samples of Ce^{3+} - doped glasses and crystals have been reported [16-18]. The PL emission spectra from SiO_2:Ce^{3+} is very similar to that of SiO_2 but with enhanced luminescence and slight shift from 448 nm to the 445 nm with addition of Ce^{3+} ions to SiO_2.
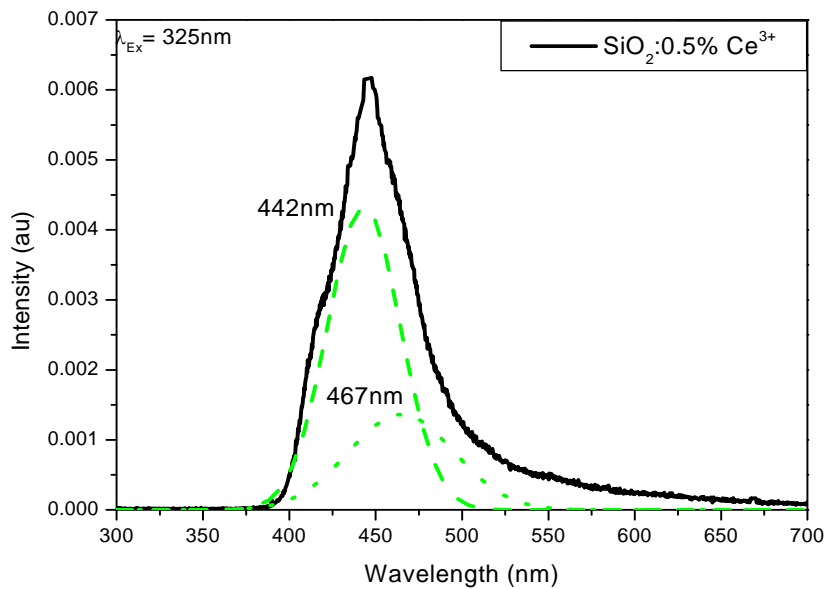
Figure 5.6(b): Photoluminescence emission spectrum for SiO_2:0.5% Ce^{3+} xerogel.

The PL emission at 445 nm could possibly be due to transition in both SiO_2 and Ce^{3+} emitting centre. This implies that there is possibility of host SiO_2 transfers energy to the emitting centre Ce^{3+} just like in the commercially used $ZnS:Ag^+$, in which the sulphide host transfers energy to Ag^+. The emission from SiO_2 at 540 nm appears to have been quenched in case of $SiO_2:Ce^{3+}$. The existence of several peaks can be attributed to non-equivalence of the Ce ions (e.g. coordination number changing with the surrounding ligands from one side to another). These luminescence bands are characteristic emission of $4f^1 \rightarrow 5d^1$ transitions of triply charged Ce^{3+} ions [13,19,20], commonly in either in the ultraviolet or visible region (blue) and it consists typically of two bands, which corresponds to the transitions from the lowest $5d^1$ crystal field component ($^2D_{3/2}$) to the two components ($2F_{5/2}$ and $2F_{7/2}$) of the 4f ground state [20]. The dependence of the luminescence spectra of SiO_2: Ce on the Ce concentration is illustrated in Figure 5.7(a). The emission intensity is related to the concentration of the Ce^{3+} activator ions. With the increase of the concentration of the activator ion, the luminescent center increases and the emission intensity is enhanced. The highest luminescent intensity yield of the particles was obtained at a Ce concentration of 0.5% and lower or higher Ce contents results in a substantial decrease in emission intensity. The luminescence spectra overlap for other mol percentages (e.g. $SiO_2:0.75\%Ce^{3+}$ and $SiO_2:1.25\%Ce^{3+}$) which are not include in Fig. 5.7(a).

Fig. 5.7(b) shows the variation of maximum luminescence intensity with Ce concentrations. The luminescence spectra depict a threshold value as the concentration of the activated elements increases as a result of concentration quenching effect. At high concentration the clustering of activator atoms may change a fraction of the activator into quenches, and may induce the quenching effect. This decrease in emission intensity commonly attributed to $^2D_{3/2} \rightarrow 2F_J$ transitions shows the presence of stronger cross-relaxation induced quenching with smaller inter-ion distance [21]. The relationship between the relative luminescence intensities by monitoring the emissions of $^2D_{3/2} \rightarrow 2F_J$ at 545 nm and doping Ce^{3+} concentrations for samples annealed at 600 °C for 2 hours is shown in Fig. 5.7(c). The quenching concentration is about 0.5%. In general, the quenching concentration effect is ascribed to transfer energy from Ce^{3+} ions to nearby quenching centers.
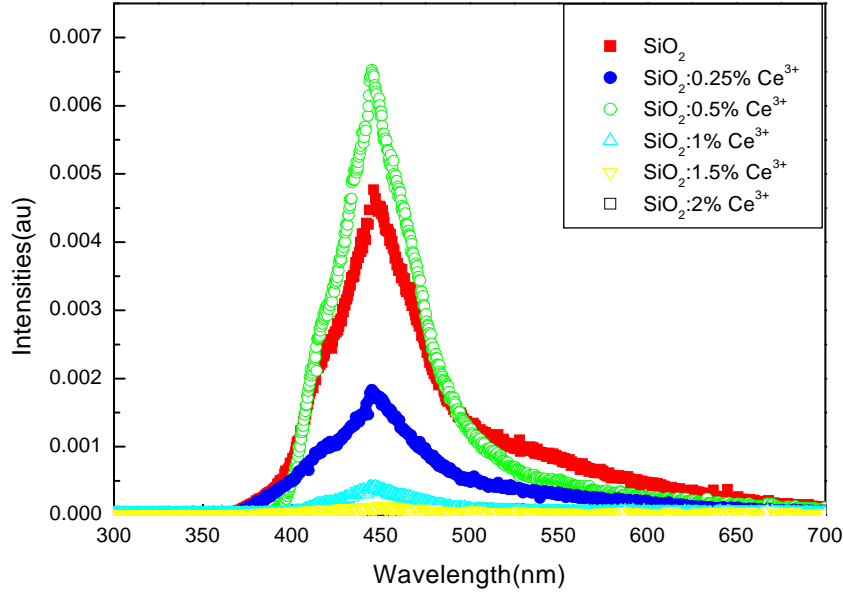
Figure 5.7: (a) Luminescence spectra of SiO₂: Ce obtained for different Ce concentration at
$\lambda_{exc} = 325$ **nm.**

The smaller nanosized particles result in the fact that the non-radiative centers distribute randomly with a considerable fluctuation in particles, at the same time, the more interfaces effect in smaller nanosized particles lead to energy transfer between Ce^{3+} ions is inhibited [22]. All of these would lead to nonradiative transfer decreased and a higher Ce^{3+} quenching concentration. The mutual interactions type of luminescence quenching in solid-state materials can concluded by analyzing the constant s from the following relational expression [23,24]:

$$\log(I/C) = -\frac{s}{d}\log C + \log f \qquad\qquad 5.1$$

where I is the relative emission intensity, C is the Ce^{3+} dopant content, s is the mutual interactions constant. When $\log C$ is the horizontal ordinate, $\log(I/C)$ is the longitudinal ordinate, the slope coefficient of curve is $s/3$. The luminescence quenching is related to the electric multipole resonant transfer between nearby Ce^{3+} ions and exchange interactions.

Figure 5.7: (b) Experimental results and Gaussian function fitted graphs of concentration dependence of the normalized emission intensity of Ce^{3+} doped SiO$_2$.

Figure 5.7: (c) The relation of the concentration of Ce^{3+} ions ($\log C$) and the $\log(I/C)$ for the ^{2}D$_{3/2}$→^{2}F$_J$ transitions in SiO$_2$:Ce phosphors.
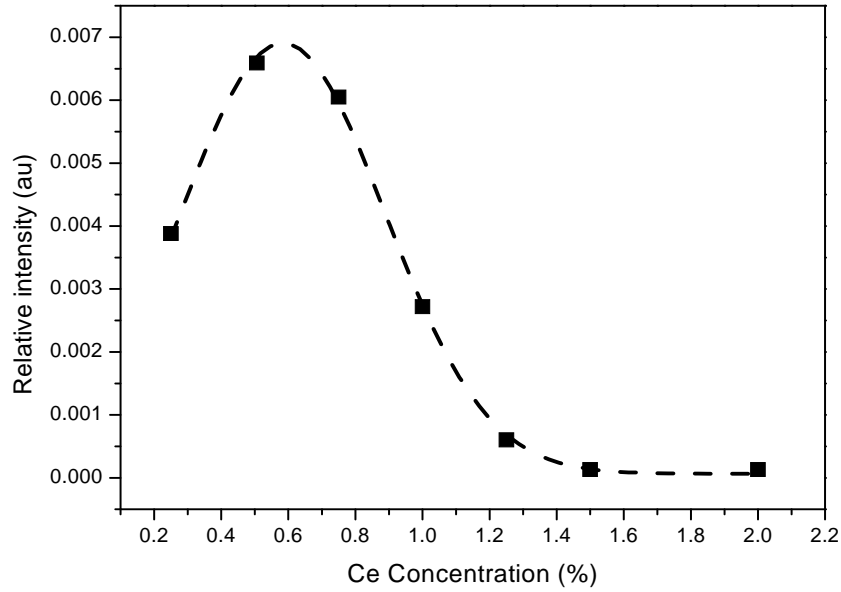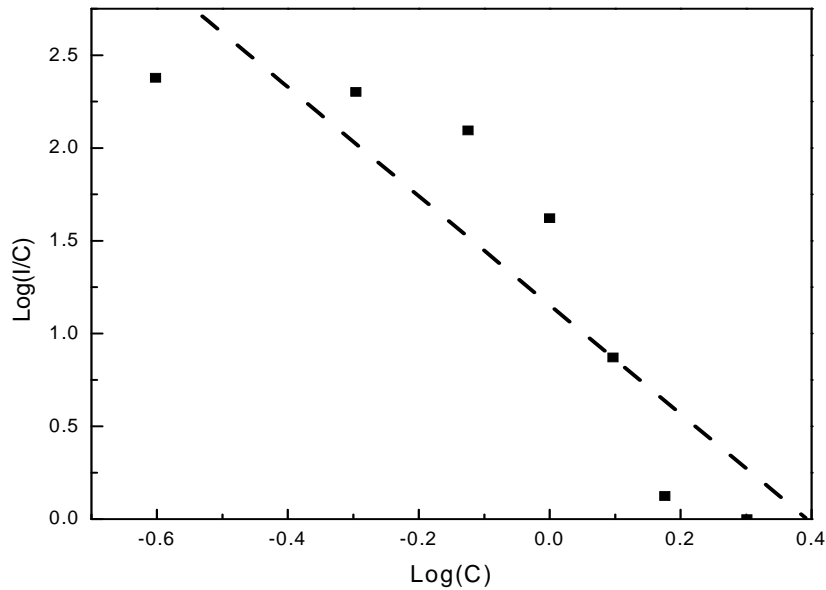
The relationships between $\log(I/C)$ and $\log C$ in SiO_2:Ce^{3+} nanoparticles prepared at 600 °C for 2 hours are plotted in Fig. 5.7(c), which can be fitted into linear, and the slope coefficient of linear is –2.9 (close to 3), according to the slope coefficient of linear, the parameter s is calculated to be 9. When s is between 8 and 10, the mutual interaction is dominated by electric dipole and electric quadrupole interactions, for the energy transfer by cross relaxation among the Ce^{3+} ions in the SiO_2:Ce phosphor. Other non-radioactive processes that could contribute to luminescence quenching effects are energy transfer to hydroxyl ions and SiO_2 deep level defects. In order to eliminate the contributions of these effects the as prepared nanoparticles are synthesized at similar experimental conditions and annealed at high temperature (around 600 °C).

5.3 Conclusion

A simple method for preparation of SiO_2 with Ce nanoparticles by using a sol-gel method has been described. The SEM results showed small spherical nano-sized particles super-imposed on some of the large agglomerated particles. The surface morphology was less dependent on the Ce concentration in SiO_2 glass. Ce-doped glasses exhibited a broad emission band in the blue region which indicates the potential for this material as the active medium for tuneable phosphor applications in this region. The PL spectrum of SiO_2 with Ce nanoparticles showed enhanced luminescence band with the maximum at about 445 nm (2.8 eV) however significant quenching occurs after total concentration of only 0.5 mol % of Ce. The luminescence band of SiO_2 is shifting from high wavelength to the short wavelength.

References

[1]. L. L. Hench and J. K. West, *Chemistry Reviews* **90 (**1991) 133.

[2]. R. Reisfeld, Opt. Mater. **16** (2001) 1.

[3]. G.E. Malashkevich, I.M. Melichenko, E.N. Poddenezhny, et al., *J. Non-Cryst. Solids* **260** (1999) 141.

[4]. H. Bi, W. Cai, L. Zhang, *Mater. Res. Bul*. **35** (2000) 1495.

[5]. R. Reisfeld, H. Minti, A. Patra, D. Ganguli, M. Gaft, *Spectrochimica Acta A* **54** (1998) 2143.

[6]. V.P. Dotsenko, I.V. Berezozskaya, N.P. Efryushina, et al., *J. Lumin.* **93** (2001) 137.

[7]. D.M. Boye, A.J. Silversmith, Thao Nguyen Nguyen, K.R. Hoffman, *J. Non-Cryst. Solids* **128** (2008) 888.

[8]. Xu Yue-hua, Zhuo-xian Zeng *Journal of Molecular Catalysis A: Chemical*   **279** (2008) 77.

[9]. U. Kreibig 1976 *Appl. Phys*. 10255.

[10]. M. Raukas, S.A. Basun, W. van Shaik, W. M. Yen and U. Happek, *Appl. Phys. Lett*. **69 (**1999) 3300.

[11]. M. Yu; J.Lin; Fu.; Y.C.Han *Phys. Chem. Lett*. **371** (2003) 178.

[12]. J. Zink, B. Dunn, *J. Ceram. Soc., Jpn*. **99** (1991) 878.

[13]. A. Patra, D. Ganguli, *J. Non-Cryst. Solids* **144** (1992) 111.

[14]. R. Reisfeld, A. Patra, G. Panczer, M. Gaft, *Optical Material*, (in press).

[15]. M. Leone, R. Boscaino, M. Cannas, F.M. Gelardi, *J. Non-Cryst. Solids* **245** (1999) 196.

[16]. A. Mohammed, T. Zaitoun, T. Kim, C.T. Lin, *J. Phys. Chem. B* **102** (1998) 1123.

[17]. G. Blasse; B.C. Grabmaier *Luminescent Materials*; ISBN 3-540-58019-0; Springe Verlag: New York, 1994, p. 91.

[18]. D. Hreniak, M. Jasiorski, K.Maruszewk, L. Kepinski, L. Krajczyk, J. Misiewics, W. J. Strek, *Non-Cryst.* **298** (2002) 146.

[19]. R. Turos-Matysiak, W. Grykm M. Grinberg, Y.S. Lin, R.S. Liu, *J. Phys. Condens. Matter.* **18** (2006) 10531.

[20]. R. Reisfeld, A. Patra, G. Panczer, et al., *Opt. Mater.* **13** (1999) 81.

[21]. D.M. Boye, A.J. Silversmith, Thao Nguyen Nguyen, K.R. Hoffman, *J. Non-Cryst. Solids* **353** (2007) 2350.

[**22**]. X.C. Jiang, C.H. Yan, L.D. Sun, Z.G. Wei, *J. Solid State Chem.* **175** (2003) 245.

[**23**]. D. Li, S.Z. Lu, H.Y. Wang, B.J. Chen, Chin. *J. Lumin.* **22** (2001) 227.

[**24**]. X. Gong, P.F. Wu, W.K. Chan, W.J. Chen, *J. Phys. Chem. Solids* **61** (2000) 115.

Chapter 6

The effect of Mg^{2+} ions on the Photoluminescence of Ce^{3+} doped silica.

6.1 Introduction

The sol-gel process is an efficient technique for the synthesis of phosphors due to the good mixing of starting material and relatively low reaction temperature. Another attractive feature of sol-gel glasses is that they can hold a higher concentration of dopants without losing their amorphous character. However, before rare-earth (RE)-doped sol-gel glasses can be used in practical applications such as phosphor materials, several luminescence quenching caused by clustering effects must be overcome. Optically active elements such as metal (Rare-earth and nanocrystals) can be doped into the so-gel matrix, with an enhanced luminescence induced by an energy transfer from host or Al^{3+} to Ce^{3+} ions [1,2]. A trivalent Ce ion is one of the most important activators in various fluoride and oxide materials for its spin allowed optical transitions of 4f-5d [3].

Researchers have reported that the fluorescence is greatly enhanced with the use of Al as co-dopants [4, 5]. The enhancement of luminescence due to Al co-doping has been ascribed to Al dispersing RE clusters, increasing the average distance between the rare-earth ions [6,7]. Rare-earth clustering and dispersing has been studied with fluorescence line narrowing, which is a laser technique that allows the detection of energy migration among the Rare-earth ions [7, 8, 9]. In this paper we present a study on absorption and luminescence properties of SiO$_2$:Ce^{3+} co-doped Mg^{2+} as characterized by UV-Vis and photoluminescence (PL) spectroscopy.

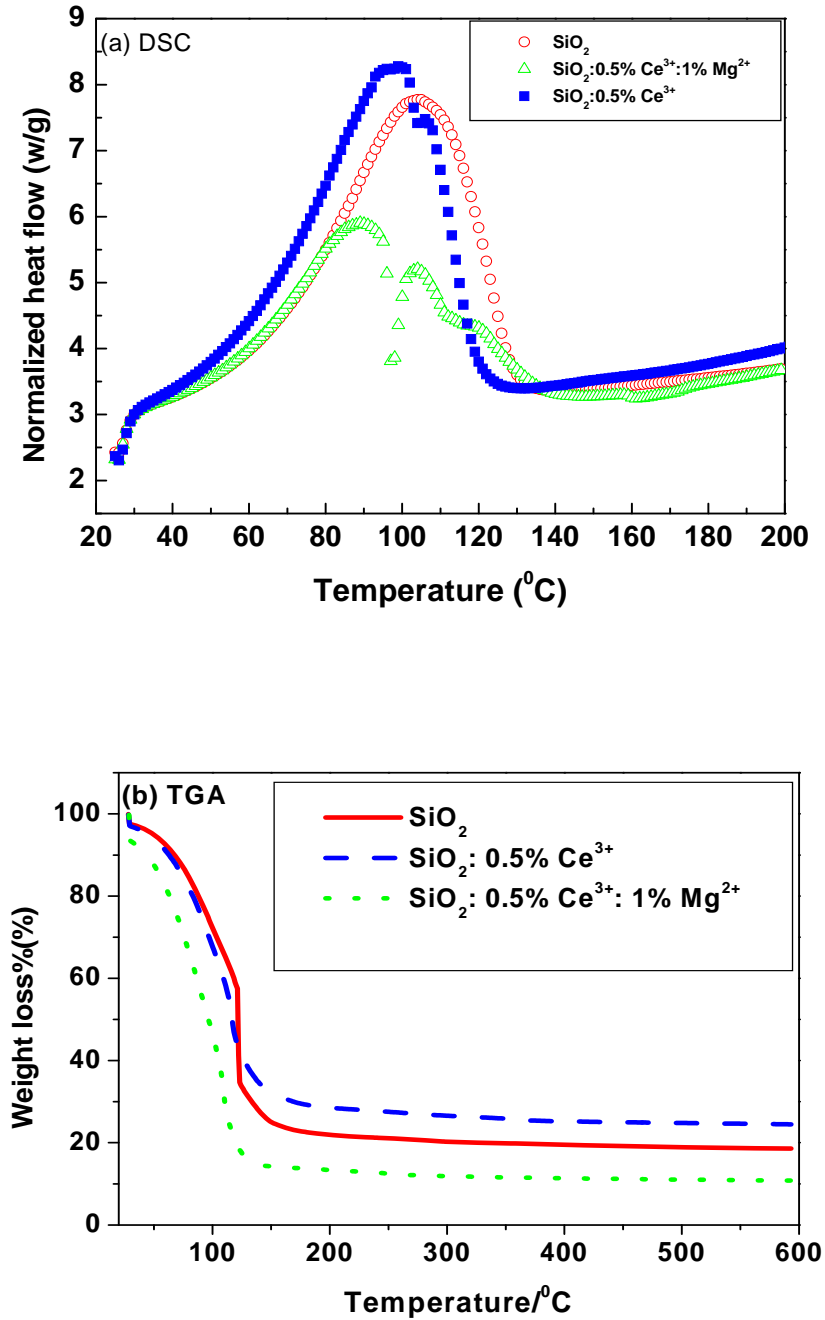## 6.2 Result and Discussion

6.2.1 Thermal analysis

Figure 6.1: DSC (a)-TGA (b), of pure SiO_2, SiO_2:0.5% Ce^{3+} and SiO_2:0.5% Ce^{3+}: 1% Mg^{2+}.

The DSC analyses of the samples are shown in Fig. 6.1 (a) SiO_2 xerogel has an endothermic peak at 105.4 °C and an enthalpy of 880.2 J/g observed in the heating and cooling process. Ce^{3+}-doped SiO_2 xerogels show the endothermic peak at 100.8 °C with enthalpy of 868.2 J/g and Mg^{2+} co-doped shows a similar peak at 90.5 °C with enthalpy of 469.9 J/g. The TGA curves in Fig. 6.1(b) show weight loss of about 45 wt. % from room temperature to 125 °C occurred. Additional weight loss of 30 wt. %, from 125 °C to 135 °C, was observed. Lastly weight loss of almost 5 wt. % from 135 °C to 600 °C was observed. Overall there was a total weight loss of 80 wt. % when undoped SiO_2 xerogels were heated from room temperature to 600 °C. The yield is highest for Ce^{3+} doped sample and lowest for the Mg^{2+} co-doped sample. The possible processes that take place as the temperature increases are, elimination of physically adsorbed water and ethanol, oxidation of residual organics, relaxation of the SiO_2 skeleton, condensation of adjacent hydroxyls and segregated hydroxyls, and viscous sintering, in that order [10]. The decrease in endothermic peak temperature due to the presence of Ce^{3+} or Mg^{2+} ions is attributed to the existence of stronger hydrogen bond between the Si-O networks and water molecules [11] or weaker intermolecular forces between the Si-O-Ce and Si-O-Mg bonds. It is suggested that the introduction of the Ce^{3+} and Mg^{2+} acts as interlayer separator in the SiO_2 network, thus facilitating the release of the water molecules to occur at lower temperatures.

6.2.2 Morphological and Structural properties.

Fig. 6.2 shows the SEM micrograph of the annealed co-doped Ce^{3+}/Mg^{2+} xerogel, after annealing at 600 °C for 2 hours. The morphology of the nanoparticles was characterized by nearly spherical individually resolved nanoparticles producing a denser morphology. The observed grain sizes are mostly between 80 – 120 nm. It is important to note that the presences of dopant and co-dopant ions in silica do not greatly influence the size and the morphology of particles. Fig. 6.3 shows the energy dispersive X-ray spectrum of (a) undoped (b) Ce^{3+} doped and (c) 1 mol % Mg^{2+} co-doped, annealed SiO_2 xerogels. The elemental analysis of the nanoparticles suggests the existence of Si, O, Mg (from the cores and the outside shell), C (from the copper (Cu) gridding for measurement) and Au (from thin gold over layer). The significantly small counts of Mg^{2+} and Ce^{3+} ions is direct indicative of small concentrations of these ions in the samples.

The typical XRD patterns of (a) undoped (b) Ce^{3+}-doped and (c) 1 mol % Mg^{2+} co-doped annealed SiO_2 xerogels are shown in Fig. 6.4. The presence of dispersive broad peak centered around $2\theta \sim 24°$ is indicative of highly disordered / or amorphous SiO_2. The heat treatment of the samples at 600 °C for 2 hours did not change the crystalline structure.
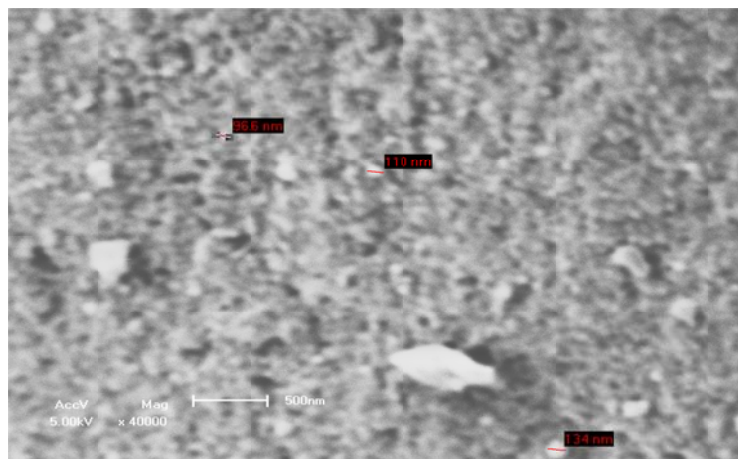
Figure 6.2: SEM micrographs depicting the typical morphological features of xerogels (SiO$_2$, Ce-SiO$_2$ and Mg co-doped SiO$_2$) annealed at 600 °C for 2 hours in air.
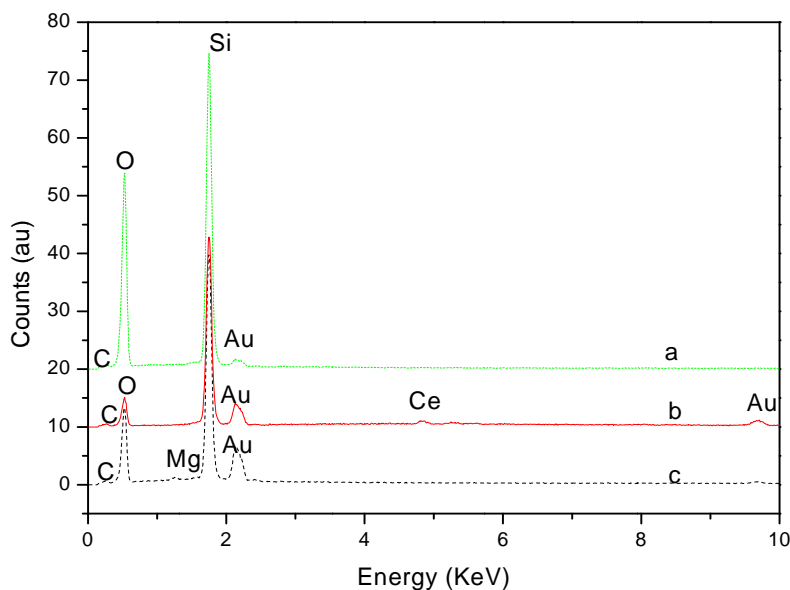
Figure 6.3: Represented EDS spectrum of (a) SiO$_2$ (b) Ce-SiO$_2$ (0.5 mol % Ce) and (c) Mg (1 mol % Mg) co-doped xerogels annealed at 600 °C for 2 hours in air.

76

Figure 6.4: Represented XRD spectra of (a) SiO$_2$ (b) Ce-SiO$_2$ (0.5 mol % Ce) and (c) Mg (1 mol % Mg) co-doped xerogels annealed at 600 °C for 2 hours in air.

6.2.3 Absorbance and Transmittance analysis.

Figure 6.5: Transmittance and absorbance spectra of (a) SiO$_2$, (b) Ce-SiO$_2$ (0.5 mol % Ce) and (c) Mg co-doped SiO$_2$ (1 mol % Mg) xerogels annealed at 600 °C in air for 2hours.

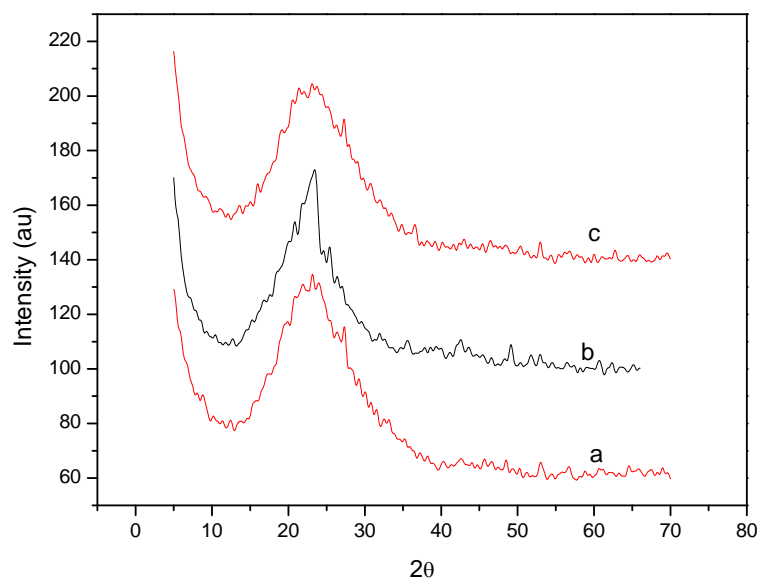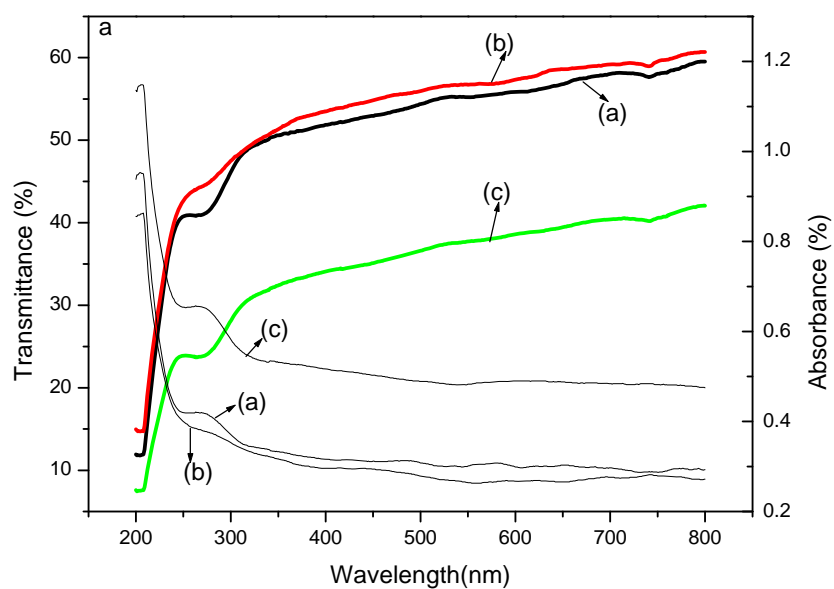Fig. 6.5 show the optical transmittance and absorbance spectra of (a) SiO_2 (b) $Ce-SiO_2$ and (c) Mg co-doped samples heat-treated at 600 °C for 2 hours in air. SiO_2 and Ce-doped samples exhibited high optical transmittance and lower absorbance in the visible region. The presence of Mg^{2+} ions drastically reduces the transmittance, but significantly increases the absorbance. The SiO_2 and Mg co-doped samples presented a weak absorption peak at 275 nm, while the Ce-doped samples quenches this peak respectively. Since no shift is observed in the position of the absorption peak it is therefore concluded that the peak is due to the host material.

6.2.4 Photoluminescence properties.
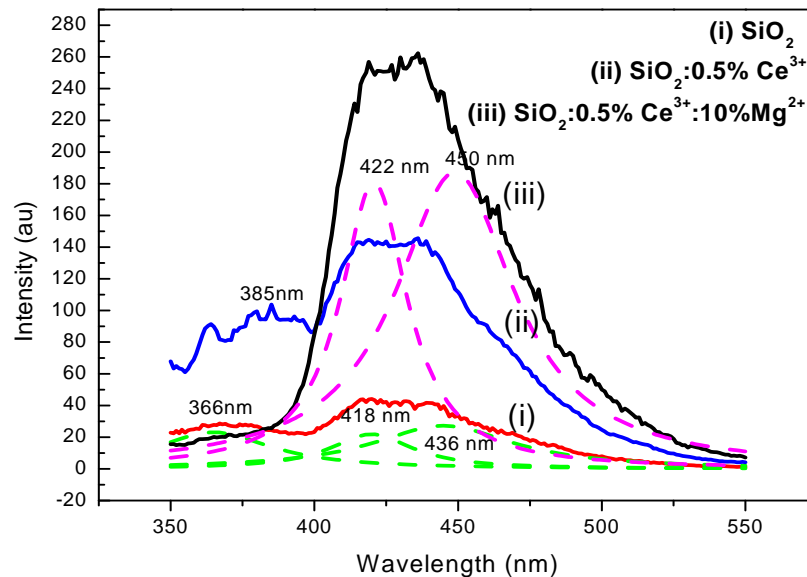
Figure 6.6: (a) Photoluminescence emission spectra of (i) SiO_2, (ii) $Ce-SiO_2$ (0.5 mol % Ce) and (iii) Mg co-doped SiO_2 (10 mol % Mg) xerogels annealed at 600 °C for 2 hours in air with its Gaussian peak fits.

Fig. 6.6 shows PL emission spectra of (i) undoped, (ii) Ce^{3+}-doped and (iii) Mg^{2+} co-doped annealed SiO_2 xerogels excited with a wavelength of 250 nm. The emission spectra of undoped silica presents defect related transitions at 366 nm, 418 nm and 436 nm, Fig. 6.6(i). The intrinsic luminescence spectrum of SiO_2 may vary slightly from sample to sample depending on the syntheses and processing conditions, but it always occurs in the blue region of the spectrum. As

shown in Fig. 6.6(iii), two peaks were fitted as a solution for the broad spectra of Ce^{3+} doped samples. The two peaks are centered at 422 and 450 nm, respectively, and differ by ~2000 cm^{-1}. Clearly the luminescence therefore can be ascribed to the electric dipole-allowed transition from the lower 5d (^{2}D) excited state to the $4f^1$ ground state (a doublet $^2F_{5/2}$ and $^2F_{7/2}$) of the Ce^{3+} ions [12]. It is well known that the emission of Ce ions is either in the UV or visible region and consists of transitions from the lowest 5d excited state to the 4f ground state [13-18].
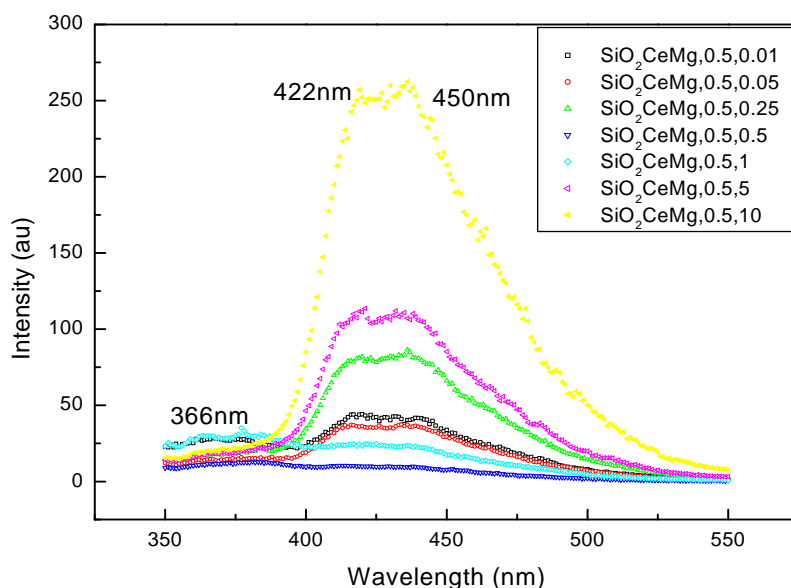
Figure 6.7: Photoluminescence emission spectrum series with two unresolved peaks at 422 and 450 nm of Mg co-doped SiO$_2$ xerogels of different concentrations: 0.01, 0.05, 0.25, 0.5, 1, 5, 10 mol % Mg annealed at 600 °C for 2 hours in air.

Fig. 6.7 contains the emission spectra of sol-gel glasses containing 0.5 mol % Ce^{3+} and varying Mg^{2+} concentrations annealed for 2 hours at 600 °C. The presence of Mg co-dopant significantly increases the luminous intensity. The Mg^{2+} ions disperses the Ce^{3+} clusters, enhancing $^2F_{5/2}$ and $^2F_{7/2}$ emissions due to increased ion-ion distances and decreased cross-relation. Also, an introduction of Mg^{2+} co-dopants with different valences from Ce^{3+}, produce defects, because of charge compensation requirements, resulting in change of energy transfer with the presence of Mg^{2+} ions. The ratio of increase in intensities of both peaks of Ce^{3+} at higher concentrations of Mg^{2+} is different from that of lower concentration of Mg^{2+} ions which indicates a change of

surrounding of the Ce^{3+} ions in the SiO_2 lattice at lower concentration of co-dopant. It was observed that intensity of emission peaks increases significantly as Mg concentrations increases with a critical value of Co-dopants/RE ratio of at least 20:1 as reported Al co-doping [18]. Previously Al [7] has been shown to be more efficient in enhancing luminescence of dopants in materials such as Ti [5], P [19], Ca [19] and thus became the standard co-dopants used by different research groups [20, 21] in the phosphor field.

6.3 Conclusion

SiO_2, Ce^{3+} doped and Mg^{2+} co-doped phosphor powders were successfully synthesized by the sol-gel process, involving the hydrolysis and condensation of organometallic precursor. The DSC and TGA showed that the presence of Ce^{3+} (or Mg^{2+}) ions decreases the endothermic peak temperature while Ce^{3+} increase the yield but Mg^{2+} reduces it. The UV showed that the presence of Ce^{3+} in the matrix slightly increases the transmission intensity and lower absorption peak of undoped SiO_2, while the presence of Mg^{2+} ions reduces the transmittance, but increases the absorbance peak. The Gaussian peak fits to the PL results showed two peaks at 422 nm and 450 nm that fit the broad band spectrum. The origin of these two peaks is due to the crystal field split of the 4f levels of Ce^{3+} ion. An increase in luminescence intensity was observed as the Mg^{2+} to Ce^{3+} ratio increases for the range investigated but significant luminescence enhancement was observed for Co-dopant:Ce ratio greater than 20. This enhanced photoluminescence was assigned to an energy transfer from the Mg nanoparticles, to result in enhanced emission from Ce^{3+}. The Mg^{2+} ions disperses the Ce^{3+} clusters, enhancing $^2F_{5/2}$ and $^2F_{7/2}$ emissions due to increased ion-ion distances and decreased cross-relation.

References

[1]. M. Morita, S. Kajiyama, T. Kai, D. Rau, T. Sakurai, *J. Lumin*., **94** (2001) 91.

[2]. M.A. Garcia, E. Borsella, S.E. Paje, J. Llopis, M.A. Villegas, R. Polloni, *J. Lumin*., **93** (2001) 253.

[3]. G.Q. Xu, Z.X. Zheng, W.M. Tang, Y.C. Wu, *J. Lumin*., **124** (2007) 151.

[4]. P. Rodnyi, E. Melchakov, N. Zakharov, I. Munro, A. Hopkirk, *J. Lumin*., **65** (1995) 85.

[5]. A.J. Silversmith, D.M. Boye, R.E. Anderman, K.S. Brewer, *J. Lumin*., **94–95** (2001) 275.

[6]. B.T. Stone, V.C. Costa, K.L. Bray, *Chem. Mater*. **9** (1997) 2592.

[7]. K. Arai, H. Namikawa, K. Kumata, T. Honda, Y. Ishii, T.Handa, *J. Appl. Phys*., **59** (1986) 3430.

[8]. M.J. Lochhead, K.L. Bray, *Chem. Mater*, **7** (1995) 572.

[9]. O.M. Ntwaeaborwa, P.H. Holloway, *Nanotechnology,* **16** (2005) 865.

[10]. L.C. Klein, *Ann. Rev. Mater. Sci*., **15** (1985) 243.

[11]. G.I. Brown, *Introduction to Inorganic Chemistry, 2nd ed., Longman, United Kingdom*, 1985, p. **47**.

[12]. E. Coetsee, J.J. Terblans, OM Ntwaeaborwa and H.C. Swart, *Physica B, in press*.

[13]. L. Skuja, K. Kajihara, Y. Ikuta, M. Hirano, H. Hosono *J. Non-Cryst. Solids*, **345&346** (2004) 328.

[14]. O.M. Ntwaeaborwa, H.C. Swart, R.E. Kroon, P.H. Holloway and J.R. Botha, *J. Phys. And Chem. of Solids*, **67** (2006) 1749.

[15]. G.E. **Malashkevich**, E.N. Poddenezhny, I.M. Melni-Chenko, and A.A. Boiko, *J. Non-Cryst Solids*, **260** (1999) 141.

[16]. H. Bi, W. Cai, L. Zhang, *Mater. Res. Bul.*, **35** (2000) 1495.

[17]. R. Reisfeld, H. Minti, A. Patra, D. Ganguli, M. Gaft, *Spectrochimica Acta A*, **54** (1998) 2143.

[18]. A.J. Silversmith, N.T. Nguyen, B. W. Sullivan, D.M. Boye, C. Ortiz and K.R. Hoffman, *J. Lumin.*, **128** (2008) 931.

[19]. A. Saitoh, S. Murata, S. Matsuishi, M. Oto, T.Miura, M. Hirano, H.Hosono*, J. Lumin.*, **122–123** (2007) 355.

[20]. A. Monteil, S. Chaussedent, G. Alombert-Goget, N. Gaumer, J. Obriot, S.J.L. Ribeiro, Y. Messaddeq, A. Chiasera, M. Ferrari, *J. Non-Cryst. Solids* **348** (2004) 44.

[21]. J. Lægsgaard, *Phys. Rev. B*, **65** (2002) 74114.

Chapter 7

The effects of the aluminum co-doping on the photoluminescence properties of Ce^{3+} doped SiO$_2$ glasses.

7.1 Introduction

The sol-gel process is of significant interest as it is synthetically flexible and allows for a more homogenous distribution in the final products. SiO$_2$ glasses doped with rare earth elements that emit in UV and visible regions are useful in many applications including laser materials and fiber optics. RE-doped sol–gel glasses are known to suffer from two fluorescence-quenching mechanisms. The first is RE clustering. RE ions have high coordination numbers and must share the limited number of non-network oxygen atoms in the matrix [1]. Clusters form through RE–O–RE bonding, and facilitate both energy migration and cross relaxation. The second important quenching mechanism is a result of residual hydroxyl groups (OH$^-$) remaining in the sol–gel material, even after annealing at high temperatures (e.g. 600 °C). Enhanced photoluminescence of trivalent rare-earth activator ions are induced by energy transfer from S^{2-}[1], Cl$^-$[1], Ti^{2+}[2] and Al^{3+} ions[2, 3, 4, 5] has been reported. The enhancement of luminescence due to Al co-doping [2-5] has been ascribed to Al dispersing RE clusters, increasing the average distance between the rare-earth ions and therefore decreasing cross relaxation [6,7]. Rare-earth clustering and dispersing has been studied with fluorescence line narrowing, which is a laser technique that allows the detection of energy migration among the Rare-earth ions [7, 8, 9]. Although the mechanisms is not yet understandable studies have clearly showed that the Al^{3+} ions co-doping is significantly effective at dispersing RE ions when the ratio of Al:RE is 10:1 or greater. In this section synthesis and characterization of Al co-doped SiO$_2$ nanoparticles in the forms of powders is presented. The concentration dependence and the influence of size on the micro-structural and luminescent properties are discussed. The investigation of luminescence properties through energy transfer between Ce^{3+} and Al^{3+}, of SiO$_2$:Ce^{3+}:Al^{3+} nanoparticles are of the main points.

7.2 Result and Discussion

7.2.1 Thermal analysis

The DSC analyses of the samples are shown in Fig. 7.1(a). SiO_2 xerogel has an endothermic peak at 105.4 °C and an enthalpy of 880.2 J/g observed in the heating and cooling process. Ce^{3+}-doped SiO_2 xerogels show the endothermic peak at 100.8 °C with enthalpy of 868.2 J/g and Al^{3+} co-doped shows a similar peak at 90.5 °C with enthalpy of 469.9 J/g. The TGA curves in Fig. 7.1(b) show weight loss of about 40 wt. % from room temperature to 125 °C. Additional weight loss of 20 wt. % was observed from 125 °C to 135 °C. Lastly an extra weight loss of almost 5 wt. % was observed from 135 °C to 600 °C. Overall there was a total weight loss of 75 wt. % when undoped or doped SiO_2 xerogels were heated from room temperature to 600 °C.
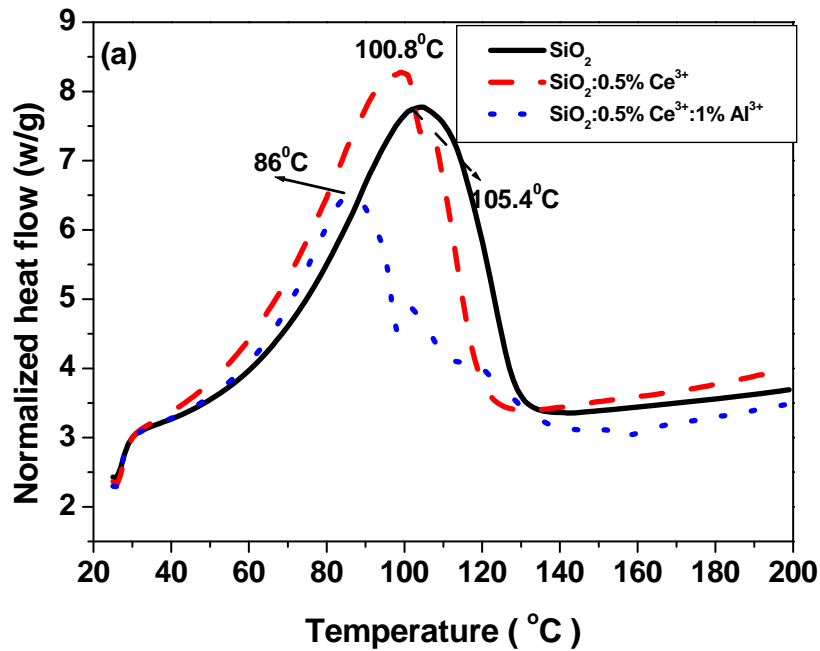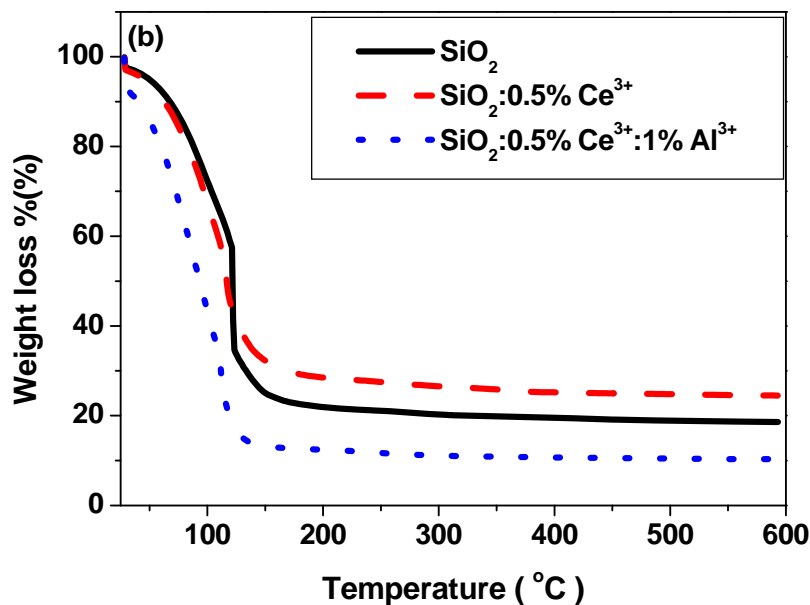
Figure 7.1: DSC (a)-TGA (b), of pure SiO$_2$, SiO$_2$:0.5% Ce^{3+} and SiO$_2$:0.5% Ce^{3+}: 1% Al^{3+}.

The possible processes that take place as the temperature increases are, elimination of physically adsorbed water and ethanol, oxidation of residual organics, relaxation of the SiO$_2$ skeleton, condensation of adjacent hydroxyls and segregated hydroxyls, and viscous sintering, in that order [9]. The decrease in endothermic peak temperature and the yield (or residual matter) due to the presence of Ce^{3+} or Al^{3+} ions is attributed to the existence of stronger hydrogen bond between the Si-O networks and water molecules [10] or weaker intermolecular forces between the Si-O-Ce and Si-O-Al bonds. It is suggested that the introduction of the Ce^{3+} and Al^{3+} acts as interlayer separator in the SiO$_2$ network, thus facilitating the release of the water molecules to occur at lower temperatures. However, the residual weight of all the samples is not the same since they did not contain the same amount of dopants. The yield product of the Ce^{3+}-doped SiO$_2$ xerogel is overlapping the xerogel SiO$_2$ because it has higher molar mass than the host (unannealed SiO$_2$). The order in which the samples melts or degrade depends on melting point of the original compound. The experimental melting point decreases according to the original melting point of the compound, for SiO$_2$ (1650 °C) and for Ce (iii) nitrate hexahydrate (200 °C) and for Al nitrate (73.5 °C). And again it depends on the intermolecular forces.

85

7.2.2 Morphological and structural properties of nanoparticles.

Fig. 7.2 shows the SEM micrographs of the annealed SiO_2 xerogel, after annealing at 600 °C for 2 hours. The morphology of the nanoparticles was characterized by nearly spherical individually resolved nanoparticles producing a denser morphology. The observed particle sizes are between 80 – 120 nm. It is important to note that the presence of dopant and co-dopant ions in SiO_2 did not greatly influence the size and the morphology of particles. Fig. 7.3 shows the EDS spectrum of (a) undoped (b) Ce^{3+} doped and (c) 1 mol % Al^{3+} co-doped, annealed SiO_2 xerogels. Samples are sputter coated with a thin gold layer in order to prevent surface charging of nonconducting sample surface by high energy electrons.

The elemental analysis of the nanoparticles suggests the existence of Si, O, Al (from the cores and the outside shell), C (from the C double sided tape) and Au (from thin gold over layer). The significantly small counts of Al^{3+} and Ce^{3+} ions is direct indicative of small concentrations of these ions in the samples.
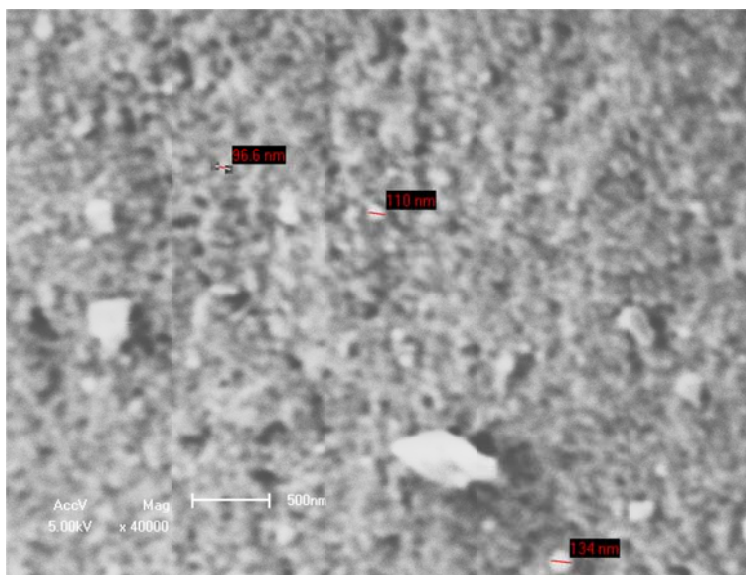

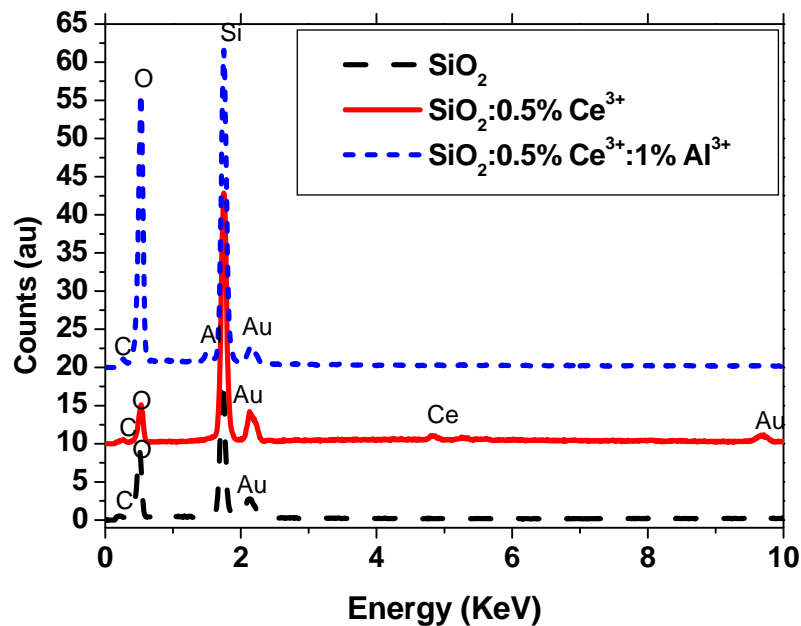**Figure 7.2: SEM images of pure SiO_2.**

Figure 7.3: EDS shows elemental component of the synthesized samples (a) SiO₂ (b) SiO₂: 0.5% Ce³⁺ and (c) SiO₂:0.5%Ce³⁺:1% Al³⁺.

The typical XRD patterns of (a) undoped (b) Ce^{3+}-doped and (c) 1 mol % Al^{3+} co-doped annealed SiO_2 xerogels are shown in Fig. 7.4. All the spectra are similar and only have one dispersive broad peak centered at $2\theta \sim 24$ degrees. The broad peak shows that the SiO_2 particles are highly disordered and / or amorphous. Heat-treatment in air using a furnace at 600 °C for 2 hours did not change the structures of the SiO_2 with Ce^{3+} and co-doped with Al^{3+}.
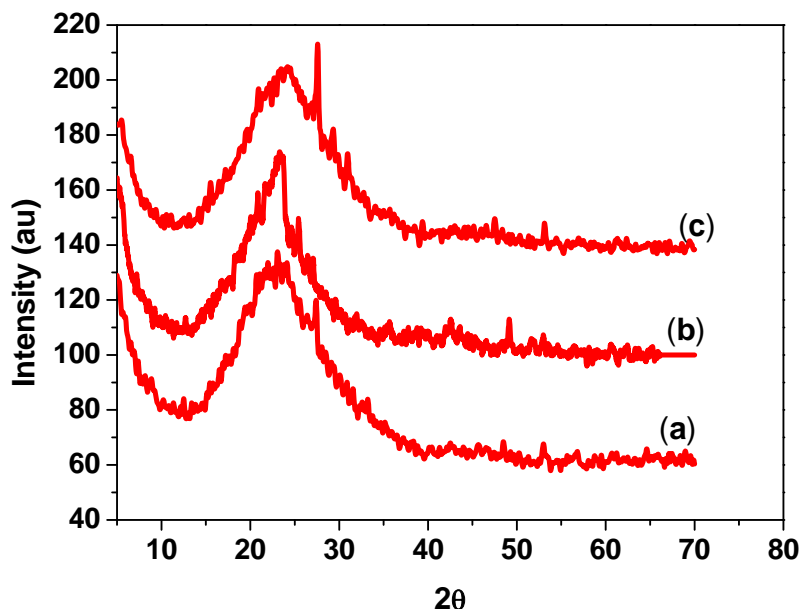
Figure 7.4: XRD spectra of (a) SiO₂ (b) Ce- SiO₂ (c) Al co-doped xerogels annealed at 600 °C for 2 hours in air.

7.2.3 Absorbance and Transmittance analysis.

Fig. 7.5 show the optical transmittance and absorbance spectra of (a) SiO_2 (b) SiO_2: 0.5% Ce^{3+} and (c) SiO_2: 0.5% Ce^{3+}: 1% Al^{3+} co-doped samples heat-treated at 600 °C for 2 hours in air. SiO_2 and Ce-doped samples exhibited high optical transmittance and lower absorbance in the visible region. The presence of Al^{3+} ions drastically reduces the transmittance, but significantly increases the absorbance intensity. The SiO_2 sample presented a weak absorption band at 270 nm, while the Ce-doped and Al co-doped samples quenches this band. This absorption band observed at 270 nm for all samples correspond to the 4f and 5d transitions [11,12], and is similar to the corresponding reference sample in this study (see transmission and absorption curve of SiO_2:Ce^{3+}) in Fig 7.5. Since no shift is observed in the position of the absorption band it is therefore concluded that the band is due to the host material.
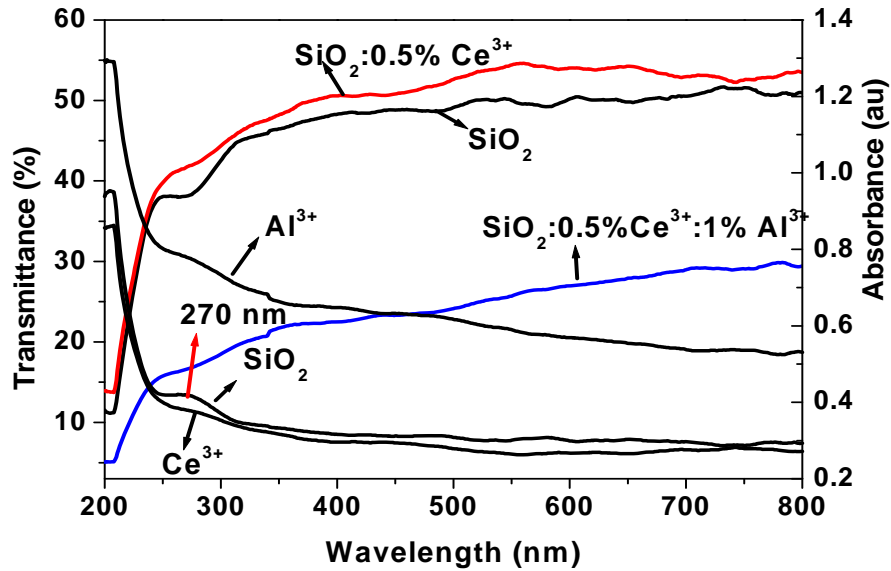
Figure 7.5: Transmittance and absorbance measurement of pure SiO$_2$, SiO$_2$: 0.5% Ce^{3+} and SiO$_2$:0.5%Ce^{3+}:1% Al^{3+}.

7.2.4 Photoluminescence properties.

Fig. 7.6 shows the excitation spectrums of SiO$_2$ and SiO$_2$: 0.5%Ce^{3+}. Both indicated a single band in the region from 250 to 300 nm. This band is attributed to allowed transitions from the ground state to the crystal-field splitting of the 5d level. The difference to these two spectrums is that the Ce^{3+}-doped SiO$_2$ has a higher intensity than the undoped SiO$_2$. The peak position of the absorption spectrum (as shown in Fig. 7.5) is in agreement with the excitation spectrum. The excitation spectrum of SiO$_2$: 0.5% Ce$^{3+:}$ 5% Al^{3+} is not included because the luminescence intensity was saturating.

Fig. 7.7(a) shows the photoluminescence spectra of undoped and Ce^{3+}-doped annealed SiO$_2$ xerogels under the excitation of 270 nm wavelengths. The emission spectra of undoped SiO$_2$ presents defect and charge transfer between Silicon (Si) and oxygen related transitions at 365 nm, 377 nm, 419 nm and 436 nm. The intrinsic luminescence spectrum of SiO$_2$ may vary slightly from sample to sample depending on the syntheses and processing conditions, but it always occurs in the blue region of the spectrum. Fig. 7.7(b) shows the luminescence patterns of undoped SiO$_2$ annealed at 600 °C in air for 2 hour.
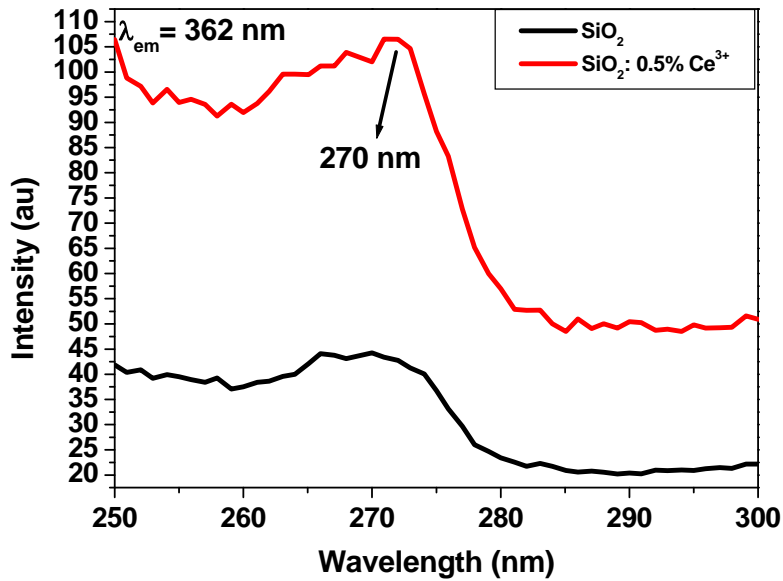
Figure 7.6: The excitation spectra of the doped and undoped SiO$_2$ samples annealed in air at 600 °C for 2 hours.
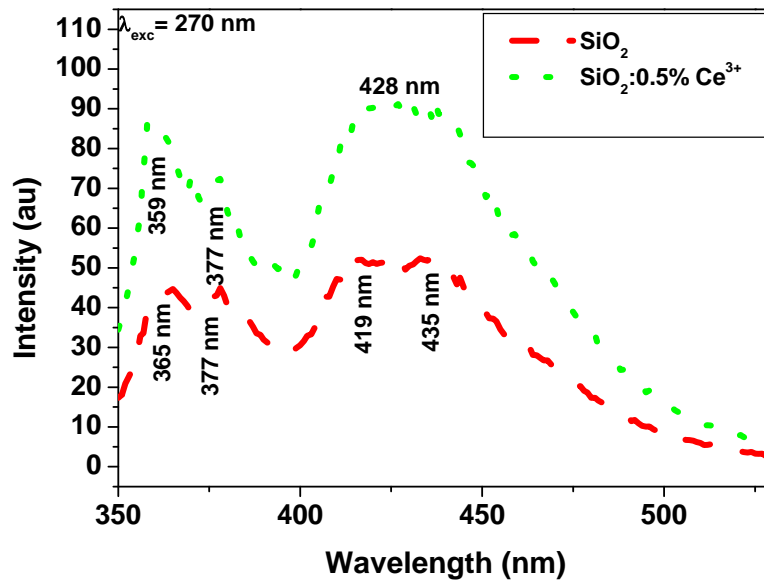

Figure 7.7(a): the emission spectra of the Ce-doped and undoped SiO$_2$ samples annealed in air at 600 °C for 2 hours both excited at λ_{ex}= 270 nm.

Two broad emissions at average of 371 nm and 427 nm were observed with an excitation wavelength of 270 nm. The analysis on these two broad bands with the Gaussian function is shown in this pattern. Three luminescence bands contribute to this two broad band with the maximum at 370, 418 and 448 nm. Fig. 7.7(c) shows the luminescence patterns of the Ce^{3+}-doped SiO_2 annealed in air at 600 °C for 2 hours and excited at 270 nm. Ce^{3+}-doped SiO_2 display unresolved peaks at short wavelength (uv-region) around 359 and 377 nm and maximum peak at 428 in long wavelength (visible region). It is well known that the emission from Ce^{3+} is either in the UV or visible region, consisting typically of two main luminescent [13, 14, 15, 16, 17] which corresponds to the transitions from the lowest $5d^1$ crystal field component ($^2D_{3/2}$) to the two components ($^2F_{5/2}$ and $^2F_{7/2}$) of the 4f ground state. These transitions are attributed to the quadruple (436 nm) and triply charged Ce ions (315 nm) [18]. As observed in section 5.2.4 of Ce-doped samples, SiO_2:0.5% Ce^{3+} produced the highest intensity, this specific sample was further co-doped with various concentrations of Al ions to investigate the effects of co-dopant on luminescence properties. Fig. 7.7(d) shows the luminescence of the Al co-doped SiO_2 annealed in air at 600 °C for 2 hours. One broad emission band was observed with the maximum at 368 nm when excited at 270 nm.
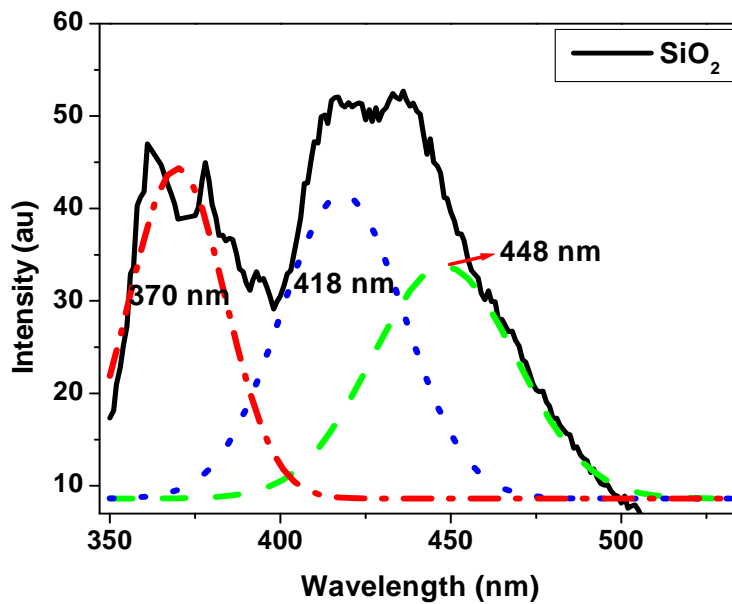

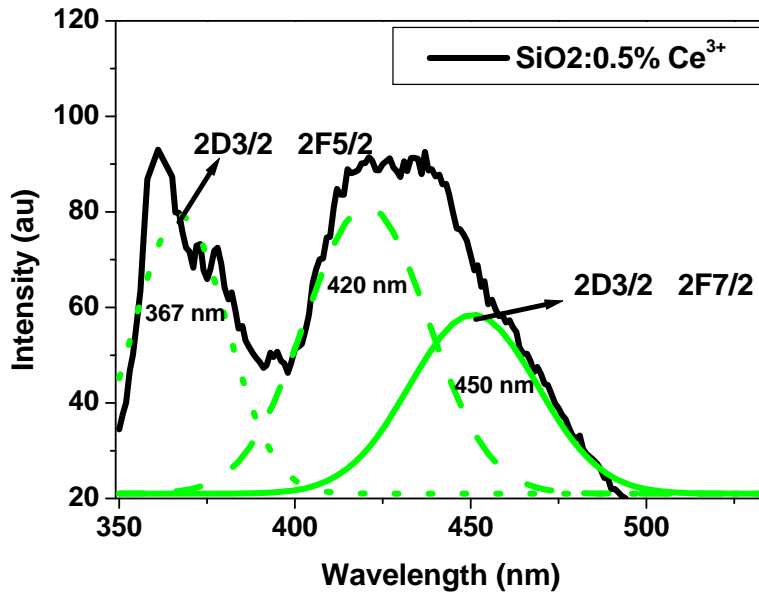**Figure 7.7(b): Shows the Gaussian fits for the PL spectra of SiO₂.**

Figure 7.7(c): Shows the Gaussian fits for the PL spectra of SiO$_2$: 0.5% Ce^{3+}.

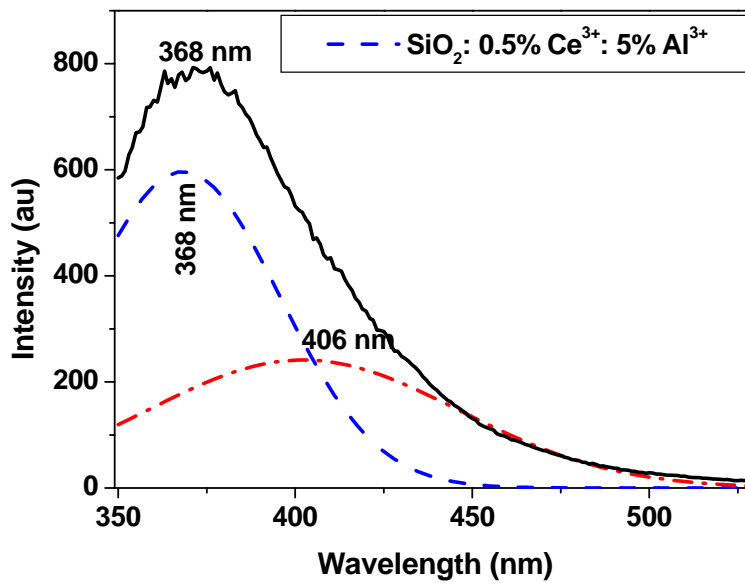**Figure 7.7(d): Shows the Guassian fits for the PL spectra of SiO$_2$: 0.5% Ce^{3+}: 5% Al^{3+}.**

The analysis on this broad band with the Guassian function is shown in this pattern. Two luminescence bands contribute to this broad band with maximum at 368 and 406 nm. Since the effect of Al co-doping on the luminescence intensities will not be clear from a graph of luminescence intensity against wavelength for all the concentrations. Therefore a graph of luminescence intensies against wavelength for low Al concentration (x< 0.5) is also presented in Fig. 7.8(a). The Al co-doped samples display two different behaviors for Al concentrations below and above 0.5% Al^{3+}. Fig. 7.8(a) depicts two unresolved broad peaks at around 370 and 429 nm. Both these luminescence bands intensities increases with increase of Al^{3+} concentrations as shown in Fig. 7.8(a). For Al^{3+} concentrations above 0.5% mol, the PL peak position enhance peak at 368 nm, which can be resolved at 414 and 436 nm. From Fig. 7.8(a) the difference in luminescence intensities at long wavelength is clear than that of short wavelength. This unresolved character of the emission band depends on the temperature and Ce^{3+} concentration [19].
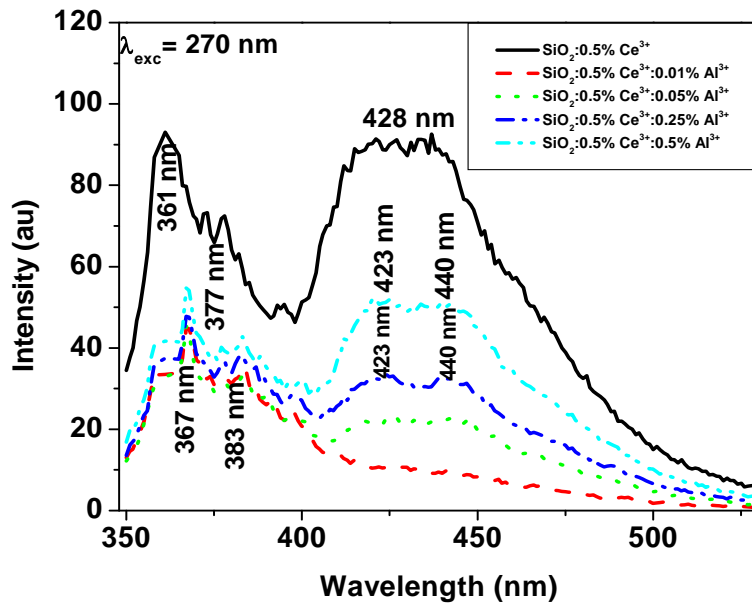

Figure 7.8(a): The PL emission spectrums of SiO_2: 0.5% Ce^{3+} and SiO_2: 0.5% Ce^{3+}: x% Al^{3+} where x is 0.0l ≤x≤0.5.

Fig. 7.8(b) shows the PL emission spectra of SiO_2 with different mol % of Al^{3+}; all excited with 270 nm photons. The effects of Al^{3+} ions are clear. When the concentrations of Al^{3+} were increased the luminescence intensity is increased up to 5% Al^{3+} ions, where the maximum luminescent intensity was obtained. Above the 5% Al^{3+} a decreases in luminescence intensity was obtained when the concentration of Al was further increased. This enhanced luminescence band at around 368 nm, possible could be due to the cross relaxation [4]. In this way, aluminium acts as a network former by distancing each Ce^{3+} ion from each other. The highest luminescent yield of the particles was obtained at a $SiO_2:0.5\%Ce^{3+}:5\% Al^{3+}$, this shows that the cerium ions are dispersed well in glasses containing Al^{3+}, but only when the Al:Ce ratio is at least 10:1. Other radioactive process that could contribute to luminescence enhancement is Al^{3+} ions reducing the residual hydroxyl groups (^-OH). From the DSC measurements, Fig 7.1 (a) it is clear that the amount absorbed is decreasing when the co-dopants are added. Lastly, the luminescence enhancement of SiO_2: 0.5% Ce^{3+}:5% Al^{3+} may be due to the energy transfer from Al^{3+} to Ce^{3+}.
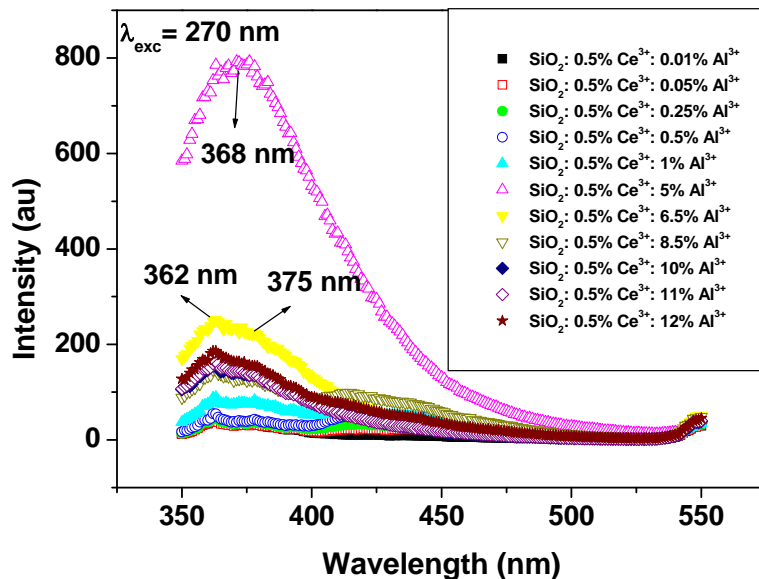

Figure 7.8(b): PL emission spectra from SiO_2: 0.5% Ce^{3+} co-doped with different percentages of Al^{3+} ions.

The energy transfer from Al^{3+} ions to Ce^{3+} ions is due to the emission rate which is faster than the radiative rate of ^-OH ions from Ce (Ce-OH bond), which makes it impossible for ^-OH states

94

to transfer energy to Ce^{3+} ions. The PL intensity of SiO_2: 0.5% Ce^{3+}: x% Al^{3+} where x is the different percentages of Al^{3+} (0.01 ≤ x ≤ 12) as a function of the Al^{3+} concentrations is shown in Fig. 7.8(c). The emission peaks intensity increased when the amount of Al increased, and a maximum value was found in the x = 5 sample, then the emission intensity was quenched gradually. After the highest luminescent intensity the PL intensity start to decrease from x = 6.5 to 8.5 and again start to increase when x = 10 to 12.
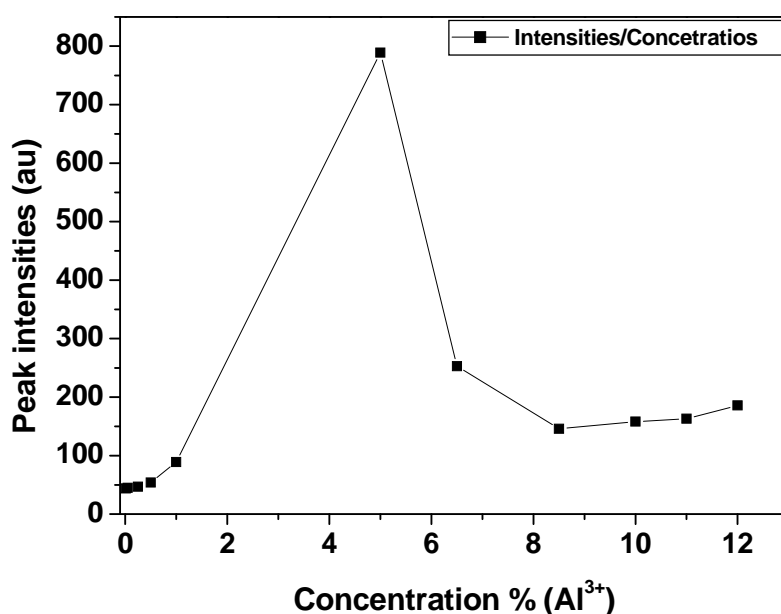
Figure 7.8(c): Shows Graph of Al^{3+} ions concentration versus maximum peak intensity.

7.3 Conclusion

Al with SiO_2 is successfully dispersing clusters of Ce^{3+} ions but not distributing the Ce^{3+} ions uniformly in all environments or regions. But at higher percentages or greater than 5% Al there is a quenching of luminous intensity. The PL spectrum of SiO_2 with different mol% Al^{3+} nanoparticles showed a luminescence band with the maximum at about 315 nm and the highest intensity was obtained with SiO_2: 0.5% Ce^{3+}:5% Al^{3+}. Even the UV spectrum shows that the Al^{3+} ions improve the absorption intensity of SiO_2 doped with Ce. This highest intensity is due to the

reduced energy transfer rate due to the interface of the nanoparticles, so that less energy can migrate to the quenching sites.

References

[1]. G.Q. Xu, Z.X. Zheng, W.M. Tang, Y.C. Wu, *J. Lumin*, **126** (2007) 475.

[2]. D.M. Boye, A.J. Silversmith, J. Nolen, L. Rumney, D. Shaye,   B.C. Smith, K.S. Brewer *J. Lumin*, **94–95** (2001) 279.

[3]. A.J. Silversmith, N.T.T. Nguyen, B.W. Sullivan, D.M. Boye, C. Ortiz, K.R. Hoffman *J. Lumin*, **128** (2008) 931.

[4]. A.J. Silversmith, D.M. Boye, K.S. Brewer, C.E. Gillespie,   Y. Lu, D.L. Campbell, *J. Lumin*, **121** (2006) 14.

[5]. J. Lægsgaard, *Phys. Rev. B*, **65** (2002) 174114.

[6]. D.M. Boye, A.J. Silversmith, A.J. Silversmith, N.T.T. Nguyen,   K.R. Hoffman, *J. Non-Cryst. Solids*, **353** (2007) 2350.

[7]. S. Shionoya, W.M. Yen (Eds.), *Phosphor Handbook*, vol. **185**, CRC   Press, 1999, p. 194.

[8]. O.M. Ntwaeaborwa, P.H. Holloway, *Nanotechnology*, **16** (2005) 865.

[9]. L.C. Klein, *Sol-Gel Processing of Silicates, Ann. Rev. Mater. Sci*., **15** (1985) 243.

[10]. G.I. Brown, *Introduction to Inorganic Chemistry*, 2nd ed., Longman, United Kingdom, 1985, p. 47.

[11]. J. Zink, B. Dunn, *J. Ceram. Soc., Jpn*, **99** (1991) 878.

[12]. A. Patra, D. Ganguli, *J. Non-Cryst. Solids*, **144** (1992) 111.

[13]. G.E. Malashkevich, E.N. Poddenezhny, I.M. Melni-Chenko, and A.A. Boiko, *J. Non-Cryst. Solids*, **260** (1999) 141.

[14]. H. Bi, W. Cai, L. Zhang, *Mater. Res. Bul*., **35** (2000) 1495.

[15]. R. Reisfeld, H. Minti, A. Patra, D. Ganguli, M. Gaft, *Spectrochimica Acta A*, **54** (1998) 2143.

[16]. V.P. Dotsenko, I.V. Berezozskaya, N.P. Efryushina, A.S.Voloshinovskii, P. Dorenbos, C.W.E. Van Eijk, *J. Lumin*. **93** (2001) 137.

[17]. L.F. Koao, H.C. Swart, E. Coetsee, M.M. Biggs, F.B. Dejene, *Physica B*, **404** (2009) 4499.

[18]. G.E. Malashkevich, E.N. Poddenezhny, I.M. Melnichenko, A.A. Boiko, *J. Non-Cryst. Solids*, **188** (1995) 107.

[19]. L.Y. Cai, X.D. Wei, H. Li, Q.L. Liu, *J. Lumin*, **129** (2009) 165.

Chapter 8

Conclusion and Future work

Conclusions

Pure, Ce^{3+}-doped and Mg^{2+} or Al^{3+} co-doped SiO_2 nanophosphors were successfully synthesized and characterized. The DSC analyses showed that the Al^{3+} and Mg^{2+} co-doped endothermic peak melt at lower temperature compared to SiO_2 and Ce-doped unannealed xerogels. TGA revealed that the unannealed co-doped samples degrade at lower temperature more than the doped and unannealed SiO_2 xerogels.

SEM images depict particles that are spherical in shape and nanosized. The presence of dopant or co-dopant has minimum effect on surface morphology. The EDS depicted the presence of expected elements in all the samples. XRD showed that all the samples are non-crystalline. Since the dopant or co-dopant is present in very small molar ratio its presence did not significantly change the crystalline structure of SiO_2.

The UV-vis showed that the presence of Ce^{3+} in matrix lowers the absorbance but increases the transmittance of annealed SiO_2 xerogels, while the presence of Al^{3+} or Mg^{2+} ions significantly increases the absorbance significantly.

The annealed SiO_2 xerogels display defects and polaron related luminescence emission. Ce-doped silica (SiO_2:Ce^{3+}) samples display Ce^{3+} characteristic luminescence transitions from 5d to 4f energy levels. It was observed that the luminescence intensity is Ce^{3+}-ion concentration dependent. The highest luminescent intensity yield of the particles was obtained at a Ce concentration of 0.5% and lower or higher Ce contents results in a substantial decrease in emission intensity. The decrease in emission intensity with increasing Ce activator concentration may be due concentration quenching as discussed in chapter 2.

An increase in luminescence intensity was observed as the Mg^{2+} or Al^{3+} to Ce^{3+} ratio increases for the range investigated but significant luminescent enhancement was observed for co-dopant:Ce ratio greater than 20. It was found that Al^{3+} luminescence almost enhances 3-times as much as Mg^{2+} ions. This enhanced luminescence is attributed to an energy transfer from the Mg^{2+} or Al^{3+} nanoparticles, to result in enhanced emission from Ce^{3+}. The co-dopants disperses

the Ce^{3+} clusters, enhancing $^2F_{7/2}$ and $^2F_{5/2}$ emission due to increased ion-ion distances and decreased cross-relaxation.

Future Work

8.1 Effect of annealing temperature on luminescence of doped SiO_2 glasses.

We have observed that apart from concentration of Ce-dopant, the luminescence intensity of doped-SiO_2 glasses is significantly affected by the presence of hydroxyl ions which are residue after hydrolysis process and annealing conditions. It is therefore important to quantify the contributions of hydroxyl ions by studying the annealing effects on the luminescence properties of these samples.

8.2 Dependence of size of the SiO_2 nanoparticles on preparations parameters.

It is our belief that the preparation conditions have significant influence on the sizes and therefore the type of defects in SiO_2 gels and powders. This will intern affects the luminescence properties of the materials. Since the observed measurement made by XRD, show that all samples are amorphous, it was not possible to use these measurements to approximate the particles sizes. Hence further studies should be done using various techniques e.g. TEM to determine the relations between particles sizes, preparation conditions and luminescence properties.

8.3 Luminescence property as functions of Ce and Al or Mg.

In all our measurements on co-doped SiO_2 samples, in the presence of different % Al or Mg, the luminescence was studied for the maximum peak observed at about 0.5% Ce. It is important to compare this result with the intensity of luminescence as a function of Ce in the presence of fixed Al or Mg as a co-dopant, since this will give us some information's whether the luminescence strongly depends on the environment and varies as the concentration of Al (Mg) or Ce or both. The information obtained will supply us with more information on the role of Al in doped glasses.

8.4. Improving the sample properties using solvent agents

In our work so far, no solvent agents such as DMF (dimethylformamide), was used during synthesis of sol-gel glasses. Our samples do come out of furnace with cracks, which negatively affects the luminescence properties of the SiO_2 glasses. However, we have been able to bring the

annealing temperature higher (600 °C) and achieve full densification of glasses that contain low concentrations of do-pants and co-dopants. In future reducing agents and further higher annealing temperature would be applied to avoid sample cracking.

8.5 Energy transfer between Al (Mg) and Ce ions

Further studies should be done to quantify and differentiate the contributions of luminescence enhancement by energy transfer between the Al (Mg) and Ce ions from that of reductions in cross relaxation due co-dopant acting as spacers between corresponding Ce ions.

Appendix A

Publications

[1]. LF Koao, HC Swart, E Coetsee, MM Biggs and FB Dejene, Synthesis and characterization of Ce^{3+} doped SiO_2 nanoparticles, J. Lumin. **Submitted September 2009**.

[2]. LF Koao, HC Swart, E Coetsee, MM Biggs and FB Dejene, The effect of Mg^{2+} ions on the Photoluminescence of Ce^{3+} doped SiO_2, Physica B **404** (2009) 4499–4503.

[3]. LF Koao, HC Swart, E Coetsee, MM Biggs and FB Dejene, The effects of the Al^{3+} ions on the photoluminescence intensity and wavelength of Ce^{3+} with SiO_2, J. Lumin. **In preparation**.

Conferences

[1]. LF Koao, HC Swart and FB Dejene, Synthesis and characterization of rare-earth metal doped SiO_2 nanoparticles, SAIP Limpopo (2008).

[2]. LF Koao, HC Swart and FB Dejene, Synthesis and characterization of SiO_2 doped with Rare-Earth metal (e.g.Ce^{3+}) and co-doped with Al^{3+} ions**,** SAIP Durban (2009).

[3]. LF Koao, HC Swart and FB Dejene, The effect of Mg^{2+} ions on the Photoluminescence of Ce^{3+} doped SiO_2, 3rd International Conference on Photonic Materials, Mabula, Limpopo (23-27 March 2009).

[4]. LF Koao, HC Swart and FB Dejene, Synthesis and characterization of Ce^{3+} doped SiO_2 nanoparticles, International Conference On Nanotechnology and Advanced Materials At University of Bahrain (4/7 May 2009).